THE UNIVERSITY OF CHICAGO

MODULATING RHOA EFFECTORS INDUCES TRANSITIONS TO OSCILLATORY AND MORE WAVELIKE RHOA DYNAMICS IN *CAENORHABDITIS ELEGANS* ZYGOTES

A DISSERTATION SUBMITTED TO
THE FACULTY OF THE DIVISION OF THE BIOLOGICAL SCIENCES
AND THE PRITZKER SCHOOL OF MEDICINE
IN CANDIDACY FOR THE DEGREE OF
DOCTOR OF PHILOSOPHY

GRADUATE PROGRAM IN CELL AND MOLECULAR BIOLOGY

BY
BAIXUE YAO

CHICAGO, ILLINOIS
JUNE 2022

TABLE OF CONTENTS

SUPPLEMENTARY FILE is available at `https://www.molbiolcell.org/doi/abs/10.1091/mbc.E21-11-0542`

LIST OF FIGURES

LIST OF TABLES

ACKNOWLEDGMENTS

To my husband, my parents, and my friends and colleagues for all of their support.

ABSTRACT

The biological world is full of patterns, from macroscopic patterns such as leaf veins to microscopic patterns that underlie processes such as cell polarization and migration. The implementation of such biological functions requires spatiotemporal control of cellular activities. A key challenge in biology is to understand the mechanisms of pattern formation. Mathematical theories on biological pattern formation were first introduced in the 1950s. Since then mathematical biologists have been trying to explain biological patterns with simple models made up of a few physical interactions. Advances in imaging, computation and the identification of many key molecular components of biological circuits in the last decade made it possible to reduce the gap between simple models and biological reality in many contexts. However, the knowledge gap is still far from closed for most biological patterns.

In this thesis, I study the mechanisms that govern the spatiotemporal patterns of pulsatile active RhoA dynamics in the *Caenorhabditis elegans* (*C. elegans*) zygote. RhoA is a small GTPase whose activation drives the assembly of actomyosin networks. Pulsatile RhoA activation underlies a wide range of cell and tissue behaviors. The circuits that produce these dynamics in different cells share common architectures based on fast positive and delayed negative feedback through F-actin, but they can produce very different spatiotemporal patterns of RhoA activity. However, the underlying causes of this variation remain poorly understood. Here I asked whether and how this variation could arise through modulation of actin network dynamics downstream of active RhoA in early *C. elegans* embryos. In particular, I asked whether it is possible to tune temporal RhoA dynamics from excitable to oscillatory and the spatial spread of of Rho activity from focal pulses to travelling waves. I combined genetic perturbations of actomyosin regulators with live multicolor microscopy and developed an image analysis pipeline to characterize and quantify patterns of RhoA activation and measure the correlation between RhoA activation and the level of inhibition from F-actin. I found that perturbing two RhoA effectors—formin and anillin—induce transitions from nonrecurrent focal pulses to either large noisy oscillatory pulses (formin depletion) or noisy oscillatory waves (anillin depletion). The observed dynamics in anillin or formin-depleted embryos could in principle be explained by simple models based on fast-positive and delayed negative feedback in which F-actin serves as the inhibitor. The underlying

mechanisms for F-actin depletion are distinct, with different dependencies on myosin II activity. The transition from wildtype to anillin or formin-depleted dynamics could be explained by reduction in the overall level of inhibition from F-actin. However, wildtype dynamics cannot be explained by the simplest models, suggesting that additional feedback mechanisms are required to generate focal pulses. Thus, the same circuit can generate different spatiotemporal dynamics of RhoA activation associated with different physiological or morphogenetic functions, which can be accessed by modulating actomyosin network dynamics.

CHAPTER 1

INTRODUCTION

1.1 Overview

How cellular activities are organized in time and space is a fundamental question in biology. Most biological processes require spatiotemporal coordination of activities. For example, cells need to decide when to divide and where to place the division site. Cells must establish and maintain polarity to direct different activities to different poles of the same cell. Groups of cells must produce complex spatial and temporal patterns of force to execute tissue shape changes during morphogenesis. Excitation and contraction of single heart cells must be coordinated across cardiac tissues to produce heartbeat and blood flow.

Complex spatiotemporal patterns of biological activity are often governed by collections of molecules that interact with each other to form complex circuits. The molecular components and their interactions have been identified in many circuits, but knowledge about individual components and pairwise interactions in the underlying molecular circuit is not sufficient to explain how the components self-organize to form complex patterns.

Theories on pattern formation provide a useful framework for understanding how spatiotemporal patterns could arise. A common approach to test whether the hypothesized model underlies the biological pattern is to compare model prediction and the biological pattern subject to the same set of perturbations. Recent developments in quantitative time-lapse microscopy have allowed researchers to characterize patterns in the accumulation/activity of molecules in cells and tissues with high temporal and spatial resolution. Advances in computational tools made it possible to simulate more detailed models. More accurate experimental measurements and model prediction work together to advance our understanding of pattern formation in biological systems.

Here I will describe efforts to understand biological pattern formation through a combination of experiments and theoretical modeling. I will focus on a class of spatiotemporal dynamics known as pulsatile dynamics. A pulse refers to a rapid increase in activity followed by a rapid return

towards baseline levels. The temporal dynamics of local pulses are used to encode information about sensory inputs such as stress response (Lagage and Uphoff 2020) and cell proliferation (Albeck et al. 2013; Aoki et al. 2013). Temporal dynamics are also used to control the timing of biological activities such as cell cycle (Ferrell 2013) and circadian oscillators (Kinmonth-Schultz et al. 2013). The propagation of pulses enables information such as depolarization, fertilization and mitosis, to transmit rapidly in space without damping.

In this introductory chapter, I will discuss how simple theoretical models guide studies on the mechanisms of complex pulsatile biological dynamics and how biological systems could utilize pulsatile dynamics to implement important biological functions. I will discuss models and biological systems exhibiting local pulses of activity. Then I will discuss the types of spatiotemporal patterns generated through the combination of local reaction kinetics and diffusion. For each type of spatiotemporal pattern, I will discuss their application in biological systems. Finally, I will discuss how contractile driven flows shape reaction diffusion dynamics.

1.2 Local pulses of activity encode information in their dynamic properties

1.2.1 Temporal dynamics of the activator-inhibitor model

The activator-inhibitor (AI) model is a popular minimal theoretical model able to generate pulses of activity at one point in space. This model considers two types of molecules that react with each other: activator and inhibitor. The activator promotes its own accumulation with nonlinear kinetics, generating a positive feedback. The inhibitor is recruited by the activator and inhibits the activator, serving as a delayed negative feedback. The positive feedback drives the initial rapid increase in activity in the rising phase of pulses. The delayed negative feedback brings the activity to the base level in the falling phase of pulses.

By modulating the strength and timing of the feedback, the AI model can generate four types of temporal dynamics. (i) A single stable steady state that the system returns to after a perturbation. (ii) Excitable dynamics. Excitable systems stay in the rest state until perturbations larger than a threshold value trigger a pulse of activity before returning to the

only stable steady state. The system is excited when the pulse of activity reaches its peak level. The transition from rest state to excited state is called excitation. (iii) Bistable dynamics. Bistable systems have two stable steady states with different levels of activity. In response to large enough external perturbations, the system can switch between the two states in both directions. (iv) Oscillatory dynamics. Oscillatory systems generate pulses of activity at regular intervals indefinitely. Excitable, bistable and oscillatory systems all experience rapid transition from low levels of activity to high levels of activity. I will refer to such transitions in all three systems as "excitation".

Pulse dynamics of models in type (ii) are affected by not only the feedback kinetics, but also temporal dynamics of the trigger which can be external perturbation or internal stochastic fluctuations. Excitable systems with rare suprathreshold triggers generate pulses separated by long periods of quiescence. As the frequency of excitation increases, the duration of quiescence decreases and approximates the duration of individual pulses. A theoretical study on the relationship between the amplitude of stochastic fluctuations and the temporal dynamics of excitable models showed that it is possible for excitable systems to generate noisy oscillatory dynamics when subject to stochastic fluctuations whose amplitude is of the same order of magnitude as the threshold value of the excitable system (Pikovsky and Kurths 1997). Given that most biological systems are subject to stochastic fluctuations, it is not possible or meaningful to distinguish whether the underlying deterministic system of noisy oscillations is excitable with small threshold or truely oscillatory. Instead, one can determine the periodicity of a given pulsatile system along the spectrum from rare stochastic excitations to noisy oscillations.

1.2.2 Pulsatile signaling dynamics allow versatile encoding of information

Overview

Cells use different signal transduction pathways (p53, ERK, $NF-\kappa B$) to convert external signals into the expression levels of target genes which are regulated by transcription factors. Examples of external input signals include environmental stress, chemoattractants or developmental signaling molecules. In general, signal transduction pathways exhibit two kinds of dynamic response: graded responses and pulsatile responses. Graded responses can only encode information in their

amplitude. Pulsatile responses can encode information in more dimensions in its dynamical properties, such as frequency, amplitude and duration. For example, consider an external signal that persists in time without changing its strength, the expression level of transcription factor remains the same overtime (static) for graded response, and exhibits pulsatile dynamics with fixed properties, for pulsatile response. When the strength of the external signal changes, the static transcription factor expression level changes for graded response, while pulsatile responses could change one or more of its dynamic properties. I will summarize how cells encode properties of external signals, such as the strength, rate of increase, in the frequency and amplitude of pulses of transcription factor expression (Figure 1.1 A).

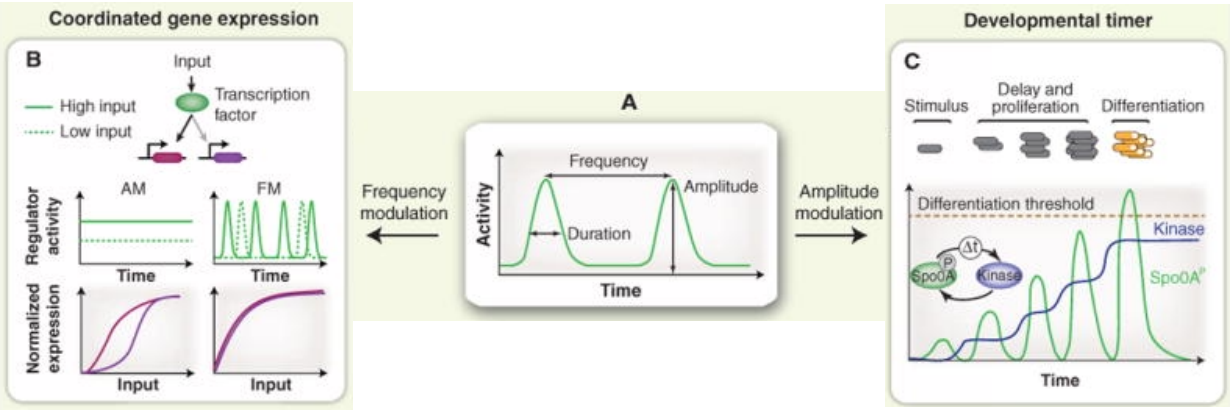

Figure 1.1. Pulsing enables diverse cellular functions. Adapted from Levine, Lin, et al. 2013. (A) Cells modulate pulse characteristics, including amplitude, frequency, and duration, to implement diverse regulatory functions. (B) A transcription factor (green) may activate different target promoters at different thresholds or with different affinities (light and dark arrows). Concentration-based regulation (amplitude modulation, AM) would therefore lead to different, nonproportional, response profiles (bottom left). In contrast, frequency-modulated (FM) pulsing, by effectively controlling the fraction of time that all target genes are expressed, leads to expression of targets in fixed proportions (bottom right), indicated by overlap of expression curves (each is normalized to its own maximum). (C) Pulsed regulation functions in a developmental timer. B. subtilis respond to sudden nutrient limitation by proliferating for multiple cell cycles before sporulating (schematic). A model of the underlying circuit (inset) is based on a positive-feedback loop (arrows) with a hypothesized time delay (δt). This circuit can generate progressive growth in pulses of phosphorylation of the sporulation master regulator Spo0A (green trace), via steplike growth in the kinase concentration (blue trace). The timer terminates when a threshold level of Spo0A is reached (dashed line).

Frequency modulation

Many cells encode the strength of external stresses in the frequency of pulses. Examples include pulses of the transcription factor Crz1 in budding yeast in response to extracellular calcium (Cai et al. 2008), pulses of the MAP kinase ERK in mammary epithelial cells in response to epidermal growth factor (Albeck et al. 2013) and pulses of the transcription factor $\sigma(B)$ in Bacillus subtilis cells in response to energy stress (Locke et al. 2011). In the absence of external signals, all three of these factors exhibit pulses of nuclear localization with a characteristic mean

frequency. Upon an increase in external signal strength, they respond with an increase pulse frequency, but not duration and amplitude.

Frequency modulation ensures that a change in the strength of the external signal alters the expression level of different target genes by the same ratio (Figure 1.1 B). Suppose that different target genes of a signal transduction pathway are activated at different thresholds. Then if the transcription factor exhibits a graded response, it activates different sets of targets at different external signal strengths. If it exhibits pulsatile response, at different external signal strengths, pulse frequencies are different while pulse amplitudes are the same. Same amplitude ensures that the same set of genes are activated. A change in pulse frequency changes the frequency with which these target genes are activated.

Pulse frequency can also encode external signal strength even when the time gap between consecutive pulses is not as regular as the examples above. For example, in 3T3 mouse fibroblast cells, the concentration of tumor necrosis factor alpha is encoded in the probability of $NF-\kappa B$ pulses (Nelson et al. 2004; Ashall et al. 2009; Tay et al. 2010).

Amplitude modulation

Another way in which cells use pulses to encode information is through amplitude modulation. In response to an increase in environmental stresses such as salt and ethanol, For example, Bacillus subtilis generates a single pulse of $\sigma(B)$ activation, a transcription factor that activates a broad set of stress response genes (Locke et al. 2011; Young et al. 2013). The amplitudes of $\sigma(B)$ pulses are governed by the rate of increase in the strength rather than the absolute strength. A sudden increase in stress triggers a stronger stress response than a gradual ramp to the same stress level.

Pulse amplitude can also encode the number of cell cycles since initial exposure to external stresses (Figure 1.1 C). When B. subtilis is placed in a culture medium with low levels of nutrients, the stress response pathway starts a timer to ensure that sporulation will initiate after 3 cell cycles (Levine, Fontes, et al. 2012; Vishnoi et al. 2013). The timer is implemented through pulsatile accumulation of the phosphorylated form of Spo0A (Spo0A-P). In this system, the positive feedback that drives the upswing of each pulse is governed by phosphorylation of

Spo0A by a kinase, whose transcription is activated by Spo0A-P. After each pulse, the kinase level increases which strengthens the positive feedback for the next pulse. Thus, the amplitude of the Spo0A-P pulse increases with time. Only during the last pulse does the level of Spo0A-P cross the threshold to transcribe sporulation genes. Since po0A-P pulses are synchronized with the cell cycle, Spo0A-P serves as a developmental timer for sporulation.

Finally, cells can encode stress signals through the simultaneous modulation of pulse frequency and amplitude. For example, the tumor suppressor p53 exhibits different pulsatile dynamics in response to different external stresses. γ-irradiation triggers a train of short p53 pulses, while UV irradiation triggers a single sustained pulse lasting more than three cycles of short p53 pulses (Purvis et al. 2012; Batchelor, Loewer, et al. 2011; Batchelor, Mock, et al. 2008). Similarly, nuclear localization of the transcription factor Msn2/4 exhibits multiple short pulses upon glucose limitation and exhibits a single sustained pulse upon oxidative stress (Hao and O'Shea 2011; Hansen and O'Shea 2013).

1.3 Reaction diffusion systems underlies many biological patterns

1.3.1 Overview

In spatially extended systems, local reactions can be spatially coupled to generate complex spatiotemporal dynamics through transport processes like thermal diffusion or active transport driven by molecular motor proteins and/or bulk flows of the cell cortex or cytoplasm. I will focus on reaction diffusion models in this section and discuss the contributions of active transport in Section 1.5.

The coupling of reaction and diffusion is often described using reaction diffusion models, which express mathematically how the concentrations or activities of specific factors change over time as a consequence of local interactions and diffusion. The resulting equations can be solved analytically or numerically to predict the kinds of patterns that can be generated for particular reactions. Most reaction diffusion models are simple, involving at most three chemical species with nonlinear reactions. In many biological contexts, the reaction kinetics of such models are challenging to constrain by experimental measurements. However, these models with

unconstrained reaction kinetics are still useful as a framework. By tuning the mathematical forms and parameters of the reaction kinetics as well as the diffusion of the activator and inhibitor, we can generate hypotheses about how the observed pattern variation could arise theoretically and test these hypotheses experimentally.

1.3.2 Activator inhibitor reaction diffusion models generate complex spatiotemporal dynamics

Here I will focus on a class of reaction diffusion models in which the activator-inhibitor kinetics described in section 1.2 are combined with thermal diffusion of the activator and inhibitor.

AI reaction diffusion models can generate a wide range of different spatiotemporal patterns depending on three factors. First, local dynamics in the absence of diffusion in section 1.2, which can be unconditionally stable, bistable, excitable and oscillatory. Second, relative rates of diffusion of activator and inhibitor which determines whether excitations propagate. Third, the temporal dynamics of local suprathreshold perturbations (triggers).

Turing patterns are stable patterns that are periodic in space and stationary in time. Turing patterns arise through diffusion-driven instability in which diffusion destabilizes the spatially uniform steady state without external perturbations (Turing 1952; Gierer and Meinhardt 1972; Kondo and Miura 2010). Intuitively, diffusion-driven instability involves the following steps. Autocatalysis of the activator amplifies infinitesimal fluctuations to generate a sharp local increase in the activator level. Locally, activator accumulation is followed with a delay by accumulation of inhibitors, which then inhibits the activator. Diffusion attenuates the local buildup of the inhibitor (which would otherwise prevent autoactivation), allowing the activator to grow locally. Diffusion also increases the level of the inhibitor in neighboring regions. So regions with high activator levels are surrounded by regions with low activator levels. On two dimensional surfaces, these static spatial waves form evenly spaced lines, spots and mazes. These patterns resemble pigmentation on the coats of cheetah, zebra and zebra fish, as well as segmental gene expression in insects. As I will discuss further below, I will refer to any static pattern with such features as Turing patterns no matter whether AIRD models are the underlying mechanisms.

AI reaction diffusion models also generate three types of locally oscillatory dynamics without external perturbations. **Synchronous oscillations** are uniform in space but periodic in time. **Traveling waves** and **standing oscillations** are periodic both in space and time. When the activator diffuses much faster than the inhibitor, local excitations propagate in space, generating traveling waves. Otherwise, excitations remain local, generating standing oscillations.

AI reaction diffusion systems with excitable or bistable local reaction kinetics can generate **trigger waves** and **focal pulses**. Excitations in both systems are triggered by suprathreshold perturbations. Trigger waves occur when the activator diffuses much faster than the inhibitor. Once initiated, excitations in trigger waves travel in space indefinitely. The condition for forming focal pulses includes that the inhibitor diffuses much faster than the activator and that suprathreshold perturbations are rare (Hecht et al. 2010). After initiation, faster build up of the inhibitor in neighboring regions restricts the propagation of excitation. So focal pulses have finite lifetime and size.

The rules of pattern formation in AI reaction diffusion systems can be generalized. The systems are not restricted to reaction diffusion systems with two types of interacting species and three reactions. They can also arise in biochemical systems with more players and interactions, and even in systems where the players are not molecules and where interactions are not described by chemical reaction and diffusion. Nevertheless, the conditions that describe when different kinds of patterns arise are very similar: the positive and delayed negative feedback circuit topology must be preserved and the two kinds of feedback must have spatial coupling mechanisms with different length scales. In the following sections, I will discuss biological systems whose dynamics resemble Turing patterns, trigger waves and traveling waves and the underlying mechanisms to generate these patterns.

1.3.3 Short range activation and long range inhibition underlies many Turing patterns

Any model that combines short-range activation and long-range inhibition can generate Turing patterns (Gierer and Meinhardt 1972). This mechanism is often called lateral inhibition to indicate that inhibition operates on a longer spatial scale than activation. Visual resemblance

of biological patterns to Turing patterns does not mean that the underlying mechanism is lateral inhibition. To show that a pattern is driven by lateral inhibition, one must first identify the molecules or cells (or other interacting players) that act as short-range activator and/or long-range inhibitor; then one must reproduce the wild-type pattern using models based on the hypothesized or observed interactions among these players; finally, one must demonstrate that the model has the same dynamic properties as the biological system. The last step can involve reproducing the temporal evolution of the pattern and the patterns under different experimental perturbations. Testing whether these three criteria are met for a given biological pattern is an intermediate level of abstraction. This intermediate level of abstraction captures the high-level topology of a complicated system of interactions despite incomplete understanding of how the interactions are mediated through specific chemical (or the types of) reactions. This abstraction can be thought of as the mapping of a high dimensional biochemical network, that can only be understood on a genomic scale, to a low dimensional space described by effective activities and effective interactions within the framework of current theories of pattern formation.

A growing number of patterns in biology have been shown to satisfy at least one but not all of the three criteria for lateral inhibition (Murray 2003; Meinhardt 2009). Below I will discuss how this intermediate level of abstraction has been applied to three example patterns.

Lateral inhibition underlies the establishment of the right-left asymmetry in early bilaterian embryos. Nodal and Lefty are members of the transforming growth factor-b (TGF-b) family of proteins. In mouse embryos, the patch of Nodal localization on the left half of the embryo is surrounded by a ring of Lefty. Nodal binds the receptor Alk4 and EGF-CFC coreceptors to promote mesendoderm induction (Gu et al. 1998). This process determines the left side. Nodal promotes the production of itself and Lefty (Chen and Schier 2002; Hamada, Meno, et al. 2002). Lefty inhibits Nodal signaling through sequestration and advantage in competitive binding. Fluorescence recovery after photo-bleaching showed that Lefty diffuses 14 times faster than Nodal (Müller et al. 2012). These molecular interactions and additional simulations (Nakamura et al. 2006) show that right-left asymmetry arises from the interaction of slowly diffusing Nodal as the activator and fast diffusing Lefty as the inhibitor.

Lateral inhibition also underlies digit patterning during vertebrate limb development. Digits

develop from small dots of prechondrogenic condensations underneath the distal tip of the growing limb bud (Zhu et al. 2008). Mesenchymal condensation is driven by the transcription factor SOX9 (Akiyama et al. 2002; Sheth et al. 2012). The small dots of SOX9 are hypothesized to form through lateral inhibition with SOX9 as the activator. The inhibitors of SOX9 are identified through two genetic screens. Microarray analysis identified major developmental signaling pathways regulated by SOX9. Wholemount in situ hybridization identified the pathways with expression patterns out of phase with SOX9. The screens identified BMP and WNT as the inhibitor of SOX9 (Raspopovic et al. 2014). It is unclear how the three signaling pathways interact with each other at the molecular level and whether the spatial range of the SOX9 is much smaller than that of BMP and WNT. A three component reaction diffusion model with SOX9 as the activator and Wnt and Bmp as the inhibitor reproduced the temporal evolution of digit growth. The model reproduced the loss of digits when Bmp is inhibited and the loss of interdigits when Wnt is inhibited. The same model reproduced the skeletal patterning of the catshark (Onimaru et al. 2016).

Lateral inhibition underlies the formation of stripes in zebrafish skin. Stripes in zebrafish skin are made up of alternating rows of melanophores (black) and xanthophores (yellow). The possibility of prepatterning is excluded by laser ablating a small part of the stripe pattern and comparing the pattern regeneration process and predictions of Turing models (Yamaguchi et al. 2007). Temporal evolution of the pattern is consistent with model prediction. More direct evidence against prepatterning comes from the observation that the regenerated stripes have the same width but different orientation. The interaction of melanophores and xanthophores is best demonstrated in primary cell cultures where cells can migrate freely (Inaba et al. 2012). Upon contact with the dendrites of xanthophores, melanophores membrane transiently depolarizes. Depolarization triggers melanophores to migrate to avoid contact with xanthophores. In real skin tissue, the segregation is driven by melanophore migration and death in the xanthophore territory (Yamanaka and Kondo 2014). This dendrite mediated segregation operates in the short range to ensure that the boundary between black and yellow stripes are not blurred. Melanophores extend long projections to promote the survival of xanthophores through Delta/Notch signaling (Hamada, Watanabe, et al. 2014). The width of stripes is modulated by the strength of Delta/Notch signaling. In summary, short dendrites mediate short-range mutual inhibition,

while long projections mediate long-range positive feedback.

Lateral inhibition are also proposed to underlie the spontaneous emergence of localized regions of Cdc-42 activity in budding yeast (Goryachev and Pokhilko 2008), the generation of evenly spaced dots on skin tissues to prepattern skin appendages such as hair follicles (Sick et al. 2006; Klika et al. 2012; Glover et al. 2017) and feathers (Jung et al. 1998; Mou et al. 2011; Painter et al. 2012), and the selection of branching points during lung development (Menshykau et al. 2012).

1.3.4 Trigger waves enable rapid long-range spatial coordination

Propagation of trigger waves involves two steps. First, spatial coupling mechanisms, such as diffusion, drive the system in neighboring regions above the threshold. Second, local reactions in the neighboring regions drive the transition from low levels of activity to high levels of activity. Trigger waves excel at transmitting information rapidly and over long distances without damping. These properties are utilized by many cells to transmit cellular signals.

Trigger waves are categorized by their local reaction dynamics, such as excitable or bistable, or by the type of molecules that mediate wave propagation, such as chemical or electrical. I will discuss three examples of trigger waves: excitable electrical trigger waves, excitable chemical trigger waves, and bistable chemical trigger waves. I will focus on feedback mechanisms and wave propagation mechanisms.

Action potentials traveling along axons is a classic example of excitable electrical trigger waves (Hodgkin and Huxley 1952). The positive and delayed negative are mediated by voltage sensitive sodium channels and potassium channels in the plasma membrane respectively. Membrane depolarization first opens sodium channels which further depolarizes the membrane to generate the upswing of the action potential. Suprathreshold depolarization opens the potassium channels to return the membrane potential to the rest state (Goldman and Schauf 1972; Hille 1976; Aldrich, Corey, et al. 1983; Aldrich and Stevens 1987). The spatial coupling mechanism is passive spread of charged ions which depolarizes the membrane and triggers sodium channel opening in neighboring regions. The rapid opening of ion channels and ion flows allows action potential to travel as fast as 200 meters per second (Kress et al. 2008; Kusano 1966).

Chemical trigger waves include calcium waves and mitotic waves, which are excitable and bistable respectively. In the *Xenopus* laevis egg/zygote, calcium waves (Hara et al. 1980; Busa and Nuccitelli 1985) and mitotic waves (Hara 1971; Hara et al. 1980; Rankin and Kirschner 1997; Pérez-Mongiovi et al. 1998) propagate through the cytoplasm like a wave. The rapidly spreading high levels of intracellular calcium reduces the probability of refertilization by a second sperm. The rapidly spreading mitotic entry ensures that the mitotic apparatus is well coordinated for successful cell divisions. Diffusion of the activator acts as the spatial coupling mechanism in both calcium waves and mitotic waves. For calcium waves, the activator is calcium ion. The positive feedback involves cytoplasmic calcium signaling to allow flow of calcium from calcium-filled endoplasmic to the cytoplasm. The negative feedback is driven by calcium pumps that transport calcium from cytoplasm back to endoplasmic. For mitotic waves, the activator is the master regulator of mitosis, active cyclin B–Cdk1. The underlying circuit for bistable active cyclin B–Cdk1 dynamics includes a fast positive feedback through the activator of Cdk1, a fast double-negative feedback through the inhibitor of Cdk1 (Pomerening et al. 2003; Sha et al. 2003) and a slow negative feedback through a complex that promotes the degradation of cyclin B (Yang and Ferrell 2013).

The combination of modern imaging and clever experimental manipulations made it possible to test whether the propagation of mitotic waves depends on diffusion of chemicals between neighboring regions. In the experiment, *Xenopus* egg extract is sealed in Teflon tubes suspended in oil. When the tube is cut into two segments, the oil creates a diffusion barrier between the two segments. Compared to the intact tube, mitotic waves are no longer coordinated (Chang and Ferrell Jr 2013). This experiment eliminates the possibility that the observed waves are phase shifted independent local oscillations.

Calcium waves and mitotic waves are used to transmit information in other large cells. Calcium waves in cultured hippocampal astrocytes (Cornell-Bell et al. 1990) modulate exocytosis of neurotransmitters (Bezzi et al. 2004). In response to salt stress, *Arabidopsis thaliana* roots generate calcium waves through the entire plant to elicit a systemic molecular response (Choi et al. 2014). Mitotic waves in the syncytial *Drosophila* embryo begin at the two poles and propagate towards the middle of the embryo (Foe and Alberts 1983). Some mulitnucleate fungi

also exhibit mitotic waves (Clutterbuck 1970).

1.3.5 Traveling waves of actin assembly underlie cell migration

Traveling waves of actin assembly drives the extension of protrusions during cell migration. Cell migration is essential for many important biology processes, for example, wound healing (Dekoninck and Blanpain 2019), cancer invasion (Friedl and Wolf 2003) and neural crest formation (Bronner 2012). Cells migrate by cycles of extending membrane rich protrusions at the leading edge, attachment to the substrate and back retraction through myosin driven contraction. The arrival of traveling waves of actin assembly precedes membrane expansion at the leading edge of many migrating cells (Vicker 2002; Asano et al. 2008; Bretschneider et al. 2009; Gerisch et al. 2004).

Traveling waves of actin assembly are observed in many migrating cell types. Examples include Dictyostelium (Vicker 2002; Arai et al. 2010; Huang et al. 2013), fish keratocytes (Barnhart et al. 2017), neutrophils (Weiner et al. 2007; Yang, Collins, et al. 2016), lymphocytes and macrophages (Lam Hui et al. 2014), breast cancer cells (Marchesin et al. 2015), U2OS cells (Baird et al. 2017; Graessl et al. 2017) and mast cells (Wu, Wu, et al. 2013; Xiong et al. 2016).

A number of different models have been proposed to explain the generation and propagation of actin waves. The first involves the intrinsic assembly dynamics of actin itself, while the other three involve dynamic interactions between actin filaments and regulators of actin assembly and disassembly.

Treadmilling of actin filaments could generate actin waves. Treadmilling refers to the process of simultaneous assembly at the barbed end and disassembly at the pointed end, which can produce a traveling wave of polymerized actin. Bretschneider et al. showed that treadmilling underlies waves of dense actin filaments at the substrate-attached surface of Dictyostelium. This model is supported by the observation that the actin assembly factor myosin-IB is enriched at the membrane to keep the growing actin barbed end near the membrane, while the actin disassembly factor coronin is located far away from the membrane (Bretschneider et al. 2009).

Actin waves could also be driven by AI reaction diffusion models with diffusion of molecules

that promote actin assembly (activator) and delayed negative feedback from immobile actin filaments (inhibitor) (Ryan et al. 2012; Carlsson 2010; Doubrovinski and Kruse 2011). Actin waves on the ventral membrane of neutrophils are proposed to be driven by such models with Hem-1 being the activator (Weiner et al. 2007). The positive feedback mechanism is not clear. It could involve membrane bound Hem-1 recruiting more Hem-1 from the cytoplasm. The delayed negative feedback through F-actin is supported by the following observations. Hem-1 is part of the Scar/WAVE complex that stimulates actin assembly at the membrane. Actin filaments are also required to remove the Hem-1 from the membrane. The Rho superfamily of small GTPases could also act as the activator. I will discuss the underlying feedback mechanisms in the following section.

Amplification of membrane curvature could drive traveling waves of actin assembly (Wu, Su, et al. 2018). Proteins with BAR domains sense and bind curved membranes near protrusions (Gov and Gopinathan 2006; Shlomovitz and Gov 2007; Ryan et al. 2012; Kabaso et al. 2011; Peleg et al. 2011). Membrane bound BAR domain proteins recruit complexes, such as WASp and Scar/WAVE, to drive actin assembly (Takenawa and Suetsugu 2007). The assembled F-actin could push against the membrane to further increase membrane curvature near protrusions. This sequence of events could form a positive feedback to amplify membrane curvature, generating traveling waves of membrane expansion and actin assembly.

1.3.6 Traveling waves of small GTPase activity are ubiquitous

Traveling waves of the Rho superfamily and the Ras superfamily of small GTPases activation are observed in two types of cellular contexts. In migrating cells, traveling waves of small GTPase activation drive traveling waves of actin assembly, which underlies cell migration. The second type of waves resemble the predicted dynamics of AIRD models with faster diffusing activators where excitations propagate at constant speed indefinitely until waves from different regions collide and annihilate each other. Nurse cell dumping in *Drosophila* is the example of traveling waves of RhoA activation in wild-type cells (Imran Alsous et al. 2021). Other cases all involve artificially boosting the activation of small GTPases. RhoA waves in the eggs and early embryos of frogs and echinoderms require expression of constitutively active RhoA GEF (Bement et al. 2015; Bhattacharya et al. 2020). RhoA waves in cultured pig kidney epithelial cells (Murthy and

Wadsworth 2008) and U2OS cells (Baird et al. 2017; Graessl et al. 2017) require disassembly of microtubules that sequester RhoA GEF. RhoA waves in mouse embryos during compaction require destruction of adherens junctions that inhibit RhoA activation (Maître et al. 2015). cdc42 waves in cultured mast cells require binding of the synthetic multivalent antigen DNP-BSA (Wu, Wu, et al. 2013; Xiong et al. 2016). Ras waves in Dictyostelium require F-actin disassembly (Huang et al. 2013).

Small GTPases are enzymes that catalyze the hydrolysis of guanosine triphosphate (GTP) to guanosine diphosphate (GDP). They bind to and diffuse within cellular membranes, where they transition between inactive (GDP-bound) and active (GTP-bound) states. Their activation is governed by guanine nucleotide exchange factors (GEFs), while inactivation is governed by GTPase activating proteins (GAPs). Cdc42 waves in cultured mast cells involve actin-dependent positive-feedback mechanisms that are calcium independent and delayed negative feedback from F-actin (Wu, Wu, et al. 2013). Ras waves in Dictyostelium involve a positive feedback loop from PIP3 to Ras activity that is independent of cytoskeletal activities, while the negative feedback mechanism is unknown. I will focus on feedback mechanisms of RhoA.

Pulsatile dynamics of small GTPases activation are driven by a positive feedback in which active small GTPases are thought to recruit their GEFs and a delayed negative feedback through recruitment of their GAPs indirectly. RhoA and cdc42 both belong to the Rho superfamily. The accumulation or activation of RhoA GEFs is thought to provide the positive feedback that drives a rapid upswing in RhoA activity in activated frog and echinoderm eggs and embryos (Bement et al. 2015), in U2OS cells (Graessl et al. 2017), and in early *C.elegans* embryos (Nishikawa et al. 2017; Michaux et al. 2018). Stabilization of RhoA activity by its effector anillin (Budnar et al. 2019), or concentration of active RhoA by myosin-dependent contractions (Munjal et al. 2015), may also provide positive feedback in some cells. F-actin-dependent inhibition of RhoA provides delayed negative feedback that helps to terminate pulses of RhoA activity in frog and echinoderm embryos (Bement et al. 2015; Michaud, Leda, et al. 2022), in early *C.elegans* embryos (Michaux et al. 2018), and on secretory vesicles (Segal et al. 2018). In *C.elegans* embryos and secretory vesicles, this inhibition is mediated by F-actin-dependent recruitment of specific RhoA GAPs, while in frog and echinoderm embryos, the molecules that mediate

inhibition remain unknown.

The functional purpose of the small GTPases activation waves is not well understood in the context of non-migrating cells. Since they are not observed in wild-type cells, traveling waves are likely to be epiphenomenon with no biological function or evolutionary advantage. The feedback mechanisms responsible for generating traveling waves may exist for functional purposes in other developmental stages or for other cellular functions such as cytokinesis. It is possible that the biological systems with functional traveling waves remain to be discovered.

1.4 Pulsed actomyosin contractions underlie cell shape changes during morphogenesis

1.4.1 Overview

Actomyosin contractility is fundamental in eukaryotic cell biology. Cells utilize actomyosin contractility to implement many important functions (Zaidel-Bar et al. 2015) including cytokinesis, migration, vesicle trafficking, apoptosis and establishment and maintenance of cell polarity. Pulsed contraction refers to short pulses of actomyosin assembly, contraction and disassembly. Pulsed contractions are driven by pulsatile RhoA activation (Munjal et al. 2015; Zhang and Glotzer 2015; Graessl et al. 2017; Nishikawa et al. 2017; Michaux et al. 2018). The spatiotemporal patterns of pulsed contractions are largely dependent on the spatiotemporal patterns of RhoA activation serving as an upstream pacemaker.

Pulsatile RhoA activation could form traveling waves or focal pulses. Traveling waves of RhoA activation are described in the last section. Focal pulses of RhoA activation occur in small patches, persist for a limited amount of time and eventually disappear. Focal pulses of RhoA activation in the *C.elegans* zygote occur during polarity establishment (Nishikawa et al. 2017; Michaux et al. 2018). It is the only cell type where many focal pulses (¿6) coexist in the same cell. So the *C.elegans* zygote is a great model system to study questions such as what determines the size of focal pulses and the spacing between them. Other examples of pulsed contractions include repair of tight junction leaks in polarized epithelium of *Xenopus* (Reyes et al. 2014; Stephenson et al. 2019) and tissue invagination and elongation in the *Drosophila* epithelia (Miao

and Blankenship 2020).

1.4.2 Pulsed contractions underlie apical constrictions during ventral furrow invagination and dorsal closure

Pulses of actomyosin contractions constrict the apical surface during gastrulation and dorsal closure (Franke et al. 2005; Jacinto et al. 2002). Apical constrictions in the presumptive mesoderm drive ventral furrow invagination to initiate gastrulation. Apical constrictions in amnioserosa cells contribute to dorsal closure. Each pulsed contraction reduces the area of the apical surface by a small amount. If the constricted cell shape is not stabilized, the apical surface could return to its original size, generating cell shape fluctuations (Figure 1.2 left) instead of stepwise shrinkage of the apical surface (Figure 1.2 right). So it is important to stabilize the constricted apical surface.

Pulsed contractions in the presumptive mesoderm and amnioserosa are stabilized with different mechanisms. In mesoderm cells, the constricted cell shape is maintained between pulses, similar to a ratchet (Martin, Kaschube, et al. 2009). Cell shape maintenance requires persistent actomyosin filaments across the apical domain. The recruitment and/or stabilization of myosin require medioapical localization of Rho Kinase driven by the transcription factor twist (Mason et al. 2013). Stabilization of the constricted apical surface in amnioserosa requires actomyosin cable that surrounds the amnioserosa tissue. Contractions from the surrounding actomyosin cable counteracts forces that would expand the apical domain after a pulse. One supporting observation is that amnioserosa exhibits continual pulsing without stepwise apical constriction when the sounding cable is disrupted. Also, persistent constriction amnioserosa starts at the periphery of the amnioserosa tissue and gradually moves inwards (Solon et al. 2009; Sokolow et al. 2012).

1.4.3 Pulsed contractions underlie junction shortening during convergent extension

Pulsatile contractions are harnessed to drive morphogenetic movements during convergent extension. Convergent extension involves the convergence of cells along one tissue axis which

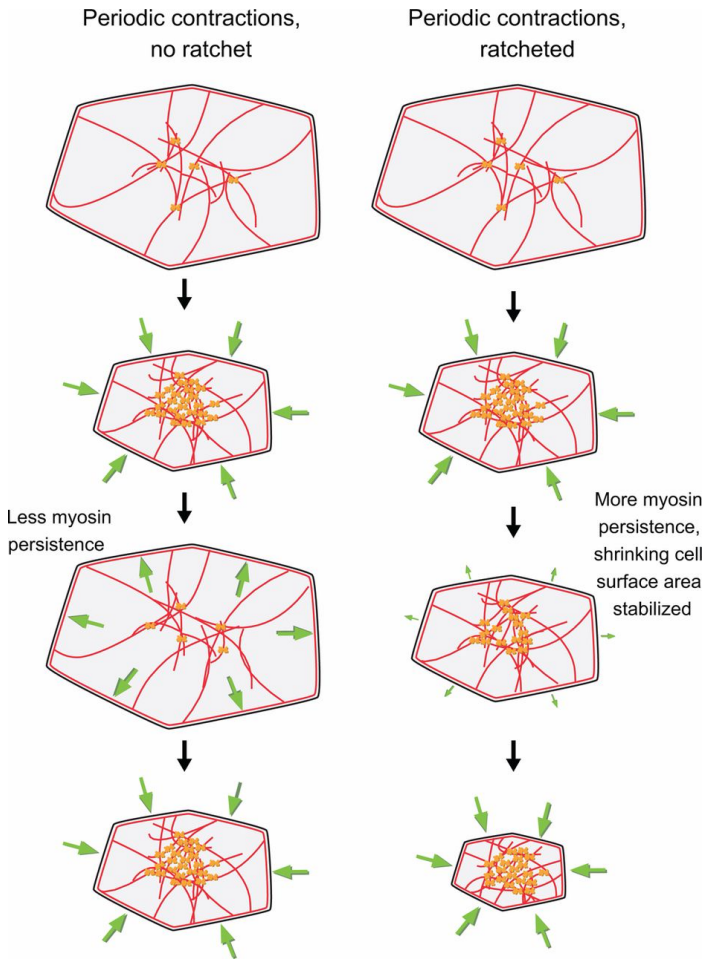

Figure 1.2. Evidence for actin-myosin-dependent ratcheting of pulsed contractions. From Martin and Goldstein 2014. Pulsed contractions can occur without stabilization of the constricted apical surface area between pulses, resulting in cell shape fluctuations (left). These unratcheted constrictions have been observed in Drosophila amnioserosa cells before the onset of dorsal closure and in Drosophila presumptive mesoderm cells mutant for twist. Alternatively, decreases in apical surface area that result from contractile pulses can be stabilized, resulting in what sometimes resembles an incremental or ratchet-like decrease in apical area (right). This behavior is observed for wild-type presumptive mesoderm cells during Drosophila gastrulation and in amnioserosa cells during dorsal closure. In both these cases, both myosin and F-actin persist to a greater degree between pulses (right), which possibly prevents relaxation, resulting in a net reduction in apical surface area. Green arrows indicate shrinkage or expansion of apical domains.

drives simultaneous extension along another perpendicular axis (Shindo 2018). Convergent extension is driven by asymmetric shortening and rearrangement of cell-cell junctions in the *Drosophila* germband, *Xenopus* kidney tube and chick neural tube. At the cellular level, junctions shrink to a singular point along one axis (vertical) and then new junctions form and expand along the orthogonal axis (horizontal) (Bertet et al. 2004; Blankenship et al. 2006; Shindo and Wallingford 2014; Nishimura et al. 2012).

One cycle of junction shortening takes three steps: actomyosin assembly at medial surfaces, contract to generate flow towards junctions, and finally contraction at the flow destination junction to reduce junction length. Medial actomyosin foci connect to junctions through E-Cadherin anchorage. Connections with weaker E-Cadherin anchorage are more likely to break. So medial actomyosin foci flow towards the junction with strong E-Cadherin anchorage (Levayer and Lecuit 2013).

Each cycle of pulsed contraction reduces the junction length by a small amount. The shortened junction needs to be stabilized to to incrementally reduce junction length. I will discuss three mechanisms to stabilize shortened junctions after each pulsed contraction.

Remodeling of the medial actomyosin network could stabilize shorten junctions. Clement et al. used optical tweezers to apply time-controlled forces on junctions in the germband epithelia right before the onset of convergent extension (Clément et al. 2017). Three observations are consistent with the proposed mechanism. Pulses with longer durations are more likely to be irreversible. The transition to irreversible pulses occurs when the pulse duration is on the same time scale as the turnover rate of actomyosin network. Inhibiting actin turnover yields more reversible contractile events. Cavanaugh et al. used optogenetics to generate pulses of contractions with different durations in a stable model epithelia that naturally exhibit very little contractility and confirmed the correlation between longer pulse duration and more irreversible junction shortening (Cavanaugh et al. 2020).

Tricellular vertices sliding could also shorten vertical junctions. At cell junctions, tricellular vertices containing myosin and E-cadherin slide when contractile medial forces from neighboring cells are asymmetric. Vertical junctions shorten when tricellular vertices move toward the contracting cell. At the molecular level, flow driven myosin accumulation consolidates E-

cadherin at the end of vertice sliding. Formation of the new tricellular vertices makes this process irreversible (Curran et al. 2017; Vanderleest et al. 2018).

Endocytosis of the plasma membrane is a general mechanism to stabilize pulsatile shape changes. At the end of each cycle of contraction, the membrane tension reaches its minimum. Internalization of the excess membrane then prevents relaxation to the original surface area or junction length. This mechanism operates during convergent extension (Levayer, Pelissier-Monier, et al. 2011; Jewett et al. 2017) and ventral furrow invagination (Lee and Harland 2010; Sumi et al. 2018; Miao, Vanderleest, et al. 2019).

1.4.4 Pulsed contractions could be more efficient than continuous contractions

One fundamental question is why some cells use multiple short pulses instead of a single long contraction with the same strength continuously? One possibility is that multiple short pulses make it easier to coordinate contractions across the epithelia to avoid catastrophic tearings. Precise control of the duration of pulsed contraction showed that multiple short contractions could overcome the saturation of a single long contraction (Cavanaugh et al. 2020). For relatively short contractions, junctional shortening is proportional to the duration of contraction. Once the duration of contraction is above a threshold, increasing the duration generates minimal junction shortening. Thus, in the context of junction shortening, structuring a single long contraction into multiple short pulses improves the efficiency of contractions. It is likely that the same rule also applies for apical constrictions.

1.5 Contraction driven flows provide additional pattern formation mechanisms

1.5.1 Contractile flows alone could drive pattern formation

Besides diffusion, contractile driven flows could also mediate spatial coupling during pattern formation. Myosin contraction is the major source of mechanical stress. Flows in the actomyosin network occur when mechanical stress is not balanced (Bray and White 1988). Pattern formation could involve flows alone or coupled to diffusion.

Contractions alone are sufficient to generate a single, stable peak of high myosin concentration in one dimension (Bois et al. 2011). The minimal model with contractile flows involves a single contractile agent, myosin, with simple exchange kinetics. This model introduced the idea of modeling the actomyosin network as a viscous contractile gel (active fluid) with a thin-film geometry. This system drives pattern formation through a positive feedback that amplifies stochastic fluctuations. The amplification process involves regions with higher levels of myosin driving flows that transport myosin from regions with lower levels of myosin towards regions with higher levels of myosin. This convergent flow provides both the short range activation and long range inhibition that underlies the formation of Turing patterns.

This minimal model is hypothesized to underlie two biological patterns. The first pattern is regularly spaced supracellular actin rings in the *Drosophila* tracheal tubule (Hannezo et al. 2015). The authors first confirmed that contractility is required for pattern formation. Both the model and experiments show that the spacing of the supracellular rings is determined by physical properties of the actomyosin network, such as contractility and turnover.

The second pattern is the trajectory of the cytokinetic ring in post-mitotic Ciona notochord cells (Sehring et al. 2015). Normally, the ring assembles at the anterior and migrates to the center. The initial anterior localization is due to polarized actin assembly factors. The migration is driven by myosin contractility that transports the assembled actomyosin network to the cell center. This behavior is reproduced using a model based on the Bois2011 model with asymmetric boundary conditions.

Two mechanisms have been proposed to generate pulsatile patterns. One involves stress dependent breakdown of the actomyosin network (Moore et al. 2014). The other involves the combination of active stress up-regulator(myosin) and down-regulator that diffuses or exchanges slower (Kumar et al. 2014). Both stress dependent breakdown and slow down-regulator serve as the inhibitor to generate locally alternating convergent and divergent flows.

1.5.2 Mechanochemical coupling

Modeling the coupling between reaction diffusion processes and contractile flows is a relatively new field of research. Staddon et al. showed that coupling an excitable circuit with contractile

flows expanded the variety of spatiotemporal patterns compared to excitable reaction diffusion systems alone (Staddon et al. 2021). Since both processes can generate patterns independently, it is not surprising that coupling them together generates more complex spatiotemporal dynamics. If neither model drives pattern formation independently, could the coupled model drive pattern formation? The answer is yes when using a two component mutual inhibition model for the reaction kinetics (Copos and Mogilner 2020). Here, local linear coupling relaxed the nonlinear reaction kinetics requirement for pattern formation. Since nonlinearity often involves feedback mechanisms, mechanochemical coupling could provide additional feedback for pattern formation.

1.6 About this project

In my thesis work, I focused on the dynamics of pulsatile RhoA activation in the one-cell *C.elegans* embryo (or zygote). Here, pulsed contractions occur during polarity establishment (Munro et al. 2004). Previous studies considered two models to explain pulsatile actomyosin dynamics: contractile flow driven pattern formation (Bois et al. 2011) and activator inhibitor reaction model. The first model is rejected based on two key observations (Nishikawa et al. 2017; Michaux et al. 2018). Pulsatile RhoA activation precedes actomyosin pulses. Contractions are not required to generate pulsatile activation of RhoA.

Michaux et al. identified the excitable reaction model underlying pulsatile activation of RhoA. In the model, active RhoA is the activator and F-actin is the inhibitor (Michaux et al. 2018). The positive feedback involves active RhoA itself, while the negative feedback is mediated by F-actin–dependent recruitment of the RhoA GTPase-activating proteins RGA-3/4 (Michaux et al. 2018). This circuit generates focal pulses of RhoA activation in the *C.elegans* zygote (Michaux et al. 2018) (Figure 1.3 B) but generates traveling waves of RhoA activation in frog and starfish cells (Bement et al. 2015; Michaud, Leda, et al. 2022) (Figure 1.3 A), which is the predicted pattern for activator inhibitor systems with faster diffusing activator. This pattern variation could come from different actomyosin dynamics because the spatiotemporal patterns of RhoA inhibition is determined by F-actin levels. However, it is challenging to determine the origins of pattern variation across different cell types. I use the one-cell *C.elegans* embryo as a model system to ask: is it possible to reproduce the pattern variants observed across different

cell types in a single cell by modulating actomyosin dynamics downstream of RhoA?

Here I combine microscopy with quantitative image analysis to characterize the spatiotemporal dynamics of pulsatile RhoA activation in one-cell *C.elegans* embryos. I find that perturbing two RhoA effectors—formin and anillin—induce transitions from nonrecurrent focal pulses to either large noisy oscillatory pulses (formin depletion) or noisy oscillatory waves (anillin depletion). In both cases, the resulting RhoA activation patterns can be explained by the patterns of F-actin depletion. However, their underlying F-actin depletion mechanisms have different dependencies on myosin II activity. These results provide new insight into how the modulation of actomyosin network assembly and contractility could shape pulsatile RhoA dynamics to achieve different physiological or morphogenetic outcomes.

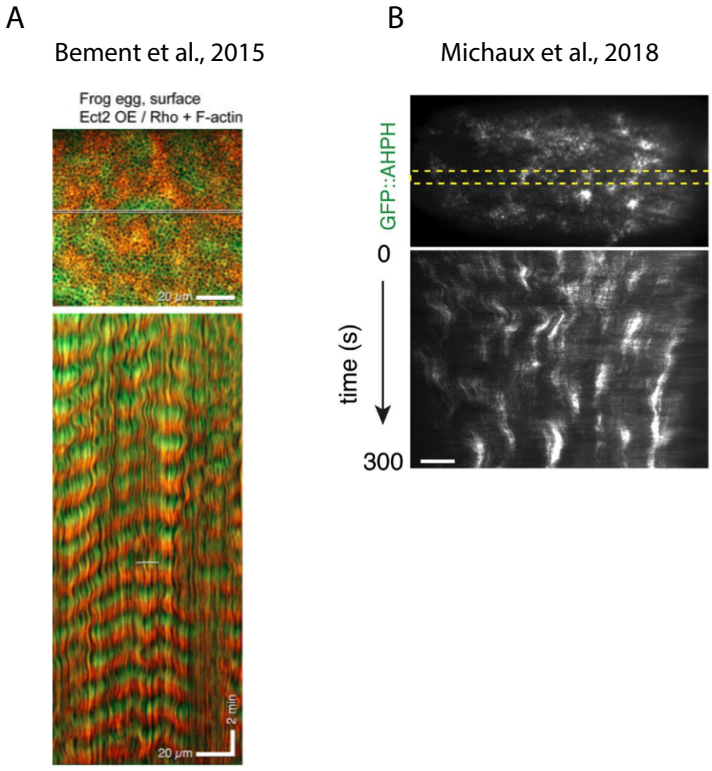

Figure 1.3. The same underlying circuit can generate both traveling waves and focal pulses. (A) Traveling waves of RhoA activation in frog egg. Green indcates active RhoA, reported by AHPH. Red indicates F-actin. (B) Focal pulses of RhoA activation in *C.elegans*. Active RhoA level is reported by AHPH. Yellow line indicates the stripe for kymograph construction.

CHAPTER 2

MODULATING RHOA EFFECTORS INDUCES TRANSITIONS TO OSCILLATORY AND MORE WAVELIKE RHOA DYNAMICS IN *CAENORHABDITIS ELEGANS* ZYGOTES

Status of the work: Published in MBOC https://www.molbiolcell.org/doi/abs/10.1091/mbc.E21-11-0542

Statement of contribution: I carried out all of the experiments, data analysis, and simulations in this project, except that Seth Donoughe give advice on data analysis and presentation.

2.1 Introduction

Pulsatile dynamics underlie the physiological control of many different cellular behaviors including gene expression (Levine, Lin, et al. 2013) hormone secretion (Brabant et al. 1992), neural and cardiac activity (DiFrancesco 1993; Clay 2005), cell migration (Arai et al. 2010; Huang et al. 2013), and tissue morphogenesis (Gorfinkiel et al. 2009; Solon et al. 2009; Rauzi et al. 2010; Maître et al. 2015; Sutherland and Lesko 2020). The circuits that produce pulsatile dynamics are composed of different molecules, but they share a common architecture in which fast positive feedback drives an initial upswing in activity, and delayed negative feedback returns activity back toward basal levels (Meron 1992). The pulses observed in different functional contexts vary widely in amplitude, duration, frequency, temporal regularity, and whether/how they propagate through space. How pulsatile dynamics arise in specific circuits and how they can be tuned to achieve different physiological outcomes remain poorly understood.

Here we focus on pulsatile dynamics of the small GTPase RhoA, which underlie intracellular remodeling, cell movement, shape change and division, epithelial tissue repair, and multicellular tissue morphogenesis (Ridley 2015; Blanchard et al. 2018; Sutherland and Lesko 2020; Michaud, Swider, et al. 2021). Like other Rho family GTPases, RhoA binds to and diffuses within cellular membranes, where it transitions between inactive (GDP-bound) and active (GTPbound) states. RhoA activation is governed by guanine nucleotide exchange factors (GEFs), while inactivation

is governed by GTPase activating proteins (GAPs). The active form of RhoA binds to various downstream effectors, including formins, Rho kinase (ROK), and anillins, to control the assembly and contraction of cortical actomyosin networks.

Recent work has begun to identify the molecular mechanisms that govern positive and negative feedback on RhoA activity to produce pulsatile dynamics in different cell types. RhoA-dependent accumulation or activation of RhoA GEFs is thought to provide the positive feedback that drives a rapid upswing in RhoA activity in activated frog and echinoderm eggs and embryos (Bement et al. 2015), in U2OS cells (Graessl et al. 2017), and in early *Caenorhabditis elegans* embryos (Nishikawa et al. 2017; Michaux et al. 2018). Stabilization of RhoA activity by its effector anillin (Budnar et al. 2019), or concentration of active RhoA by myosin-dependent contractions (Munjal et al. 2015), may also provide positive feedback in some cells. F–actin-dependent inhibition of RhoA provides delayed negative feedback that helps to terminate pulses of RhoA activity in frog and echinoderm embryos (Bement et al. 2015), in early *C. elegans* embryos (Michaux et al. 2018), and on secretory vesicles (Segal et al. 2018). In *C. elegans* embryos and secretory vesicles, this inhibition is mediated by F–actin-dependent recruitment of specific RhoA GAPs, while in frog and echinoderm embryos, the molecules that mediate inhibition remain unknown. Overall, these studies suggest a potentially important role for actomyosin networks in shaping pulsatile RhoA dynamics. The spatiotemporal patterns of pulsatile RhoA activity observed in different cells or tissues vary in terms of how pulses recur in time and whether/how they propagate through space. However, they can be classified into two main types: focal pulses, with variable frequency and regularity of recurrence and limited propagation, and oscillatory waves, which recur at regular intervals and propagate over longer distances. Focal pulses have been observed in cultured cells (Baird et al. 2017; Graessl et al. 2017), in early *C. elegans* embryos (Roh-Johnson et al. 2012; Nishikawa et al. 2017; Michaux et al. 2018, Drosophila embryos and egg chambers (Gorfinkiel et al. 2009; Rauzi et al. 2010; Azevedo et al. 2011), and at cell contacts in epithelial tissues (Reyes et al. 2014; Stephenson et al. 2019). Oscillatory waves have been observed in the eggs and early embryos of frogs and echinoderms (Bement et al. 2015; Bhattacharya et al. 2020), in mouse embryos during compaction (Maître et al. 2015), and in tissue culture cells subjected to experimental perturbations (Murthy and Wadsworth 2008; Xiong et al. 2016; Michaud, Swider, et al. 2021). With one exception (Graessl et al. 2017), focal

pulses and oscillatory waves have not been observed in the same cells. Interestingly, artificial cortices prepared using extracts of frog egg cytoplasm can produce both locally oscillatory patches and single traveling waves of RhoA activity, suggesting the potential for a broader range of tunable variation in this system (Landino et al. 2021). In general, the mechanistic basis for observed variations in pulsatile RhoA dynamics remains unknown. Reaction diffusion models provide a useful framework for understanding how such variation could arise in simple activator/inhibitor systems (Allard and Mogilner 2013). Depending on the relative strengths and timing of positive and negative feedback, the same circuit can exhibit excitable dynamics, in which a local perturbation, whose amplitude exceeds some threshold, is required to drive the system away from a stable rest state to induce a single pulse of activity, followed by a return to the rest state, or oscillatory dynamics, in which pulses recur with a fixed frequency in the absence of external perturbations (Strogatz 2019). Similarly, the same circuit can generate focal pulses (also known as standing pulses) when the inhibitor diffuses faster than the activator (Hecht et al. 2010), or traveling pulses, when the activator diffuses faster than the inhibitor (Koga and Kuramoto 1980; Ermentrout et al. 1984; Klaasen and Troy 1984; Dockery and Keener 1989). Thus in principle, the range of variation in RhoA pulse dynamics observed in different contexts could be explained by differences in the relative strength/timing of activation and inhibition and/or the relative mobilities of activators and inhibitors.

However, efforts to use such simple models to explain pulsatile RhoA dynamics observed *in vivo* highlight a basic puzzle: echinoderm, frog, and nematode cells appear to use the same basic circuit architecture combining fast autoactivation of RhoA with delayed negative feedback via local F-actin assembly (Figure 2.1 A). Simple reaction diffusion models, treating RhoA as a fast-diffusing activator and F-actin (and associated GAPs) as a slow-diffusing inhibitor, recapitulate the oscillatory waves of RhoA activity observed in frog and echinoderm cells (Bement et al. 2015) but not the focal pulses observed in nematodes. Thus the focal pulses observed in nematodes must involve additional forms of feedback and/or through different mechanisms of coupling RhoA activity to the dynamics of actomyosin assembly and contractility. However, incomplete knowledge of circuit components, difficulties in measuring the strength and timing of positive and negative feedback, and differences in actomyosin network architecture and assembly dynamics make it challenging to determine the origins of pattern variation by comparisons

across different cell types. Here we take an alternative approach, using the one-cell *C. elegans* embryo as a model system to ask: is it possible to reproduce the pattern variants observed across different cell types in a single cell by modulating actomyosin dynamics downstream of RhoA? We perturbed proteins that regulate actomyosin architecture, assembly dynamics, and contractility; developed new computational tools to quantify the local recurrence and spread of RhoA activity; and looked for perturbations that induce shifts from excitable to oscillatory dynamics and from focal to traveling pulses. We identified perturbations to two different RhoA effectors-formin and anillin-that induce an apparent shift from excitable to oscillatory dynamics. Both conditions also induce increased spread of RhoA activity but with qualitatively different spatial patterns: formin depletion produces larger, but still spatially delimited, focal pulses, Anillin depletion produces a noisy version of the oscillatory waves observed in other systems, in which pulses spread locally and continuously, frequently merging and splitting, to explore large regions of the cell cortex. For both perturbations, the increase in local recurrence and the spread of pulsatile RhoA activity are accompanied by a decrease in overall F-actin levels and enhanced local F-actin depletion that is tightly synchronized with local pulse initiation. However, the transition to large recurrent focal pulses produced by inhibiting formin requires actomyosin contractility and is associated with local contractile instabilities, while the transition to noisy oscillatory waves produced by anillin depletion is independent of contractility. These results provide new insight into how the modulation of actomyosin network assembly and contractility could shape pulsatile RhoA dynamics to achieve different physiological or morphogenetic outcomes.

2.2 Results

2.2.1 Modulating actomyosin dynamics can induce shifts in both spatial and temporal pulse dynamics

During polarization of *C. elegans* zygotes, focal pulses of RhoA activity and actomyosin contractility are superimposed on long-range cortical flows, which are induced by a posterior centrosomal cue (Cowan and Hyman 2004; Munro et al. 2004; Mayer et al. 2010). These flows progressively segregate actomyosin, polarity factors, and RhoA activity toward the future anterior pole (Munro et al. 2004; Motegi and Sugimoto 2006; Dickinson et al. 2017; Rodriguez

et al. 2017); thus they introduce an additional level of spatial and temporal variation in RhoA pulse dynamics. To focus on local changes in pulse dynamics without the confounding effects of longrange flows (Nishikawa et al. 2017), we perturbed actomyosin dynamics in embryos depleted of the centrosomal scaffold protein SPD-5 (Hamill et al. 2002), which lack functional centrosomes.

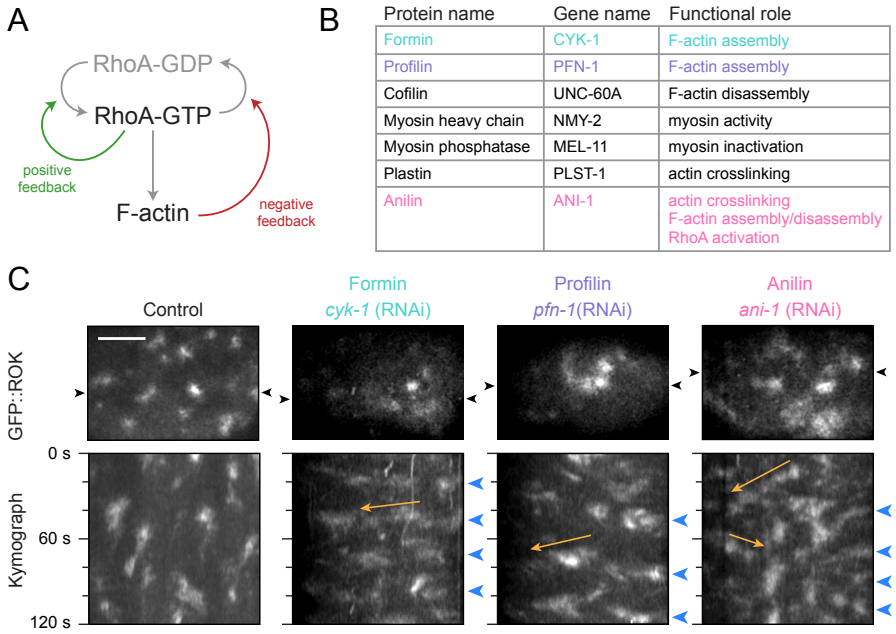

Figure 2.1. Modulating actomyosin dynamics generates qualitatively distinct patterns of RhoA activation. (A) Schematic representation of the molecular circuit for RhoA pulse dynamics. (B) Regulators of actomyosin dynamics that were perturbed in this study. (C) Single frames (top) and kymographs (bottom) showing patterns of ROK distribution in control, *cyk-1(RNAi)*, and *ani-1(RNAi)* embryos. Fluorescence intensity is scaled differently across phenotypes to highlight variations in ROK distribution. Black arrowheads indicate the vertical position where the kymograph is generated. Blue arrowheads indicate recurrence of ROK accumulation at regular intervals. Orange lines and arrows indicate diagonally oriented streaks. Scale bar is 10 μm.

We began by looking for perturbations to cortical actin assembly, disassembly, architecture, and contractility that induce changes in the frequency and regularity of local excitation or in the spatial spread of excitation (Figure 2.1B). We used endogenously tagged ROK (GFP::LET-502, hereafter GFP::ROK) as a reporter for RhoA activity (Piekny, Johnson, et al. 2003; Maddox, Lewellyn, et al. 2007; Bell et al. 2020). We reduced F-actin assembly by depleting formin/CYK-1 or its cofactor profilin/PFN-1 (Neidt, Skau, et al. 2008; Neidt, Scott, et al. 2009), and we reduced F-actin disassembly by depleting cofilin/UNC-60A (Ono et al. 2003). We used a temperature-sensitive mutation in the nonmuscle myosin II heavy chain NMY-2 [*nmy-2(ts)*; (Liu et al. 2010)] to sample reduced contractility and we enhanced contractility by depleting the myosin phosphatase/MEL-11 (Piekny, Johnson, et al. 2003). We used embryos mutant for the cross-linker plastin/PLST-1 [*plst-1(tm2455)*] to sample reduced network connectivity (Ding

et al. 2017). We also depleted the scaffolding protein anillin/ANI-1 (Maddox, Habermann, et al. 2005; Maddox, Lewellyn, et al. 2007; Piekny and Glotzer 2008; Tse et al. 2011, which cross-links actin filaments and is also reported to affect actin turnover (Tian et al. 2015), myosin dynamics (Pacquelet et al. 2015), and RhoA activity (Budnar et al. 2019).

We used time-lapse analysis and kymography to assess qualitative changes in pulsatile RhoA dynamics in response to these different perturbations (Figure 2.1C; Supplemental Figure S1, A and B; Supplemental Movies S1–S3; see Methods). We observed three general classes of spatiotemporal patterns. First, in control embryos, GFP::ROK appeared as small transient focal pulses with no obvious pattern of recurrence (Figure 2.1C), as previously observed with a different RhoA biosensor (Michaux et al. 2018). The general pattern of nonrecurrent focal pulses was also observed in embryos with reduced or enhanced contractility [*nmy-2(ts)* and *mel-11(RNAi)*, respectively], or in embryos with reduced cross-linking by PLST-1 [*plst-1(tm2455)*] (Supplemental Figure S1A; Supplemental Movie S2). Second, cofilin depletion induced a higher density of focal pulses, and these recurred with higher frequency, producing long vertical streaks of GFP::ROK with fluctuating intensities in kymographs (Supplemental Figure S1B; Supplemental Movie S3). Finally, three perturbations [*ani-1(RNAi)*, *cyk-1(RNAi)* and weak *pfn1(RNAi)*] induced shifts toward higher frequency, more regular recurrence, and larger domains of RhoA activity, consistent with a shift toward oscillatory dynamics and increased spread of RhoA activity (Figure 2.1C). In *ani-1(RNAi)* embryos, pulses of GFP::ROK accumulation often appeared to propagate locally at approximately constant speeds; this could be readily seen in time-lapse movies (Supplemental Movie S1) and as diagonal streaks of GFP::ROK in kymographs (orange arrows in Figure 2.1C). In *cyk1(RNAi)* or *pfn-1(RNAi)* embryos, pulsed accumulations of GFP::ROK are synchronized across larger regions producing wide, nearly horizontal streaks in kymographs (orange arrows in Figure 2.1C). In summary, multiple ways of perturbing actomyosin dynamics lead to increased frequency and regularity and greater spread of RhoA excitation, consistent with a shift toward oscillatory and wavelike RhoA dynamics. We therefore focused on analyzing the differences in spatiotemporal dynamics produced by these perturbations.

2.2.2 A computational pipeline to identify regions undergoing RhoA excitation

To quantify and compare spatiotemporal patterns of RhoA activity across different perturbations, we developed computational methods to automate the detection of regions undergoing the initiation of RhoA pulses, which we will refer to here as RhoA excitation (see Methods for details). We based our approach on a simple observation: for each perturbation in manually chosen pulsing regions, after smoothing the raw data (Figure 2.2A: [1] and [2]), we could detect the sharp rising phase of RhoA excitation at individual pixels (Figure 2.2B). To automate detection of the rising phase, we computed the temporal derivative of the smoothed data divided by its standard deviation to normalize (Figure 2.2A: [3]) and then applied a threshold to produce binary masks representing all pixels currently undergoing excitation (Figure 2C). From these binary masks, we identified excitation regions as contiguous groups of pixels undergoing excitation (i.e., with temporal derivatives above threshold) (Figure 2.2A: [4]) and new excitation regions as groups of pixels crossing the excitation threshold for the first time (Figure 2.2A: [5]).

To account for genotype-specific variations in the amplitude of the temporal derivative of GFP::ROK, we set the excitation threshold for each genotype as follows: we computed the average amplitude of the temporal derivative across many manually labeled pulsing regions. Then we multiplied by a single scale factor S = 0.4, shared across all perturbations, to obtain a perturbation-specific threshold value (Figure 2.2D). Overlaying new excitation regions on the raw GFP::ROK signal shows that, for a single choice of scale factor, our algorithm accurately captures pulses for three different perturbations (Figure 2.2E). These and the results of our subsequent analysis of spatiotemporal excitation dynamics were largely insensitive to variation in the magnitude of the scale factor up or down by 10/

2.2.3 Depleting formin/CYK-1 or anillin/ANI-1 induces a shift from locally excitable to noisy oscillatory dynamics

To characterize changes in temporal dynamics induced by formin and anillin depletion, we analyzed the recurrence of excitation at individual pixels. Comparing embryowide frequency maps (Figure 2.3A) and kymographs of new excitation events (Figure 2.3B) revealed an increase

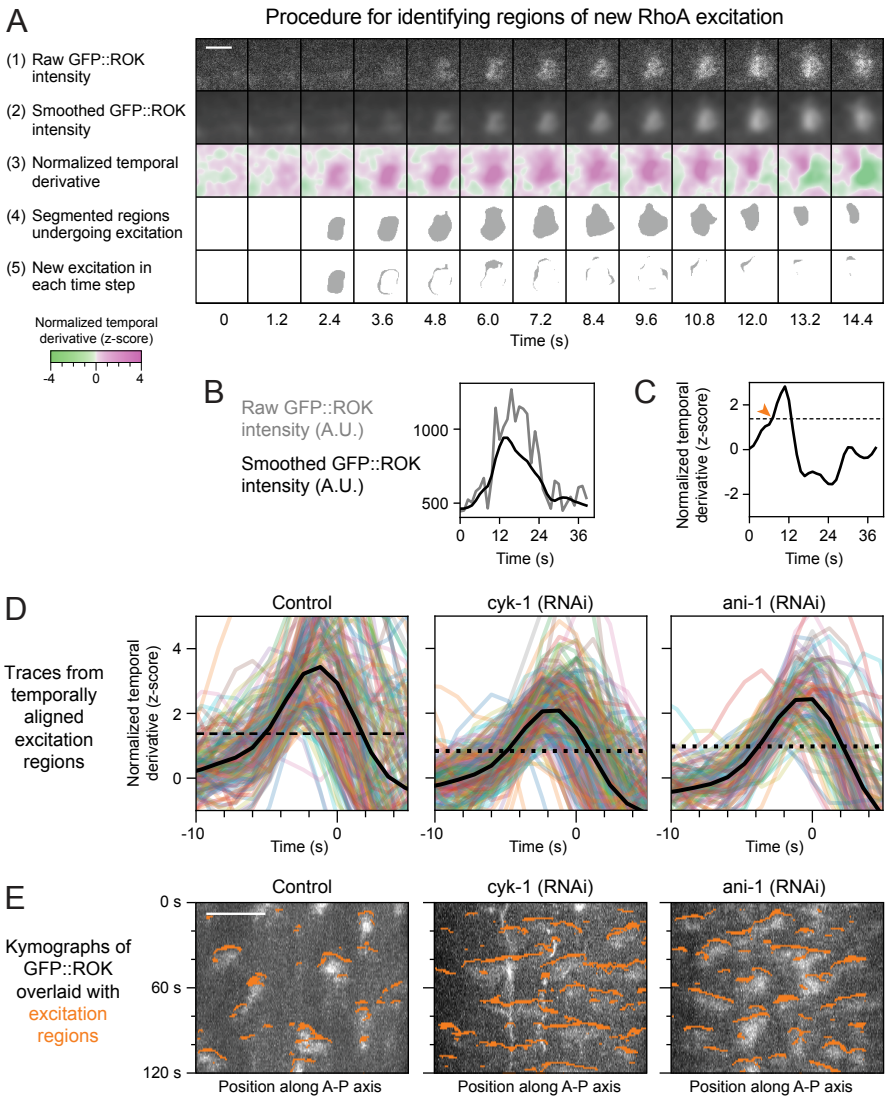

Figure 2.2. A pipeline for automated detection of RhoA excitation. (A) Time evolution of a single pulse illustrating image processing steps that convert the raw GFP::ROK signal into binary masks representing RhoA excitation. Top row: raw GFP::ROK intensity. Second row: smoothed signal obtained by averaging raw signal in space and time (see Methods). Third row: normalized temporal derivative calculated by subtracting the smoothed signal at t −2.4 s from the smoothed signal at t + 2.4 s and then dividing by its standard deviation. Fourth row: binary excitation mask obtained by thresholding the normalized temporal derivative (see panel C). Bottom row: binary subtraction of excitation in previous frame from current frame yields new excitation. The time delay between frames is 1.2 s. The selected region is 7 μm square. (B) Time evolution of the raw and smoothed intensities for the center pixel of the region in A. The gray line indicates the raw GFP::ROK signal; the black line indicates the smoothed signal. (C) Time evolution of normalized temporal derivative values for the center pixel in A. The black line indicates the normalized temporal derivative; the dotted black line indicates the threshold used in A; the orange arrowhead indicates the new excitation time point. (D) Time evolution of the normalized temporal derivative value of ROK over time. The thin colored lines show the normalized temporal derivative for pixels within many manually labeled regions in embryos subjected to the indicated perturbation. The thick black line is their average. The dotted black line is the selected threshold for all embryos subjected to the indicated perturbation. (E) Kymographs showing new excitation in orange superimposed on the raw GFP::ROK intensities for the indicated perturbations. Scale bar is 10 μm.

in both the frequency and the regularity of new excitation in *cyk-1(RNAi)* and *ani-1(RNAi)* embryos compared with controls. To quantify these differences, we plotted distributions of new excitation frequency and wait times between new excitations for control, *cyk-1(RNAi)*, and *ani-1(RNAi)* embryos (Figure 2.3, C and D). In control embryos, the distribution of frequencies was highly skewed, with a peak near 0, and the distribution of wait times was approximately uniform with a refractory period near 0 (Figure 2.3, C and D; Supplemental Figure S2B). By contrast, in *cyk-1(RNAi)* or *ani-1(RNAi)* embryos, the distribution of frequencies was nearly symmetric with peaks near 0.04/s, while the distribution of wait times was unimodal with strong peaks near 23 s (Figure 2.3, C and D; Supplemental Figure S2B). For all three phenotypes, there was a slight peak in the wait time distribution at around 10 s which likely reflects small cortical displacements that we do not account for in this analysis. We also measured the average temporal autocorrelation function (tACF) of smoothed GFP::ROK intensities (see Methods) in control, *cyk-1(RNAi)*, and *ani-1(RNAi)* embryos. In control embryos, the tACF was monotonically decreasing, while in *cyk1(RNAi)* and *ani-1(RNAi)* embryos, the tACF had a small secondary peak at around 23 s (Supplemental Figure S3), confirming that pulses of RhoA excitation become more regular on depletion of formin or anillin.

To help interpret these differences, we compared the experimental distributions with those produced by simulations of the Fitzhugh–Nagumo (FHN) model (Nagumo et al. 1962), a generic model of an excitable system subjected to stochastic input (Supplemental Figure S4A; see Methods for details). We held the amplitude and frequency of the stochastic input fixed and gradually reduced the value of a single parameter (α) so that the deterministic behavior of the FHN model transitions from excitable to oscillatory (Supplemental Figure S4B). When α was tuned to yield excitable dynamics with a large threshold relative to the amplitude of the stochastic input, the FN model predicted frequency and wait time distributions that were qualitatively similar to those observed in controls (Supplemental Figure S4, C and D; $\alpha = 0.95$). As α increased, the excitation threshold decreased; the frequency distribution shifted right and became more symmetric, and a peak appeared in the wait time distribution (Supplemental Figure S4, C and D; $\alpha = 0.9$). As α approached the bifurcation point at which the deterministic dynamics switched from excitable to oscillatory, the peak in the frequency distribution approached the frequency of the oscillation and the wait time distribution tightened around its natural period.

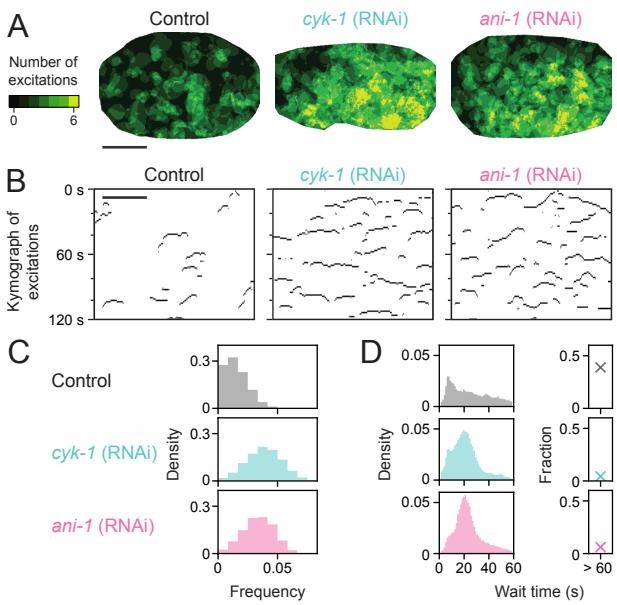

Figure 2.3. Depletion of CYK-1 or ANI-1 induces a shift from locally excitable to noisy oscillatory RhoA dynamics. (A) Colormaps showing the total number of excitations in 120 s for each pixel in representative control, *cyk-1(RNAi)* and *ani-1(RNAi)* embryos. The number of excitations is color coded using the colorbar on the left. (B) Kymograph showing new excitation events (black) over time for the center row of pixels in A. (C) Distributions of excitation frequencies for all pixels in embryos with the indicated perturbations. Frequency is the total number of excitations divided by 120 s. The dotted line is the best Poisson fit. (D) Distributions of wait times between new excitations for all new excitation events in embryos with the indicated perturbations. On the right is the fraction of pixels at which new excitation did not recur within 60 s. The numbers of embryos used for the analysis in C and D are control/spd-5(RNAi) (n = 6). *spd-5(RNAi)*; *cyk-1(RNAi)* (n = 8) and *spd-5(RNAi)*; ani-1(RNAi) (n = 5). The total numbers of excitation events examined are control/*spd-5(RNAi)* (n = 615914), spd-5(RNAi); *cyk-1(RNAi)* (n = 561054), and for all *cyk-1(RNAi)* embryos and *spd-5(RNAi)*; *ani-1(RNAi)* (n = 349737). Scale bar is 10 μm.

As α passed through this bifurcation point, qualitative features of the distributions of frequency and wait time were preserved (Supplemental Figure S4, C and D; $\alpha = 0.85, 0.65$). Thus in the presence of fixed stochastic input, when the system is close to a transition from excitable to oscillatory dynamics, it is not possible to infer from the observed dynamics alone whether the underlying deterministic system is excitable or oscillatory. We will use the term noisy oscillations to describe this type of observed dynamics. Comparing predictions of the FHN model with stochastic forcing with the frequency and wait time distributions measured in *cyk-1(RNAi)* and *ani-1(RNAi)* embryos suggests that depleting either cyk-1/CYK-1 or anillin/ANI-1 induces a transition from excitable RhoA dynamics to noisy oscillatory dynamics.

2.2.4 Depleting formin and anillin induces different spatiotemporal patterns of excitation

To visualize and compare the spread of RhoA excitation across different perturbations, we assigned grayscale values to excitation pixels based on the time since last excitation. The resulting movies (Supplemental Movie S4) show that local spread of new excitation occurs across all perturbations. but the patterns of spread are markedly different in *cyk-1(RNAi)* or *ani-1(RNAi)* embryos than in controls. In control embryos, excitations tend to initiate and spread locally before terminating. In forminand anillin-depleted embryos, regions of locally spreading excitation cover a larger fraction of the cortex and frequently merge with one another or split to form more complicated spatial patterns of excitation. To quantify these differences, we first measured the speeds at which the boundaries of excitation regions (excitation fronts) advance locally between successive frames (Figure 2.4A; see Methods for details). If the dominant mode of propagation were coherent excitation wavefronts as observed in other cells (Bement et al. 2015; Maître et al. 2015; Bhattacharya et al. 2020), the distribution of speeds would have a single dominant peak centered on a nonzero value. Instead, the distributions that we observe in *C. elegans* zygotes are monotonically decreasing with a peak near zero velocity and long tails (Figure 2.4B). However, the distributions of speeds were remarkably similar in control, *ani-1(RNAi)*, and *cyk-1(RNAi)* embryos, suggesting that differences in the speeds at which excitation spreads locally are not responsible for larger differences in spatiotemporal patterns of excitation.

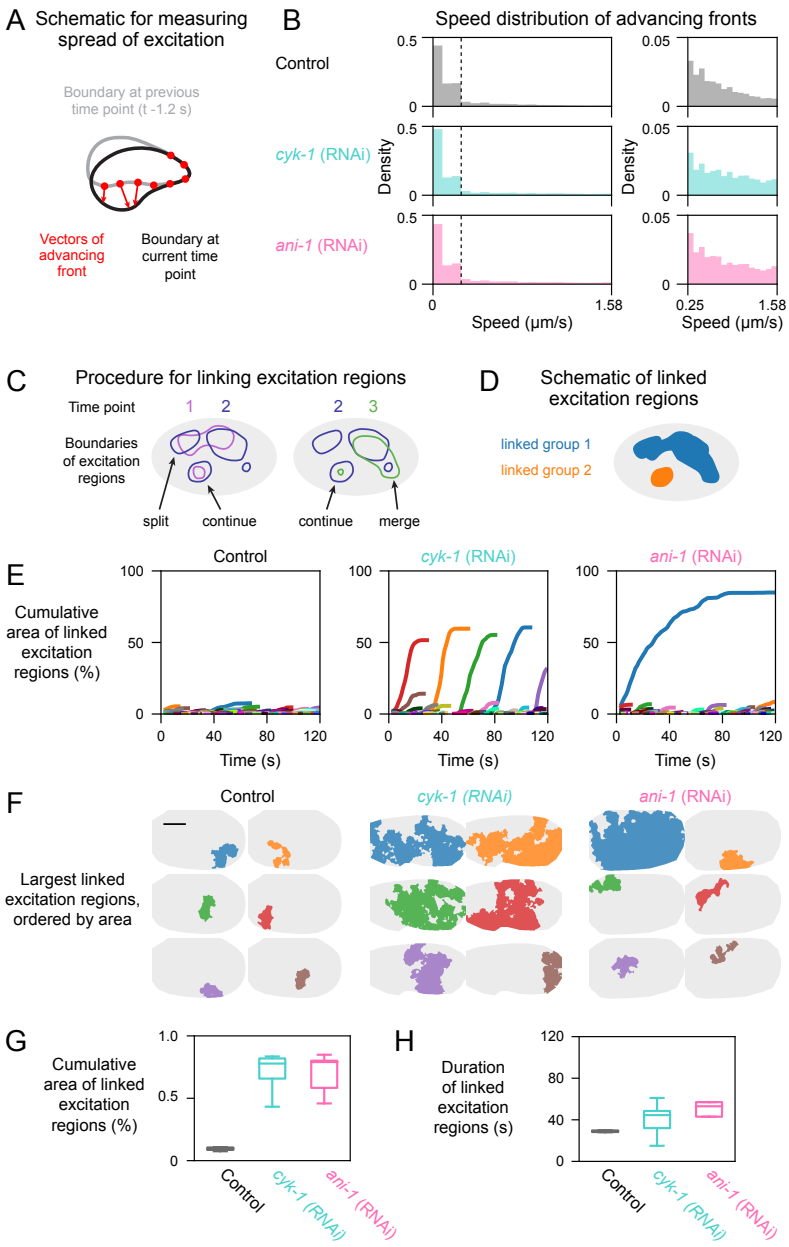

Figure 2.4. Depletion of CYK-1 and ANI-1 induce distinct spatiotemporal patterns of RhoA excitation. (A) Schematic showing the method for quantifying local spread of excitation. Black and gray lines are the boundaries of excitation regions at times t and t−1.2 s, respectively. Red dots are equally spaced points along the part of the excitation front at time t that advanced by time t−1.2. Red arrows show displacement normal to the local excitation front at time t. (B) Distribution of local speeds in embryos of the indicated perturbation. Magnified view at the right shows the tail of the distributions for speeds ¿0.25 μm/s shown as black dotted line at the left. (C) Schematic illustration of linking excitation regions across successive frames. Closed lines show the contours of excitation regions. Line colors indicate successive time points. Left shows examples of splitting and continuation between time points 1 and 2. Right shows examples of continuation and merger between time points 2 and 3. (D) Schematic illustration of linked excitation regions corresponding to the linkage sequences in C. (E) Curves showing the growth of cumulative area vs. time for all linked excitation region in representative embryos for the indicated perturbation. Each colored line indicates the growth of a single linked excitation regions over time. (F) Areas explored by the six largest excitation regions for each representative embryo. Colors correspond to the lines in E. The "representative" embryos in E and F were chosen to best highlight qualitative differences across perturbations. (G) Box plots showing the distribution of cumulative areas of the largest linked excitation regions in embryos with the indicated perturbations. (H) Box plots showing the duration of the largest linked excitation regions in embryos with the indicated perturbations. The numbers of embryos used for the analysis in G and H are control/*spd-5(RNAi)* (n = 6). *spd-5(RNAi)*; *cyk-1(RNAi)* (n = 8) and *spd-5(RNAi)*; *ani-1(RNAi)* (n = 5). The numbers of vectors at advancing fronts in B are control/*spd-5(RNAi)* (n = 45496), *spd-5(RNAi)*; *cyk-1(RNAi)* (n = 82638), and for all *cyk-1(RNAi)* embryos and *spd-5(RNAi)*; *ani-1(RNAi)* (n = 47574).

To characterize differences in spatiotemporal patterns of excitation, we linked excitation regions that overlap in successive frames (Figure 2.4D; see Methods for details). We applied this linkage recursively over the entire observation window to identify a set of "linked excitation regions" connecting excitation regions that spread locally, merge with one another or split over time (Figure 2.4, C and D). Visualizing and quantifying the cumulative growth, duration, and distribution of linked excitation regions in representative control, *cyk-1(RNAi)*, and *ani-1(RNAi)* embryos revealed different patterns of spreading excitation (Supplemental Movie S5; Figure 2.4, E and F). In control embryos, linked excitation regions have small cumulative areas and durations (Figure 2.4, E and F), reflecting the tendency for excitations to initiate locally, expand rapidly and then terminate quickly without merging or splitting (Supplemental Movie S5). We also observe linked excitation regions with small areas and short durations in forminand anillin-depleted embryos, but in these embryos, the frequent merging and splitting of excitation regions also generate a few linked excitation regions that persist longer and cover much of the embryo surface. We confirmed these basic differences by plotting the durations and cumulative areas of the largest linked excitation regions for multiple embryos with each perturbation (Figure 2.4, G and H; Supplemental Figure S2C). Closer inspection suggested that differences in the spatial synchronization of excitation produces different spatiotemporal patterns of excitation in forminand anillindepleted embryos (Figure 2.4, G and H; Supplemental Movie S5). In formin-depleted embryos, the larger linked excitation groups represent multiple excitation regions that initiate synchronously and then rapidly expand and merge into larger regions before terminating (Supplemental Movie S5). Multiple rounds of synchronous excitation recur at intervals comparable to the mean wait time for excitation (Figure 2.4E) and in overlapping regions of the embryo (Figure 2.4F). In anillin-depleted embryos, new excitation regions initiate throughout the cortex without apparent synchrony. They often form adjacent to existing or recent excitation regions and frequently merge with one another or split, giving the overall impression of noisy waves that expand locally and persistently in different directions, colliding with one another to create larger linked excitation regions that span most of the embryo (Figure 2.4, E and F; Supplemental Movie S5). In summary, depleting either formin/ CYK-1 or anillin/ANI-1 has only minor effects on the distribution of speeds at which excitation spreads locally but large effects on spatiotemporal patterns of RhoA excitation. In control embryos,

many excitations initiate and spread locally and terminate rapidly. In formin-depleted embryos, recurrent episodes of excitation are synchronized over larger regions of the cortex. In anillin-depleted embryos, excitations initiate asynchronously, spread locally, and frequently merge and split to explore larger regions of the cell cortex.

2.2.5 Lower levels and enhanced depletion of F-actin underlie the shift in spatiotemporal patterns of RhoA excitation in formin- and anillin-depleted embryos

Our data suggest that depleting either formin or anillin induces a transition from locally excitable to noisy oscillatory dynamics. In simple activator/inhibitor models, such transitions can be induced by reducing overall inhibitor levels and/or by enhancing the depletion of inhibitor after individual pulses. Consistent with the first possibility, we observed an overall reduction in F-actin levels in both anillinand formin-depleted embryos relative to controls [Figure 2.5A, control: 440 ± 29; *ani-1(RNAi)*: 403 ± 23; *cyk-1(RNAi)*: 350 ± 6 (mean ± SD in arbitrary units of intensity)].

To assess whether enhanced depletion of F-actin after pulses accompanies the transition to noisy oscillatory dynamics in forminand anillin-depleted embryos, we imaged embryos coexpressing ROK::GFP and Lifeact::mCherry as a marker for F-actin (Pohl et al. 2012). As above, we used the GFP::ROK signal to identify pixels undergoing new excitation and then used kymographs and movies to compare new excitation with F-actin levels (Supplemental Figure S5A) or their temporal derivatives (Figure 2.5B; Supplemental Figure S2D; Supplemental Movie S6) in space and time. In forminand anillin-depleted embryos, local depletion of F-actin occurs shortly before the majority of RhoA excitations (and the majority of excitations follow shortly after Factin depletion). In control embryos, the relationship between F-actin depletion and RhoA excitation was more variable; some excitations follow F-actin depletion; others do not (Figure 2.5B; Supplemental Figure S5A; Supplemental Movie S6). To quantify the strength of temporal correlations between F-actin depletion and RhoA excitation under different perturbations, we measured the average Lifeact::mCherry intensity (Supplemental Figures S5C and S2D), and its temporal derivative (Figure 2.5C) in excitation pixels at a range of temporal offsets relative to

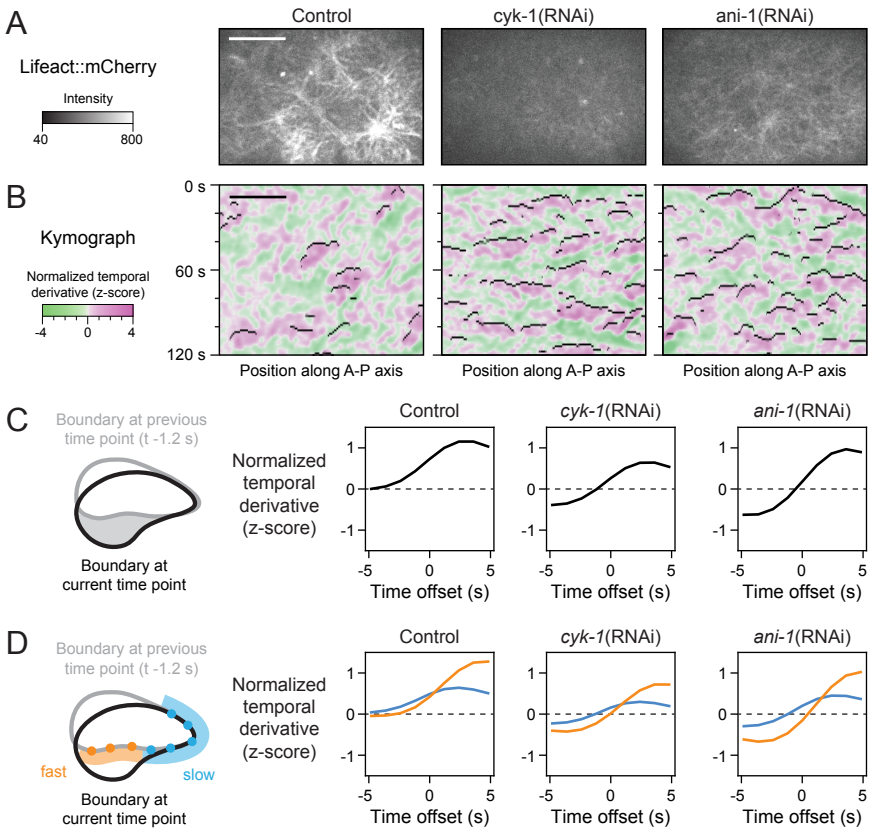

Figure 2.5. Reduced levels and more rapid depletion of F-actin accompanies the transition to noisy oscillatory dynamics in formin- and anillin-depleted embryos. (A) Single spinning disk images of embryos expressing mCherry::Lifeact. Images were acquired with identical settings and identically processed to allow direct comparison of intensities across perturbations. (B) Kymographs showing the normalized temporal derivative of mCherry::Lifeact intensity, calculated as shown in Figure 2A, for the vertically centered row of pixels from the embryos in A, overlaid with new excitation pixels in black, which were calculated as in Figure 2A. (C) Left: schematic showing new excitation region at time t in solid gray. Right: average normalized temporal derivative of mCherry::Lifeact intensity measured over all new excitation pixels in embryos with the indicated perturbations. (D) Left: schematic representation of pixels evenly spaced along the advancing boundary of an excitation front, color coded with respect to the instantaneous speed of advance; orange indicates large instantaneous speed ($S >= 0.25 \mu m/s$); blue indicates small instantaneous speed ($S < 0.25 \mu m/s$). Right: average normalized temporal derivative of mCherry::Lifeact intensity measured over all new excitation pixels with fast (orange) or slow (blue) instantaneous speeds in embryos with the indicated perturbations. (C, D) The 95 % confidence intervals for average F-actin level are smaller than the thickness of the average line. the dotted black line indicates a temporal derivative = zero; that is, no change in F-actin level. The numbers of embryos used for the analysis in C and D are control/*spd-5(RNAi)* (n = 6). *spd-5(RNAi)*; *cyk-1(RNAi)* (n = 8) and *spd-5(RNAi)*; *ani-1(RNAi)* (n = 5). The total numbers of excitation events examined are control/*spd-5(RNAi)* (n = 615914), *spd-5(RNAi)*; *cyk-1(RNAi)* (n = 561054), and for all *cyk-1(RNAi)* embryos and *spd-5(RNAi)*; *ani-1(RNAi)* (n = 349737). Scale bar is 10 μm.

new excitation. We found that on average, Lifeact::mCherry intensities decreased sharply just before new excitation in *cyk-1(RNAi)* and *ani-1(RNAi)* embryos but not in control embryos (Figure 2.5C; Supplemental Figure S5C, discussed further below). Thus overall reduction in levels and enhanced local depletion of F-actin accompanies the shift to noisy oscillatory dynamics in both forminand anillin-depleted embryos. To ask whether local spread of excitation correlates with local depletion of F-actin in forminand anillin-depleted embryos, at each time point we partitioned pixels along the advancing boundaries of excitation regions ("excitation fronts") into fast and slow groups based on the speed of local advance. For each pixel, we measured Lifeact::mCherry intensity or its temporal derivative in regions just ahead of the excitation front (see Figure 5D schematic: orange and blue regions) at different times relative to the current time point (Figure 2.5D; Supplemental Figure S5D; see Methods). In forminand anillin-depleted embryos, the average F-actin levels decreased in regions ahead of excitation fronts shortly before the time of entry (Figure 2.5D; Supplemental Figures S5D and S2D; note that slow-moving excitation fronts enter but do not spread through these regions). The average rate and extent of decrease were lower ahead of slowly advancing excitation fronts than faster moving ones (Figure 2.5D; Supplemental Figures S5D and S2D). In control embryos, there was a slight decrease in average F-actin levels in regions ahead of fast advancing excitation fronts but none ahead of slowly advancing fronts. These observations suggest that local depletion of F-actin plays a role in channeling the spread of RhoA excitation in forminand anillindepleted embryos.

2.2.6 Heterogeneous F-actin dynamics precede RhoA excitation in control embryos

We have shown that, on average, local depletion of F-actin does not precede RhoA excitation in control embryos. However, this does not rule out a role for F-actin inhibition in control embryos because these average measurements hide significant heterogeneity in the local F-actin dynamics preceding RhoA excitation (Figure 2.5B; Supplemental Figure S5B; Supplemental Movie S6). To better understand the origins of this heterogeneity, we used nearTIRF microscopy (see Methods) to image control embryos expressing GFP::ROK and Lifeact::mCherry (Figure 2.6; Supplemental Movie S7). In control embryos, as previously described (Munro et al. 2004), the cortex contains a dynamic network of actin foci interconnected by bundles that surround

"depletion regions" with relatively lower levels of F-actin. The foci are coenriched in F-actin and GFP::ROK. They typically form as condensations of larger RhoA pulses, and they often persist for tens of seconds and propagate slowly through regions with high levels of F-actin (Figure 2.6A; see also Michaux et al, 2018), suggesting that additional mechanisms may exist to sustain and/or propagate RhoA activity in regions with high levels of F-actin.

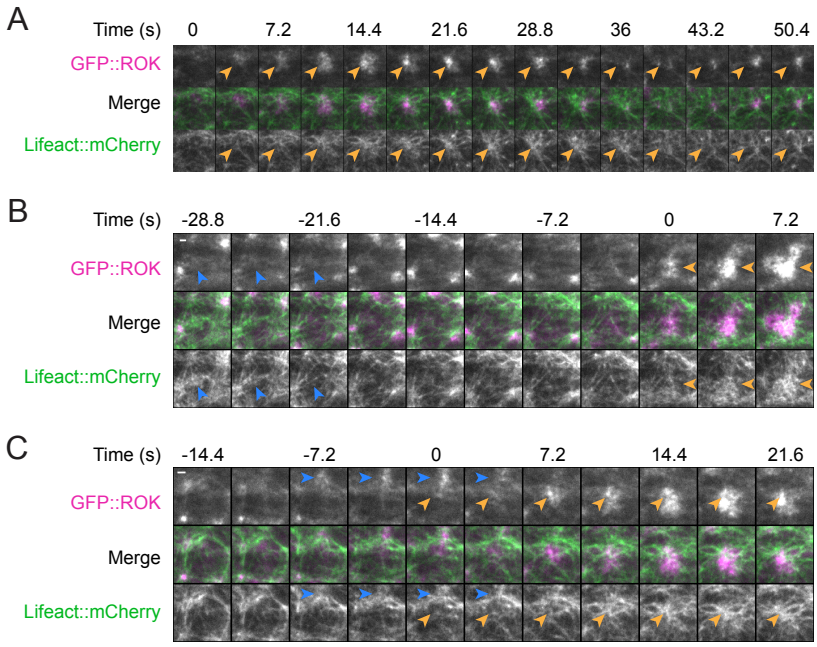

Figure 2.6. Heterogeneous dynamics of pulse initiation and spread in control embryos. Time series of TIRF images from Supplemental Movie S7 showing examples of pulse initiation and spread in a control embryo expressing GFP::ROK and mCherry::Lifeact. Time zero indicates initiation of pulses. (A) A GFP::ROK focus forms from a larger pulse and then persists in a region with high levels of mCherry::Lifeact (orange arrowheads). (B) Local cortical tearing and dilation (blue arrowheads) creates a region with reduced F-actin levels where a new pulse initiates (orange arrowheads). (C) A new pulse initiates near an existing GFP::ROK focus (blue arrowheads) and then spreads into a region with lower levels of mCherry::Lifeact (orange arrowheads). Scale bar is 10 μm.

We observed that new RhoA pulses tend to form and spread within F-actin depletion regions. But where excitation first initiates within these regions is more variable. Pulses can initiate within the interiors of depletion regions where F-actin levels are relatively low, and this is sometimes (¡10% of pulses) preceded by spontaneous local tearing and dilation of the cortical network (Figure 2.6B). However, pulses often initiate near the boundaries of depletion regions, and near existing foci where F-actin levels are persistently high and/or increasing (Figure 2.6C). These observations suggest that local depletion of F-actin helps to shape, but does not determine, patterns of RhoA excitation in control embryos.

2.2.7 Contractility is required for the shift from locally excitable to noisy oscillatory dynamics in embryos depleted of formin but not anillin

Both formin and anillin depletion induce a transition to noisy oscillatory dynamics but with qualitatively distinct spatiotemporal patterns of RhoA excitation (Figures 2.1C and 2.4, E–G). Since local reduction in Factin levels correlates with RhoA excitation in both cases (Figure 2.5, C and D), we reasoned that these differences in spatiotemporal RhoA excitation patterns could reflect differences in the mechanisms that drive local reduction in F-actin levels. Consistent with this possibility, we observed different patterns of actomyosin contractility in forminand anillin-depleted embryos (Figure 2.7; Supplemental Movie S8). In *cyk-1(RNAi)* embryos, cycles of local actomyosin accumulation and disappearance are correlated with local contraction and dilation, respectively (Figure 2.7B; blue arrows indicate accumulation/contraction; orange asterisks indicate disappearance/dilation). Accumulation preceded contraction, while disappearance preceded cortical tearing and dilation, which was followed by another round of accumulation. These cycles were synchronized across large regions of the embryo (best seen in Supplemental Movie S7), matching the rapid recurrent spread of RhoA activity (Figure 2.4E). We observed very similar dynamics in profilin-depleted embryos (Supplemental Figure S6; Supplemental Movie S9). Recurrent cycles of local tearing followed by GFP::ROK accumulation and contraction were particularly apparent in embryos weakly depleted of profilin (Supplemental Figure S6; Supplemental Movie S9, left). In more strongly depleted embryos, the dynamics became increasingly chaotic (Supplemental Figure S6; Supplemental Movie S9, middle and right); however, the correlation between local tearing and subsequent accumulation and contraction of GFP::ROK persisted. By contrast, in *ani-1(RNAi)* embryos, F-actin and myosin II undergo cycles of accumulation and rapid disappearance with very little cortical movement (Figure 2.7).

These observations suggest that actomyosin contractility could play different roles in producing the different spatiotemporal patterns of RhoA excitation in *cyk-1(RNAi)* and *ani-1(RNAi)* embryos. To test this possibility, we compared the effects of depleting formin and anillin in control [*spd-5(RNAi)*] embryos and in temperaturesensitive myosin mutant (*nmy-2(ts)* (Liu et al. 2010) embryos produced at the restrictive temperature (25°C). Specifically, we compared

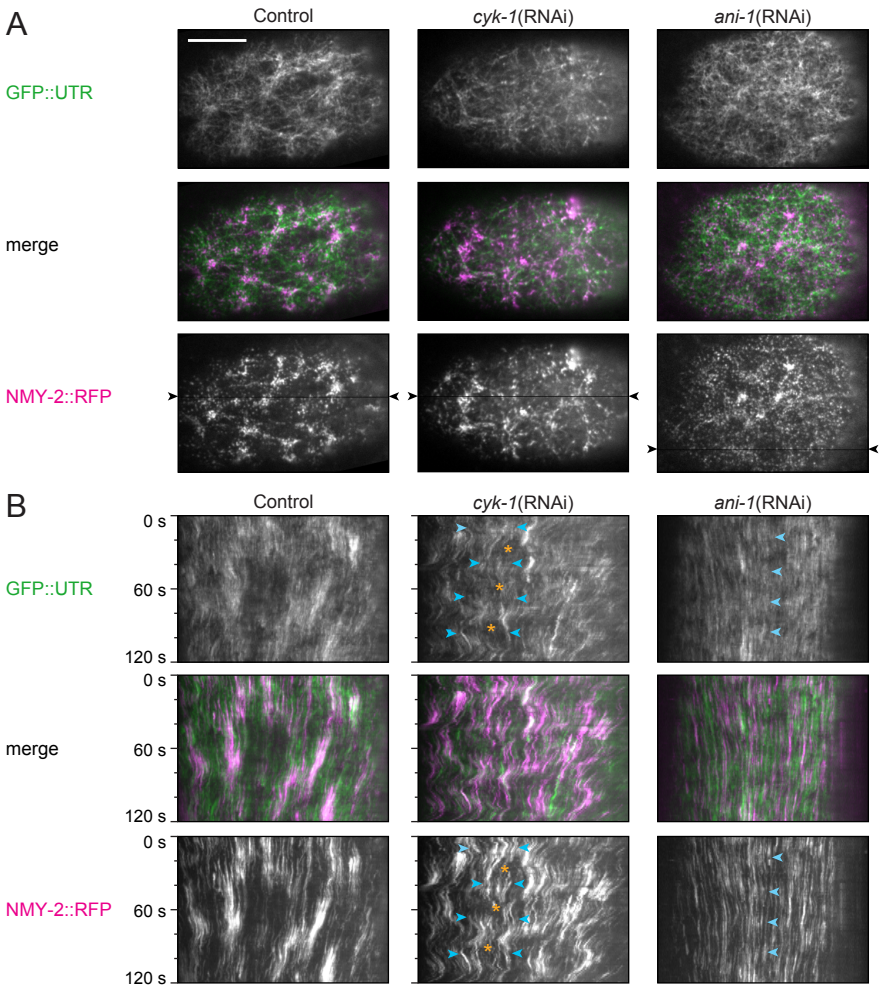

Figure 2.7. Distinct patterns of local contractility underlie the transition to noisy oscillatory dynamics in formin- and anillin-depleted embryos. (A) Single frames from the TIRF Supplemental Movies shown in Supplemental Movie S8 of embryos with the indicated perturbations expressing GFP::UTR and NMY-2::mKate2. Fluorescence intensities are scaled differently across perturbations to highlight actomyosin structures. (B) Kymographs from the same Supplemental Movies shown in A. Black arrowheads indicate the vertical position where each kymograph was generated. Paired cyan arrowheads overlaying the kymographs for *cyk-1(RNAi)* indicate a sequence of local contractions, each accompanied by accumulation of NMY-2::mKate2 and preceded by local cortical tearing/dilation events (orange asterisks). Cyan arrowheads overlaying the kymographs for *ani-1(RNAi)* indicate the recurrent accumulation of GFP::UTR and NMY- 2::mKate2 without local contraction or dilation. Scale bar is 10 μm.

the recurrence (excitation frequency and wait time distributions; Figure 2.8, A–F) and spatial pattern (cumulative area and duration of the largest linked excitation regions; Figure 2.8, G and H) of RhoA excitation. In *nmy-2(ts)* embryos observed at 25°C, the recurrence and spatial pattern of RhoA excitation were similar to those observed in controls (Figure 2.8, A, D, G, and H). Inhibiting myosin contractility in formin-depleted embryos [*cyk-1(RNAi)*; *nmy-2(ts)*; 25°C] produced a sharp decrease in the recurrence of RhoA excitation (Figure 2.8, B and E) and in the cumulative area and duration of linked excitation regions (Figure 2.8, G and H), indicating a loss of the spatial synchrony of RhoA excitation observed in *cyk-1(RNAi)* alone. The resulting dynamics were similar to those observed in *nmy-2(ts)* alone. In contrast, inhibiting myosin contractility in anillindepleted embryos [*ani-1(RNAi)*; *nmy-2(ts)*] produced dynamics similar to those observed in *ani-1(RNAi)* alone (Figure 2.8, C, F–H), except for a small increase in excitation frequency. Thus the shift toward spatially synchronized noisy oscillatory dynamics produced by depleting formin requires myosin II activity, while the shift toward noisy oscillations and the spatiotemporal patterns of spreading excitation produced by depleting anillin do not.

2.3 Discussion

Pulsatile RhoA activity underlies the control of many different cell and tissue behaviors. Here we asked whether variations in spatial and temporal patterns of pulsatile RhoA activity observed in different contexts could be recapitulated in the *C. elegans* zygote by modulating actin network assembly dynamics, architecture, and contractility. We identified perturbations that induce variations along two axes: from locally excitable to noisy oscillatory temporal dynamics and from focal (standing) pulses to traveling waves. In particular, we found that reducing actin assembly rates by depleting formin/ CYK-1 or profilin/PFN-1 induces a transition to locally oscillatory dynamics that are synchronized across larger cortical regions, while depleting anillin/ANI-1 induces spatiotemporal activity patterns that are reminiscent of, albeit more irregular than, the oscillatory propagating waves observed in other cells. Our analysis suggests that these pattern variants can be understood as a consequence of changes in local F-actin dynamics, leading to different dynamics of RhoA inhibition.

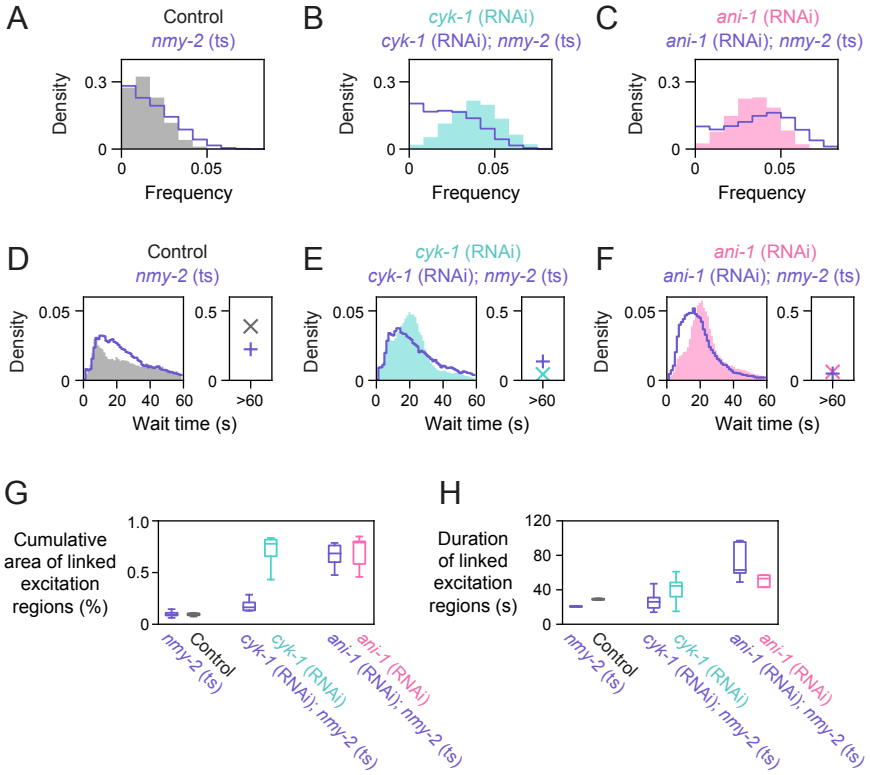

Figure 2.8. Contractility is required for the shift from locally excitable to noisy oscillatory dynamics in embryos depleted of formin but not anillin. (A–C) Distributions of excitation frequencies for all pixels in embryos with the indicated perturbations. Filled histograms show the data from Figure 3C. Overlaid blue histograms show the data from *nmy-2(ts)* embryos alone (A, for comparison with *spd-5(RNAi)* controls) or in combination with formin (B) or anillin (C) depletion. (D–F) Distributions of wait times between new excitations for all new excitation events in embryos with the indicated perturbations. Filled histograms show the data from Figure 3D. Overlaid blue histograms show the data from *nmy-2(ts)* embryos alone (D, for comparison with *spd-5(RNAi)* controls) or in combination with formin (E) or anillin (F) depletion. (G) Box plots showing the distribution of cumulative areas of the largest linked groups in embryos with the indicated perturbations. (H) Box plots showing the duration of the largest linked groups in embryos with the indicated perturbations. The number of embryos used for analysis in A–H are control/*spd-5(RNAi)* (6), *spd-5(RNAi)*;*cyk-1(RNAi)* (n = 8). *spd-5(RNAi)*;ani- 1(RNAi) (n = 5), *nmy-2(ts)* (n = 7), *nmy-2(ts)*; *cyk-1(RNAi)* (n = 5), *nmy-2(ts)*; *ani-1(RNAi)* (n = 7).

2.3.1 Reduced levels and faster depletion of F-actin induce a shift from excitable to noisy oscillatory dynamics

In simple activator/inhibitor systems, transitions from excitable to oscillatory dynamics can be induced by decreasing the overall level of inhibition or by enhancing the release of inhibition following a pulse. Consistent with these possibilities, we find that i) the overall density of F-actin is reduced in forminand anillin-depleted embryos relative to controls and ii) on average, local depletion of Factin precedes pulse initiation in forminand anillin-depleted embryos but not in controls. Thus we propose that in control embryos, higher overall levels of F-actin set a higher threshold for pulse initiation, making it hard to trigger pulses through local fluctuations in RhoA activity or F-actin levels. In forminand anillin-depleted embryos, lower overall levels of F-actin and faster and stronger depletion of F-actin after a pulse drive a shift to locally oscillatory pulse dynamics.

2.3.2 Distinct mechanisms for local F-actin depletion distinguish different spatiotemporal pulse dynamics induced by formin and anillin depletion

In embryos depleted of formin or profilin, local dilation of the cortex precedes the initiation and spread of RhoA activity; in *cyk-1(RNAi)* [and likely *pfn-1(RNAi)*] embryos, these dilations do not occur in the absence of contractility. We propose that the noisy oscillations induced by formin or weak profilin depletion are driven by coupling excitable RhoA dynamics with a local cortical tearing instability. As RhoA, F-actin, and myosin II disappear locally following a pulse, reduced contractility (and connectivity) relative to neighboring regions induces local dilation, cortical tearing, and further depletion of Factin, and this in turn leads to rapid RhoA activation and new pulse initiation. Accumulation of F-actin at the edges of dilated regions may ultimately limit this spread to produce larger but still spatially restricted pulses of RhoA activity. Whether RhoA activation is purely a response to local reduction in F-actin levels or involves a more complicated mechanical response to network tearing, as observed in other contexts (Smith et al. 2010; Sun et al. 2020; Winkelman et al. 2020), remains to be determined.

The instabilities that we observe in forminand profilin-depleted embryos are reminiscent of cortical tearing instabilities that underlie bleb formation and cell shape oscillations in other cells

(Paluch et al. 2005; Charras and Paluch 2008). Interestingly, spontaneous local tearing occurs with low frequency in both wild-type (Mayer et al. 2010) and SPD–5-depleted zygotes (Figure 6B; Supplemental Movies S7 and S8), suggesting that *C. elegans* zygotes are poised close to such a tearing instability. Thus we propose that reducing rates of filament assembly by formin or profilin depletion increases the tendency for local depletion of F-actin after a pulse to trigger a local contractility instability and re-excitation of RhoA, leading to oscillatory dynamics.

A related behavior occurs in epithelial cells of gastrula stage frog embryos, where local breakage of tight junctions along contractile cell–cell contacts leads to the production of local RhoA pulses (called "flares" in this system), which in turn promote local assembly of actomyosin to repair the break (Reyes et al. 2014; Stephenson et al. 2019). In this system, local depletion of tight junction components, but not F-actin, precedes spontaneously occurring RhoA flares. However, reducing F-actin assembly rates by treating embryos with Latrunculin can induce local tearing instabilities that result in local depletion of both F-actin and tight junction components and recurrent activation of RhoA flares (Reyes et al. 2014; Stephenson et al. 2019), similar to what we describe here in *C. elegans* embryos depleted of formin or profilin. Together these observations highlight a general route to oscillatory RhoA dynamics in contractile systems by enhancing the tendency toward tearing instabilities in the presence of a Rho-based repair mechanism.

By contrast, in anillin-depleted embryos, F-actin and myosin II disappear rapidly after each pulse in the absence of significant cortical contractions or dilations. Our analysis suggests that the rapid depletion of F-actin promotes local oscillations in anillin-depleted embryos, but in the absence of cortical tearing instabilities, these oscillations are not synchronized across larger cortical regions. Instead, asynchronous oscillations create local zones of F-actin depletion in neighboring regions, and these appear to serve as channels through which activation can propagate (Supplemental Movie S6), allowing continuous exploration of the cortex by locally propagating wavefronts.

What drives the rapid disappearance of F-actin in anillin-depleted embryos? Previous studies have shown that the rate of F-actin disassembly increases before the initiation of RhoA pulses in early *C. elegans* embryos (Michaux et al. 2018). Anillin accumulates locally during individual

pulses (Tse et al. 2011; Michaux et al. 2018), and studies in *C. elegans* larvae and in vitro suggest that anillin can stabilize F-actin by antagonizing the severing activity of cofilin/UNC-60A Tian2015. If anillin plays a similar role in stabilizing F-actin during individual pulses, then increased disassembly on its removal could explain the more rapid depletion that we observe. Anillin has also been shown to promote formin-dependent actin assembly in some contexts (Watanabe et al. 2010), and thus local reduction in F-actin assembly may also contribute to the more rapid depletion of F-actin in anillin-depleted embryos. Local measurements of actin filament assembly/disassembly (Robin et al. 2014) will allow us to distinguish these and other possibilities in future studies.

2.3.3 A comparison with previous observations of RhoA dynamics in polarizing zygotes

Nishikawa et al (2017) described pulsatile dynamics of RhoA activation, myosin II accumulation, and cortical flow in polarizing *C. elegans* zygotes. They hypothesized that these dynamics arise through coupling between an autonomous (actomyosin-independent) RhoA oscillator and a form of contractile instability in which RhoA promotes myosin-dependent contractile flows which in turn advect and concentrate RhoA. In Nishikawa et al. (2017), oscillatory dynamics were inferred from cross-correlation analysis at the posterior cortex of polarizing zygotes that are undergoing long-range pulsatile flows (Munro et al. 2004; Mayer et al. 2010; Nishikawa et al. 2017; Naganathan et al. 2014). In these embryos, posterior RhoA activity is modulated by signals associated with the sperm-derived centrosomes in addition to negative feedback from F-actin/RhoGAPs (Cowan and Hyman 2004; Motegi and Sugimoto 2006; Kapoor and Kotak 2019; Zhao et al. 2019; Bolado-Carrancio et al. 2020).

Here we used spd-5(RNAi) to block the centrosome-dependent inhibition of RhoA and the confounding effects of long-range flows, and we used an alternative approach to analyze pulsatile dynamics in which we track the local recurrence and propagation of excitation events. Our current analysis and previous work (Michaux et al. 2018) suggest that in these conditions, pulsatile RhoA dynamics are intrinsically excitable, not oscillatory, although we cannot exclude the possible existence of low amplitude oscillations that lie below our threshold for detecting the rapid rise in RhoA activity during pulse initiation. Moreover, during individual pulses in

SPD–5-depleted zygotes, or in AB cells that do not polarize, the rapid rising phase of RhoA activation precedes the onset of local contraction (Michaux et al. 2018), arguing against a contractile instability in which local contraction concentrates RhoA. Instead, our data reveal an alternative mechanism by which coupling a cortical tearing instability to excitable RhoA dynamics through local F-actin depletion can induce oscillatory pulse dynamics. It will be interesting to see how this mechanism contributes to shaping pulsatile flow dynamics during polarization.

2.3.4 What controls the initiation and spread of RhoA pulses in control embryos?

Our data suggest that the higher overall levels of F-actin in control embryos increase the threshold for initiation of RhoA pulses and reduce the frequency with which they occur. Pulses still tend to form and spread within "depletion regions" containing lower levels of Factin, consistent with an inhibitory role for F-actin. However, the relationship between local F-actin depletion and RhoA excitations is more complex. In some cases, as discussed above, local depletion of F-actin by cortical tearing appears to trigger RhoA pulses. But in many other cases, RhoA pulses initiate at the edges of depletion regions near existing RhoA foci in regions where F-actin levels are persistently high. We hypothesize that these foci serve as local sources of active RhoA that can diffuse into and trigger pulses in adjacent regions containing lower levels of F-actin. However, it remains unclear how RhoA activity can persist in and even spread through regions with high levels of F-actin. One possibility that we will explore in future studies is that one or more additional positive feedback loops, perhaps involving anillin (Maddox, Lewellyn, et al. 2007; Budnar et al. 2019), could locally counter the inhibitory effects of F-actin.

It also remains unclear what restricts the spread of active RhoA to produce focal pulses in control embryos. Simple activator/inhibitor models predict that if active RhoA can freely diffuse while the inhibitory GAPs RGA-3/4 are immobilized through binding to F-actin, then RhoA pulses should tend to propagate as waves. In principle, focal pulses could be achieved by reducing the spread of activation and/or increasing the spread of inhibition. Higher overall levels of F-actin could limit the speed at which RhoA excitation spreads in control embryos. Alternatively, local binding of active RhoA to its effectors (e.g., anillin/ANi-1 and formin/CYK-1) could reduce

its effective mobility. However, these effects are likely to be small, because we observe only small differences in distribution of speeds at which RhoA activation spreads locally in control versus forminand anillin-depleted embryos. It is also possible that local differences in F-actin architecture could shape its ability to inhibit the spread of RhoA (Bement et al. 2015; Michaud, Swider, et al. 2021). For example, the F-actin bundles that bound depletion regions could in principle provide more effective inhibition than a more diffuse network. However, pulses remain focal in *nmy-2(ts)* embryos that lack robust F-actin bundles. Finally, recent work suggests that during pulse initiation, active RhoA recruits cytoplasmic formin/CYK-1 in pulsing regions that subsequently elongate filaments at $\sim$1.5 μm/s (Costache et al. 2021; Li and Munro 2021). Thus in principle, rapid filament elongation could project a zone of F-actin assembly beyond the front of active RhoA and limit its spread. It will be interesting to test these and other possibilities in future studies.

2.3.5 Concluding remarks

In conclusion, our work highlights the importance of actomyosin dynamics in shaping spatiotemporal patterns of pulsatile RhoA activity. It suggests that some of the different patterns of activity observed in other cellular or developmental contexts could arise from differences in the underlying actomyosin dynamics. It also highlights the inadequacy of very simple models for explaining the rich diversity and heterogeneity of pulsatile dynamics observed in living cells or more recently in. While deeper understanding may require the identification and characterization of additional feedback loops, it will likely also require the use of new experimental approaches, such as the use of cell free cytoplasmic extracts (Landino et al. 2021) and/or more detailed models that consider the complex and heterogeneous dynamics of the actomyosin cytoskeleton which forms the physical scaffold on which these dynamics unfold.

2.4 Experimental Procedures

2.4.1 C. elegans *culture and strains*

We cultured *C. elegans* strains at 22°C under standard conditions (Brenner 1974). This study used 3 strains: mc74(GFP::let-502)I; zbIs2[pie-1::Lifeact::mCherry, unc-119(+)], mc74(GFP::let-

502)I; NMY-2(ne1490) I, zuIs151[nmy-2::NMY-2::mRFP, unc-119(+)]; mgSi3[cb-UNC-119 (+) GFP::UtrophinABD]II. The first two strains are created in the study. The last strain is from Michaux *et al.*, 2018.

2.4.2 RNAi

We performed RNAi using the feeding method as previously described (Timmons et al. 2001). We obtained bacteria targeting spd5, cyk-1, and pfn-1 from the Kamath feeding library (Kamath et al. 2003). The bacteria targeting ani-1 is from the Glotzer lab at the University of Chicago. The RNAi sequence spans residues 40–170 aa and is cloned into the KpnI site of L4440. Briefly, we grew bacteria to log phase in LB with 50 μ g/ml ampicillin and then seeded ~300 μ l of these bacteria onto NGM plates supplemented with 50 μ g/ml ampicillin and 1 mM IPTG. For double RNAi treatments, we grew the bacteria for both treatments separately to log phase, mixed equal volumes of the individual bacteria cultures and then seeded ~300 μ l of culture onto NGM plates supplemented with 50 μ g/ml ampicillin and 1 mM IPTG. We incubated the seeded plates at room temperature (21–23°C) for 2 d and then stored them at 4°C for up to 1 wk before use. We transferred L4 larvae to feeding plates and then cultured them at room temperature (21–23°C) for GFP::ROK; Lifeact::mCherry and GFP::UTR; NMY-2::mRFP and at 16°C for GFP::ROK; *nmy-2(ts)*. The culture time for feeding strains are 16-22 h, with 3 exceptions. spd-5 (RNAi); cyk-1 (RNAi) is 14–18 h. spd-5 (RNAi); pfn-1 (RNAi) is 8–22 h. spd-5 (RNAi); pfn-1 (RNAi) is 8–22 h.

2.4.3 Microscopy

We performed imaging on a Nikon Ti-E inverted microscope equipped with a Yokogawa CSU-X1 spinning disk scan head, a motorized TIRF illuminator, and a Ti-ND6-PFS Perfect Focus Unit. A laser merge module (Spectral Applied Research) controlled tunable delivery of 481-nm and 561-nm laser excitation from 50 mW solidstate lasers (Coherent Technology) to either the confocal scanhead or the TIRF illuminator with fast (ms) control of laser power and switching between lasers. All image acquisition was controlled by Metamorph software. We collected images using a Nikon CFI Apo 1.45 NA oil immersion objective combined with 1.5× intermediate magnification onto an Andor iXon3 897 EMCCD camera.

2.4.4 Imaging conditions

We mounted embryos as described previously (Sailer et al. 2015) in 3–5 μ l of standard egg salts (118 mM NaCl, 48 mM KCl, 3 mM CaCl2, 3 mM MgCl2, 5 mM HEPES, pH 7.2) on 3% agarose pads (3% agarose in standard egg salts) under #1.5 coverslips. For all experiments, we imaged embryos in early establishment phase (mitotic interphase), during which there is no qualitative change in pulsatile RhoA dynamics in control [spd-5(RNAi)] embryos. To quantify patterns of RhoA excitation and correlations with F-actin levels under different RNAi perturbations, we used a strain coexpressing GFP::ROK (Bell et al. 2020) and Lifeact::mCherry (Pohl et al. 2012). To quantify patterns of RhoA excitation in a myosin mutant background in response to different RNAi perturbations, we used a temperature-sensitive myosin mutant strain (*myo(ts)*; (Liu et al. 2010) expressing GFP::ROK. For both experiments, we used spinning disk confocal imaging and alternated between 488 nm (30% laser power, 300 ms exposure time) and 561 nm (50% laser power, 300 ms exposure time) excitation. To visualize actomyosin network dynamics in response to different RNAi perturbations, we imaged worms expressing mKate::NMY-2 and GFP::UTR with near-TIRF illumination as described previously ((Li and Munro 2021), alternating between 488 nm (20% laser power, 200 ms exposure time) and 561 nm (30% laser power, 200 ms exposure time) excitation. To visualize GFP::ROK and F-actin in control [spd-5(RNAi)] embryos, we used near-TIRF illumination, alternating between 488 nm (30% laser power,300 ms exposure time) and 561 nm (50% laser power, 300 ms exposure time) excitation. We performed all imaging experiments at room temperature (21–23°C), except for temperature-sensitive myosin mutants (*myo(ts)*, which we imaged at 25°C.

2.4.5 Kymograph analysis

To produce the kymographs shown in Figures 1C, 2E, 5B, and 7B and Supplemental Figures S1, S2, S5A, and S6B, we rotated images so that the anterior–posterior axis of the embryo coincided with the horizontal (x) image axis. We selected rectangular regions aligned with the x image axis whose width (in x) coincided with the embryonic ROI and whose height (in y) was 10 pixels. From the original image stack, we extracted an xyt substack corresponding to this rectangular region; we resliced this stack with respect to the xt plane, and then we used a maximum-intensity projection to collapse the individual slices in y to obtain a kymograph in x

versus t.

2.4.6 Image analysis

We performed all image processing using custom functions written in Python. The code is available at https://github.com/baixue0/ excitability. We developed custom image segmentation algorithms to identify regions of RhoA excitation in noisy microscopy images by thresholding the temporal derivative of smoothed GFP::ROK intensities. This approach transforms ROK levels to binary masks, allowing us to quantify the temporal recurrence and spatial spread of RhoA excitation at pixel resolution.

2.4.7 Segmenting regions of RhoA excitation

We performed all analyses described below on data collected within a standard observation window lasting 120 s. To correct for photobleaching, we measured M1(n), the mean intensity of ROK::GFP for all pixels in the embryo at frame n over the 120 s observation window (n = 1, 2, ..., 100 frames). We then calculated its temporal trend M2(n) by applying the Scipy filter savgol_filter (window_length = 6 s, polyorder = 1) to M1(n). To calculate the correction factor C(n), we subtracted M2(n) from its mean value. We then added C(n) to the raw intensity value for each pixel at frame n. To determine local regions of RhoA excitation within individual frames, we first smoothed each frame of the image stack in space and time. We smoothed in space using sequential application of the Scipy functions medianBlur (5 pixels diameter) and GaussianBlur (19 pixels diameter). We smoothed in time using sequential application of a 5-frame centered moving average, followed by a 2-frame grouped average). We then computed a pixelwise temporal difference signal using a 5-frame (6s) window centered on the current frame. We set the derivative time window to be half the duration of the rapid rising phase so that short-lived intensity fluctuations from other sources were suppressed. Then we scaled the temporal difference values at each pixel by the standard deviation of the temporal difference, taken over all pixels in all frames, to obtain the normalized temporal difference. Finally, we thresholded the normalized temporal difference at each pixel to obtain a binary mask with 1 representing pixels above threshold and 0 representing below threshold.

To determine appropriate threshold values, for each phenotype we measured the average

normalized temporal difference signal within manually labeled pulsing regions (∼25 disks with 1 μm diameter per embryo) over the duration of a pulse. We used 40% of the average peak signal for all conditions, which captured distinct pulses with different amplitudes while excluding noisy fluctuations. Using these binary masks, we defined excitation pixels as pixels that are above the threshold in the current frame and new excitation pixels as pixels that are above threshold in the current frame, but below the threshold in the previous frame. Similarly, in a given frame, we defined excitation regions as contiguous groups of excitation pixels and new excitation regions as contiguous groups of new excitation pixels.

Measuring the distribution of frequency and wait times between successive new excitations We computed the distribution of frequencies over all pixels by counting the number of excitation events recorded at each pixel and dividing by the duration of the observation time window. For each new excitation event at a given pixel, we monitored the pixel's excitation state over the following 60 s. If we detected a new excitation event within 60 s, we computed the wait time as the difference between the first and the second excitation times. We thus report the fraction of pixels for which the wait time >60 s and the distribution of wait times over all pairs of excitation events with wait times <60 s.

2.4.8 Linking excitation regions across frames

We considered two excitation regions to be linked across consecutive frames if their area of overlap was greater than 8 pixels and greater than 10% of the total area of both regions. Note that this definition allows merging and splitting of excitation regions. We compute linked excitation regions by extending pairwise linkage recursively, backward and forward in time using the connected components function from the Python package networkx. To compute the duration of linked excitation regions, we determined the first frame (f0) and the last frame (fl) in which an individual excitation region belonging to the linked group appeared. Then we computed duration = 1.2*(fl–f0). To plot the cumulative area of linked excitation regions versus time, for each frame f in the image sequence we computed the total number of unique pixels belonging to excitation regions appearing in frames preceding f. To determine the total areas, we computed the total number of unique pixels belonging to all excitation regions.

2.4.9 Measuring the speed of advance of local excitation fronts

In each frame, we identified the boundaries of excitation regions whose area was larger than 0.04 μm^2. We identified a set of points spaced at $\sim$0.5 μm intervals along the boundary. We considered that a boundary point belongs to an excitation front if it lies within a new excitation region. For every boundary point along an excitation front, we constructed a local displacement vector extending from that point, outward normal to the boundary, and intersecting the nearest excitation boundary in the next frame. We then took the instantaneous speed of advance to be the length of this displacement vector divided by time between frames (1.2 s). We divided boundary points into "fast" and "slow" groups based on instantaneous velocity using 0.25 μm/s as a threshold.

2.4.10 Sampling pixels ahead of advancing excitation fronts

At each time point, we selected all boundary points belonging to excitation fronts. For each point, we defined a rectangular region extending 0.5 μm from the boundary point in the outward normal direction (i.e., ahead of the advancing front) and extending 0.6 μm in the perpendicular direction centered on the boundary point. Then we sampled F-actin intensity values or time derivatives on all pixels within the rectangular region at different times relative to the current time point; that is, relative to when the advancing front begins to enter the rectangular region—which we refer to as "time of entry." We constructed plots of average F-actin intensity or time derivatives relative to time of entry for "fast" and "slow" advancing fronts by averaging these measurements over all "fast" or "slow" boundary points.

2.4.11 Measuring the tACF of GFP::ROK intensities

For each pixel in the embryo, we extracted a time series of smoothed ROK intensities measured at 1.2-s intervals over 120 s. Then we computed the standard time autocorrelation function (tACF) using the Python package statsmodels.tsa.stattools.acf. The tACF shown in Supplemental Figure S3 is the average over all pixels in embryos of a given phenotype.

2.4.12 Simulating the temporal dynamics of the FHN model with stochastic forcing

We considered a nonspatial stochastic version of the FHN model (equations shown in Supplemental Figure S4A), where ξt defines a random sequence of perturbations, each described by a rectangle function R(h,d) with amplitude h = 0.1 and duration d = 3 s. For each simulation, we selected seven initiation times randomly from a uniform probability distribution over the simulation time window (0– 240 s), yielding an average perturbation frequency of 0.03/s. We fixed values for parameters (I = 0.5, b = 0.6, $\tau = 10$) and then varied the value of α to tune the deterministic dynamics of the system from excitable to oscillatory. For each value of α, we repeated the simulation 16,384 times. For each simulation, we thresholded the temporal derivative of u to identify individual excitation events. Then we computed frequency and wait time distributions using the same method described above for RhoA excitations.

CHAPTER 3

IMAGE ANALYSIS TOOLS

Statement of contribution: I implemented all the data analysis and simulations in Python. The code is available at `https://github.com/baixue0/excitability`. A tutorial containing the code and result of each step of image analysis is available at `https://baixue0.github.io/excitability/build/html/Example_jupyter_notebook.html`.

3.1 Pipeline architecture

The goal of this image analysis pipeline is to quantify differences in the local temporal dynamics and spatial spread of excitation and its relationship with changes in the level of F-actin. The general approach of detecting rapid changes in noisy signals can be adopted for other systems exhibiting pulses of activity.

The pipeline architecture is shown in Figure 3.1. First, I identified pixels in the rapid rising phase of pulsatile ROK::GFP accumulation by calculating its temporal derivative. Second, I assigned a binary value to each pixel to indicate whether the temporal derivative of a given pixel is above the threshold value (in the excited state). The threshold value used in the second step depends on the amplitude of the temporal derivative for all embryos of the same phenotype. Then I used the binary excitation videos to calculate the frequency and waittime of new excitations as well as edge velocity and extent of wave-like spread of excitation regions. Using the excitation masks and F-actin intensities, I calculated the average F-actin intensity of pixels in new excitation pixels before and after its excitation.

3.2 Using python dictionary to organize data

The intermediate steps in the pipeline generates data, that often needs to be used for later steps in the pipeline. It can be challenging to keep track of the meaning of each value in the saved data file. I propose saving the output of each step as python dictionaries. A python dictionary is composed of multiple items. Each item has a key and a value. The value can be an array or any custom objects.

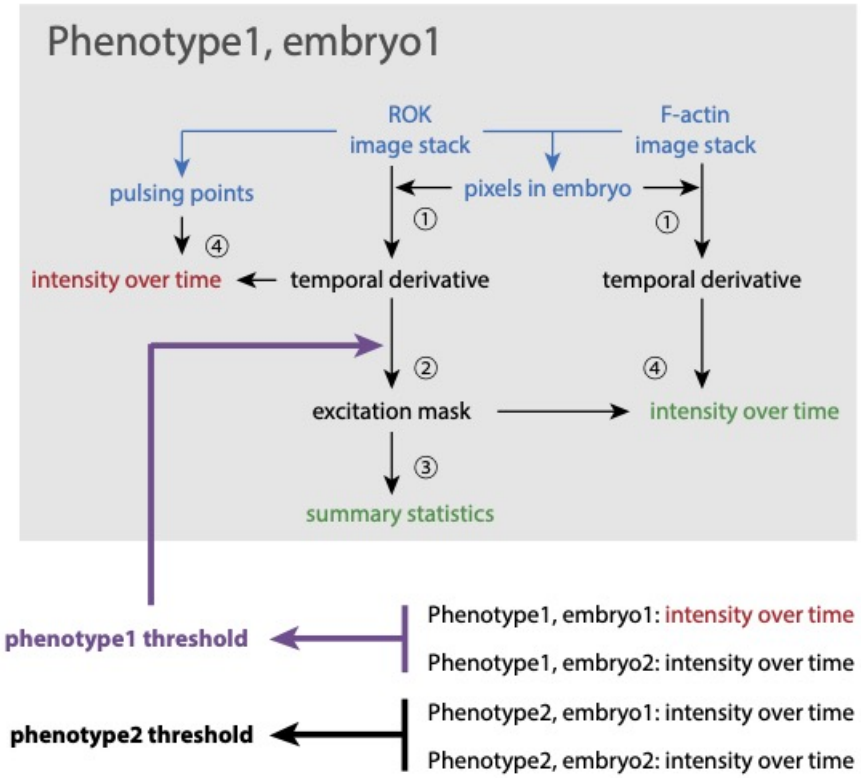

Figure 3.1. Image analysis pipeline. The gray box shows the data and image processing for one embryo. The texts represent data, with blue indicating input and green indicating output of the pipeline. Red texts indicate that they are the same data. Purple indicates that calculation of the threshold requires intensity overtime for all embryos of the same phenotype. Circled numbers represents image processing steps.

Table 3.1: Name of python functions in Figure 3.1

step number	step name	functions
1	compensate for photobleach over time	measure.segmentation.bleach_correction
1	calculate temporal derivative image stack	measure.segmentation.group_diff
2	apply threshold to get excitation imagestack	measure.segmentation.excitation
3	measure pixel-wise temporal dynamics from new excitation imagestack	measure.recurrence.frequency measure.recurrence.waittime
3	measure spatial spread from excitation imagestack and new excitation imagestack	measure.contour.findContours measure.edgespeed.point_velocity measure.link.connected_components
4	measure pixel intensity at a range of time offsets	measure.pixel_intensity.intensity_ts

For a single embryo, I identified the key variables that communicate between steps and give them unique and intuitive names. The output variables of each step are packed in a dictionary with the name of the variable as the dictionary key and the value of the variable as the dictionary value. Output dictionaries from different steps of the same embryo can be combined to use as input data for another step. Packing variable in a dictionary is implemented using a python decorator. The content of the decorator and usage examples are shown in Figure 3.2.

After iterating through all embryos for a given step, output dictionaries from different embryos can be combined together in a larger dictionary of the format `{ID0:{'x':x,'y':y},ID1:{'x':x,'y':y},...}`. The keys ID0 and ID1 represent the unique name of each embryo. The values x and y are output variables from different steps of the pipeline.

Calculation of the summary statistics require the same output variable from all embryos. So the previous dictionary needs to be reordered into `{'x':{ID0:x,'ID1':x},'y':{ID0:y,'ID1':y},...}`. This conversion is implemented through a single line of code `pandas.DataFrame(dict_to_convert).transpose().to_dict()`. Each item in the converted dictionary can be saved as a separate file. To calculate a summary statistic that depends on x but not y, only the file corresponding to x needs to be loaded.

```python
def return_dict(func):
    """convert returned variables to a dictionary, when used as a decorator

    Parameters
    ----------
    func : function
        the function to decorate

    Returns
    -------
    dict
        variables returned by the decorated function as a dictionary

    Note
    --------
    Results from different functions can be combined by

    .. code-block:: python

        dict(**dict1,**dict2)

    """

    import functools
    @functools.wraps(func)
    def wrapper(*args, **kwargs):
        # get the names of the returned variables
        import inspect
        lines = inspect.getsource(func).replace(' ','').split('\n')
        lines = list(filter(None, lines))
        vnames = lines[-1][len('return'):].split(',')

        # execute function
        value = func(*args, **kwargs)
        if value is None:
            return
        if not isinstance(value, tuple):# when a single variable is returned
            return {vnames[0]:value}

        # construct dictionary of the returned variables
        result = dict(zip(vnames,value))
        return result
    return wrapper
```

```python
@ return_dict
def func(x):
    y = x*2
    return y

func(1)
```

```
{'y': 2}
```

```python
@ return_dict
def func(*args):
    times2 = [x*2 for x in args]
    times3 = [x*3 for x in args]
    return times2,times3

func(1,2)
```

```
{'times2': [2, 4], 'times3': [3, 6]}
```

Figure 3.2. Return result as dictionary. The first gray box contain the source code for the decorator. The next two gray boxes are usage examples.

CHAPTER 4

DISCUSSION

4.1 Inhibition from F-actin partially explains the transition from focal pulses to traveling waves of RhoA activation

4.1.1 Overview

Pulsatile RhoA dynamics exhibits a range of spatiotemporal patterns. Different patterns are associated with different biological functions. A key question is whether the same pulse circuit can be tuned to generate the range of observed patterns. Focal pulses and traveling waves are two common types of RhoA activation patterns. I focused on focal pulses in the *C. elegans* zygote (Michaux et al. 2018) and traveling waves in frog and starfish (Bement et al. 2015; Michaud, Leda, et al. 2022) because they share the same underlying pulse circuit involving active RhoA and F-actin. The shared circuit is made up of a positive feedback in which active RhoA promotes its own activation and a delayed negative feedback through F-actin dependent recruitment of RhoA GAP. Pulsatile RhoA in *C. elegans* form focal pulses while pulsatile RhoA in *C. elegans* form traveling waves. I am interested in how the circuit is tuned differently to generate focal pulses and traveling waves.

I used the one-cell *C. elegans* embryo as a model system to reproduce pattern variants and to study the tuning mechanisms underlying the pattern variants. I found that the knockdown of formin or anillin generates patterns that resemble synchronous oscillations and traveling waves respectively. This shows that the same underlying circuit operating in *C. elegans* embryos can produce a range of different pattern variants.

I measured the extent to which the observed RhoA activation patterns can be explained by inhibition from F-actin. The inhibitory rule of F-actin predicts that the average F-actin level of all excitation regions should decrease before excitation and that reduction in the average F-actin level of regions near faster spreading fronts should be larger. Thus, inhibition from F-actin alone could explain traveling waves and synchronous oscillations but not focal pulses of activation.

The transition from focal pulses to synchronous oscillations or traveling waves is partially consistent with the hypothesis that inhibition from F-actin governs RhoA activation pattern. (i) Consistent with the hypothesis, higher overall F-actin levels reduced the frequency and spread of RhoA activation. (ii) In wildtype embryos, focal pulses occur in regions with a wide range of inhibition levels, both in "depletion regions" containing lower levels of F-actin and near existing actomyosin foci where F-actin levels are persistently high. The second case suggests that additional positive feedback mechanisms promote RhoA activation. In summary, the initiation of focal pulses is governed by a strong global inhibition and additional positive feedback from existing focal pulses. (iii) Activator inhibitor reaction diffusion models predict that traveling waves involve faster diffusing the activator while focal pulses involve faster diffusing the inhibitor. The activator active RhoA can diffuse in the membrane or bind immobile effectors. The inhibitor RGA-3/4 are immobilized through binding to F-actin. The transition from traveling waves to focal pulses can be achieved through immobilizing active RhoA and/or increasing the range of inhibition. I will discuss potential mechanisms for each of the three hypothesized mechanisms.

4.1.2 Additional positive feedback

Anillin is a good candidate for mediating the additional positive feedback. This hypothesis is supported by three observations. Anillin binds myosin and localizes to the foci (Tse et al. 2011; Maddox, Lewellyn, et al. 2007; Tse et al. 2011; Michaux et al. 2018). The existence of actomyosin foci depends on anillin. The amplitude of Rho Kinase accumulation is reduced in anillin KD embryos.

Anillin is required for contractile processes, such as the cytokinetic ring (Field and Alberts 1995; Piekny and Glotzer 2008; Straight et al. 2005) and adherens junctions (Reyes et al. 2014). Anillin is predicted to bind many targets based on its sequence, including F-actin, myosin, RhoA, RhoA GEF and RhoA GAP, septins, phospholipids and microtubules. I will discuss three possible positive feedback mechanisms through recruitment of septins, phospholipids and RhoA GEF respectively. Genetically modifying anillin sequences to subtract or add binding sites could disentangle these three potentially interconnected feedbacks.

The positive feedback could involve anillin directly recruiting RhoA GEF which then activates more RhoA. Examining whether RhoA GEF localizes to the foci can be an initial test.

Anillin could mediate a positive feedback by crosslinking the actomyosin network to the septins. Septins are conserved GTP-binding proteins and form hetero-oligomers to serve as scaffolds to recruit proteins at the plasma membrane and in the cytosol (Spiliotis and Nakos 2021). In the cytokinetic ring, anillin recruits septins to form dense networks of both actin filaments and septin hetero-oligomers. This network, in turn, recruits more anillin (Maddox, Lewellyn, et al. 2007). This positive feedback amplifies stochastic fluctuations in the distribution of anillin to promote the asymmetric closure of the contractile ring in *C. elegans*. Septin dependent positive feedback could contribute to the formation and stabilization of the actomyosin foci.

Finally, reducing the cortical dissociation of active RhoA by binding to anillin could serve as a positive feedback (Budnar et al. 2019). At the molecular level, cycles of the following sequence of events increase the membrane dwell time of active RhoA. Anillin concentrates phosphoinositide-4,5-P_2 (PIP2). Active RhoA binds anillin temporally, then dissociates from anillin and finally is retained at the membrane in its free state by PIP2. Dense anillin accumulation in the foci may retain a pool of active RhoA in PIP2 patches, which could diffuse into neighboring regions to ignite new pulses.

4.1.3 Immobilizing active RhoA

The effective mobility of active RhoA can be reduced by binding to immobile RhoA effectors, such as those that also bind the actomyosin cortex. The small difference in the distribution of local spreading speed for focal pulses and traveling waves suggests that reduction in active RhoA effective mobility is small. However, additional tests are required to rule out this possibility.

4.1.4 Increasing the range of inhibition

Formin mediated actin assembly could outrun the diffusion of active RhoA to generate focal pulses. This hypothesis is theoretically plausible because formins elongate actin filaments at around 1.5 $\mu m/s$ (Costache et al. 2021; Li and Munro 2021) while active RhoA diffuses in the membrane at around $0.1\mu m^2/s$. The exact conditions for faster spread of inhibition can be

solved through modeling. Another test involves reducing the speed of formin mediated actin assembly through profilin KD. The expectation is that RhoA should form traveling waves when formins are slow enough. The caveat is that reduced overall F-actin assembly could change more than the speed of formins. The final test involves measuring whether the time delay between RhoA activation and F-actin assembly is negatively correlated with the distance to the center of actomyosin foci. The time delay between RhoA activation and F-actin assembly should be positive near the initiation region and negative near the boundaries of the pulse.

4.2 Molecularization of pattern formation models in biology requires balance between abstract models and molecular reality

This project is one of the many studies that try to reduce the gap between minimal theoretical models and complex molecular circuits involving many feedbacks. The journey often starts with testing how much of the pattern can be explained with minimal theoretical models. In this project, the mutant patterns are in general consistent with the model while the wildtype pattern is only partially consistent. The failure to explain all observations with the minimal theoretical model is not a surprise. The reason is that the molecular reality likely involves a large network of molecules and interconnected feedbacks, which can take several decades of collaborative work to disentangle.

I proposed possible mechanisms that can explain the observations inconsistent with the model. Adding this additional complexity may improve the accuracy of the model, but testing the new hypothesis takes time and effort. If the system does not serve important function but has high probability of being conserved through evolution, one need to decide how much complexity is appropriate to preserve the ability to generalize to other biological systems. This project belongs to this category because the active RhoA and GAP RGA-3/4 circuit is conserved in *C. elegans*, frog and starfish (Michaud, Leda, et al. 2022). If the system serve important biological function, one can add as much complexity as necessary until the hypothesized interactions are sufficient to reproduce the biological patterns. The ultimate test can be reconstitution experiments using artificial membranes and purified proteins to reproduce the biological pattern and design genetically modify proteins to reproduce model predicted patterns.

4.3 Challenges in image collection and analysis

Quantification of dynamic patterns is common in cell and developmental biology. Such projects often involve the following steps. The protein of interest is labeled with fluorescent tags such as GFP and RFP. Cells or tissues expressing the fluorescent protein are then imaged using fluorescent microscopes at evenly spaced time points. In the resulting videos, pixel intensities represent local concentrations of the protein of interest. Quantifications of spatiotemporal patterns based on pixel intensity share many technical challenges. I hope what I learned through trial and error will be helpful for future researchers.

The image analysis goal in my project is to identify robust metrics that distinguish focal pulses, synchronous oscillations and traveling waves. Segmentation of pixels in the videos into pulsing and non-pulsing regions is the major challenge and could be generalizable to other segmentation problems. I will discuss three challenges: selecting the appropriate imaging conditions, transformations of the videos to amplify signals that best distinguish pulsing pixels and non-pulsing pixels, and the method to choose the threshold value for each embryo.

I used two imaging conditions. I chose near-TIRF microscopy to start with because of its relatively high signal to noise ratio and slow photobleaching rate. However, for one mutant phenotype, the near-TIRF microscopy can not capture the entire cortex at the same time. So I had to switch to spinning disk microscopy that is not as sensitive to the depth of the sample. My advice is to sample several imaging conditions and phenotypes before investing a lot of time collecting data for biological duplicates.

Amplifying the signals of interest in noisy microscopy images often involve many transformation steps. Each step is defined by hyperparameters such as type, parameters, and order of transformations. The number of hyperparameters increases very quickly as more transformations are included in the analysis pipeline. Setting a concrete goal for the quality of segmentation can help avoid unnecessary optimizations.

Dealing with variations across biological replicates is the largest challenge for me. Due to the low signal to noise ratio in the data, the segmentation is sensitive to the threshold used. I initially determined the threshold by manually adjusting the threshold for each embryo so that the

segmentation seemed reasonable to my eyes. To improve reproducibility and consistency, I came up with a simple rule to determine the threshold value for biological replicas. I normalized the signal using summary statistics measured in the same embryo. I confirmed that the normalized signals in biological replicas have the same distribution so that the same threshold value can be applied. The thresholds are different across phenotypes because the amplitude of the signal varies across phenotypes. I estimated the amplitudes for all phenotypes by manually labeling pulsing regions. The threshold for each phenotype is determined by multiplying its measured amplitude with a tunable constant.

REFERENCES

Akiyama, Haruhiko et al. (Nov. 2002). "The transcription factor Sox9 has essential roles in successive steps of the chondrocyte differentiation pathway and is required for expression of Sox5 and Sox6". en. In: *Genes & Development* 16.21. Company: Cold Spring Harbor Laboratory Press Distributor: Cold Spring Harbor Laboratory Press Institution: Cold Spring Harbor Laboratory Press Label: Cold Spring Harbor Laboratory Press Publisher: Cold Spring Harbor Lab, pp. 2813–2828. ISSN: 0890-9369, 1549-5477. DOI: 10.1101/gad.1017802. URL: http://genesdev.cshlp.org/content/16/21/2813 (visited on 03/09/2022).

Albeck, John G., Gordon B. Mills, and Joan S. Brugge (Jan. 2013). "Frequency-Modulated Pulses of ERK Activity Transmit Quantitative Proliferation Signals". English. In: *Molecular Cell* 49.2. Publisher: Elsevier, pp. 249–261. ISSN: 1097-2765. DOI: 10.1016/j.molcel.2012.11.002. URL: https://www.cell.com/molecular-cell/abstract/S1097-2765(12)00933-1 (visited on 10/20/2021).

Aldrich, R. W., D. P. Corey, and C. F. Stevens (Dec. 1983). "A reinterpretation of mammalian sodium channel gating based on single channel recording". eng. In: *Nature* 306.5942, pp. 436–441. ISSN: 0028-0836. DOI: 10.1038/306436a0.

Aldrich, R. W. and C. F. Stevens (Feb. 1987). "Voltage-dependent gating of single sodium channels from mammalian neuroblastoma cells". eng. In: *The Journal of Neuroscience: The Official Journal of the Society for Neuroscience* 7.2, pp. 418–431. ISSN: 0270-6474.

Allard, Jun and Alex Mogilner (Feb. 2013). "Traveling waves in actin dynamics and cell motility." In: *Current Opinion in Cell Biology* 25.1, pp. 107–115. DOI: 10.1016/j.ceb.2012.08.012. URL: http://dx.doi.org/10.1016/j.ceb.2012.08.012 (visited on 09/17/2020).

Aoki, Kazuhiro et al. (Nov. 2013). "Stochastic ERK activation induced by noise and cell-to-cell propagation regulates cell density-dependent proliferation". eng. In: *Molecular Cell* 52.4, pp. 529–540. ISSN: 1097-4164. DOI: 10.1016/j.molcel.2013.09.015.

Arai, Yoshiyuki et al. (July 2010). "Self-organization of the phosphatidylinositol lipids signaling system for random cell migration". en. In: *Proceedings of the National Academy of Sciences* 107.27. Publisher: National Academy of Sciences Section: Biological Sciences, pp. 12399–

12404. ISSN: 0027-8424, 1091-6490. DOI: 10.1073/pnas.0908278107. URL: https://www.pnas.org/content/107/27/12399 (visited on 10/10/2021).

Asano, Yukako, Akira Nagasaki, and Taro Q.P. Uyeda (2008). "Correlated waves of actin filaments and PIP3 in Dictyostelium cells". en. In: *Cell Motility* 65.12. _eprint: https://onlinelibrary.wiley.com/doi/pd pp. 923–934. ISSN: 1097-0169. DOI: 10.1002/cm.20314. URL: https://onlinelibrary.wiley.com/doi/abs/10.1002/cm.20314 (visited on 04/01/2022).

Ashall, Louise et al. (Apr. 2009). "Pulsatile stimulation determines timing and specificity of NF-kappaB-dependent transcription". eng. In: *Science (New York, N.Y.)* 324.5924, pp. 242–246. ISSN: 1095-9203. DOI: 10.1126/science.1164860.

Azevedo, Dulce et al. (Sept. 2011). "DRhoGEF2 regulates cellular tension and cell pulsations in the Amnioserosa during Drosophila dorsal closure." In: *Plos One* 6.9, e23964. DOI: 10.1371/journal.pone.0023964. URL: http://dx.doi.org/10.1371/journal.pone.0023964 (visited on 04/09/2020).

Baird, Michelle A. et al. (Jan. 2017). "Local pulsatile contractions are an intrinsic property of the myosin 2A motor in the cortical cytoskeleton of adherent cells". In: *Molecular Biology of the Cell* 28.2. Publisher: American Society for Cell Biology (mboc), pp. 240–251. ISSN: 1059-1524. DOI: 10.1091/mbc.e16-05-0335. URL: https://www.molbiolcell.org/doi/10.1091/mbc.e16-05-0335 (visited on 09/02/2021).

Barnhart, Erin L. et al. (Jan. 2017). "Adhesion-Dependent Wave Generation in Crawling Cells". en. In: *Current Biology* 27.1, pp. 27–38. ISSN: 0960-9822. DOI: 10.1016/j.cub.2016.11.011. URL: https://www.sciencedirect.com/science/article/pii/S0960982216313367 (visited on 02/11/2022).

Batchelor, Eric, Alexander Loewer, et al. (May 2011). "Stimulus-dependent dynamics of p53 in single cells". eng. In: *Molecular Systems Biology* 7, p. 488. ISSN: 1744-4292. DOI: 10.1038/msb.2011.20.

Batchelor, Eric, Caroline S. Mock, et al. (May 2008). "Recurrent initiation: a mechanism for triggering p53 pulses in response to DNA damage". eng. In: *Molecular Cell* 30.3, pp. 277–289. ISSN: 1097-4164. DOI: 10.1016/j.molcel.2008.03.016.

Bell, Kathryn Rehain et al. (June 2020). "Novel cytokinetic ring components drive negative feedback in cortical contractility". In: *Molecular Biology of the Cell* 31.15. Publisher: American

Society for Cell Biology (mboc), pp. 1623–1636. ISSN: 1059-1524. DOI: 10.1091/mbc.E20-05-0304. URL: https://www.molbiolcell.org/doi/full/10.1091/mbc.E20-05-0304 (visited on 11/02/2020).

Bement, William M et al. (Nov. 2015). "Activator-inhibitor coupling between Rho signalling and actin assembly makes the cell cortex an excitable medium." In: *Nature Cell Biology* 17.11, pp. 1471–1483. DOI: 10.1038/ncb3251. URL: http://dx.doi.org/10.1038/ncb3251 (visited on 04/09/2020).

Bertet, Claire, Lawrence Sulak, and Thomas Lecuit (June 2004). "Myosin-dependent junction remodelling controls planar cell intercalation and axis elongation". eng. In: *Nature* 429.6992, pp. 667–671. ISSN: 1476-4687. DOI: 10.1038/nature02590.

Bezzi, Paola et al. (June 2004). "Astrocytes contain a vesicular compartment that is competent for regulated exocytosis of glutamate". eng. In: *Nature Neuroscience* 7.6, pp. 613–620. ISSN: 1097-6256. DOI: 10.1038/nn1246.

Bhattacharya, Sayak et al. (Aug. 2020). "Traveling and standing waves mediate pattern formation in cellular protrusions". In: *Science Advances* 6.32, eaay7682. ISSN: 2375-2548. DOI: 10.1126/sciadv.aay7682. URL: https://www.ncbi.nlm.nih.gov/pmc/articles/PMC7413732/ (visited on 10/11/2021).

Blanchard, Guy B., Jocelyn Étienne, and Nicole Gorfinkiel (Aug. 2018). "From pulsatile apicomedial contractility to effective epithelial mechanics". eng. In: *Current Opinion in Genetics & Development* 51, pp. 78–87. ISSN: 1879-0380. DOI: 10.1016/j.gde.2018.07.004.

Blankenship, J. Todd et al. (Oct. 2006). "Multicellular rosette formation links planar cell polarity to tissue morphogenesis". eng. In: *Developmental Cell* 11.4, pp. 459–470. ISSN: 1534-5807. DOI: 10.1016/j.devcel.2006.09.007.

Bois, Justin S, Frank Jülicher, and Stephan W Grill (Jan. 2011). "Pattern formation in active fluids." In: *Physical Review Letters* 106.2, p. 028103. DOI: 10.1103/PhysRevLett.106.028103. URL: http://dx.doi.org/10.1103/PhysRevLett.106.028103 (visited on 04/09/2020).

Bolado-Carrancio, Alfonso et al. (July 2020). "Periodic propagating waves coordinate RhoGTPase network dynamics at the leading and trailing edges during cell migration." In: *eLife* 9. ISSN:

2050-084X. DOI: 10.7554/eLife.58165. URL: https://elifesciences.org/articles/58165 (visited on 08/10/2020).

Brabant, G, K Prank, and C Schofl (July 1992). "Pulsatile patterns in hormone secretion." In: *Trends in Endocrinology and Metabolism* 3.5, pp. 183–190. DOI: 10.1016/1043-2760(92)90169-2. URL: http://dx.doi.org/10.1016/1043-2760(92)90169-2 (visited on 09/10/2020).

Bray, D. and J. G. White (Feb. 1988). "Cortical Flow in Animal Cells". In: *Science* 239.4842. Publisher: American Association for the Advancement of Science, pp. 883–888. DOI: 10.1126/science.3277283. URL: https://www.science.org/doi/10.1126/science.3277283 (visited on 04/08/2022).

Brenner, S. (May 1974). "The Genetics of Caenorhabditis Elegans". en. In: *Genetics* 77.1. Publisher: Genetics Section: INVESTIGATIONS, pp. 71–94. ISSN: 0016-6731, 1943-2631. URL: https://www.genetics.org/content/77/1/71 (visited on 11/01/2021).

Bretschneider, Till et al. (Apr. 2009). "The Three-Dimensional Dynamics of Actin Waves, a Model of Cytoskeletal Self-Organization". en. In: *Biophysical Journal* 96.7, pp. 2888–2900. ISSN: 0006-3495. DOI: 10.1016/j.bpj.2008.12.3942. URL: https://www.sciencedirect.com/science/article/pii/S0006349509004159 (visited on 03/29/2022).

Bronner, Marianne E. (Aug. 2012). "Formation and migration of neural crest cells in the vertebrate embryo". In: *Histochemistry and cell biology* 138.2, pp. 179–186. ISSN: 0948-6143. DOI: 10.1007/s00418-012-0999-z. URL: https://www.ncbi.nlm.nih.gov/pmc/articles/PMC3425661/ (visited on 03/05/2022).

Budnar, Srikanth et al. (June 2019). "Anillin Promotes Cell Contractility by Cyclic Resetting of RhoA Residence Kinetics". en. In: *Developmental Cell* 49.6, 894–906.e12. ISSN: 15345807. DOI: 10.1016/j.devcel.2019.04.031. URL: https://linkinghub.elsevier.com/retrieve/pii/S1534580719303284 (visited on 10/24/2020).

Busa, W B and R Nuccitelli (Apr. 1985). "An elevated free cytosolic Ca2+ wave follows fertilization in eggs of the frog, Xenopus laevis." In: *Journal of Cell Biology* 100.4, pp. 1325–1329. ISSN: 0021-9525. DOI: 10.1083/jcb.100.4.1325. URL: https://doi.org/10.1083/jcb.100.4.1325 (visited on 02/23/2022).

Cai, Long, Chiraj K. Dalal, and Michael B. Elowitz (Sept. 2008). "Frequency-modulated nuclear localization bursts coordinate gene regulation". eng. In: *Nature* 455.7212, pp. 485–490. ISSN: 1476-4687. DOI: 10.1038/nature07292.

Carlsson, Anders E. (June 2010). "Dendritic Actin Filament Nucleation Causes Traveling Waves and Patches". In: *Physical Review Letters* 104.22. Publisher: American Physical Society, p. 228102. DOI: 10.1103/PhysRevLett.104.228102. URL: https://link.aps.org/doi/10.1103/PhysRevLett.104.228102 (visited on 02/25/2022).

Cavanaugh, Kate E. et al. (Jan. 2020). "RhoA Mediates Epithelial Cell Shape Changes via Mechanosensitive Endocytosis". eng. In: *Developmental Cell* 52.2, 152–166.e5. ISSN: 1878-1551. DOI: 10.1016/j.devcel.2019.12.002.

Chang, Jeremy B. and James E. Ferrell Jr (Aug. 2013). "Mitotic trigger waves and the spatial coordination of the Xenopus cell cycle". en. In: *Nature* 500.7464. Bandiera_abtest: a Cg_type: Nature Research Journals Number: 7464 Primary_atype: Research Publisher: Nature Publishing Group Subject_term: Cell biology Subject_term_id: cell-biology, pp. 603–607. ISSN: 1476-4687. DOI: 10.1038/nature12321. URL: https://www.nature.com/articles/nature12321 (visited on 11/28/2021).

Charras, Guillaume and Ewa Paluch (Sept. 2008). "Blebs lead the way: how to migrate without lamellipodia". eng. In: *Nature Reviews. Molecular Cell Biology* 9.9, pp. 730–736. ISSN: 1471-0080. DOI: 10.1038/nrm2453.

Chen, Yu and Alexander F Schier (Dec. 2002). "Lefty Proteins Are Long-Range Inhibitors of Squint-Mediated Nodal Signaling". en. In: *Current Biology* 12.24, pp. 2124–2128. ISSN: 0960-9822. DOI: 10.1016/S0960-9822(02)01362-3. URL: https://www.sciencedirect.com/science/article/pii/S0960982202013623 (visited on 03/08/2022).

Choi, Won-Gyu et al. (Apr. 2014). "Salt stress-induced Ca2+ waves are associated with rapid, long-distance root-to-shoot signaling in plants". en. In: *Proceedings of the National Academy of Sciences* 111.17. Publisher: National Academy of Sciences Section: Biological Sciences, pp. 6497–6502. ISSN: 0027-8424, 1091-6490. DOI: 10.1073/pnas.1319955111. URL: https://www.pnas.org/content/111/17/6497 (visited on 02/23/2022).

Clay, John R (May 2005). "Axonal excitability revisited." In: *Progress in Biophysics and Molecular Biology* 88.1, pp. 59–90. DOI: 10.1016/j.pbiomolbio.2003.12.004.

URL: http://dx.doi.org/10.1016/j.pbiomolbio.2003.12.004 (visited on 04/12/2020).

Clément, Raphaël et al. (Oct. 2017). "Viscoelastic Dissipation Stabilizes Cell Shape Changes during Tissue Morphogenesis". en. In: *Current Biology* 27.20, 3132–3142.e4. ISSN: 0960-9822. DOI: 10.1016/j.cub.2017.09.005. URL: https://www.sciencedirect.com/science/article/pii/S0960982217311697 (visited on 03/06/2022).

Clutterbuck, Arthur (Feb. 1970). "Synchronous Nuclear Division and Septation in Aspergillus nidulans". In: *Journal of general microbiology* 60, pp. 133–5. DOI: 10.1099/00221287-60-1-133.

Copos, Calina and Alex Mogilner (July 2020). "A hybrid stochastic–deterministic mechanochemical model of cell polarization". In: *Molecular Biology of the Cell* 31.15. Publisher: American Society for Cell Biology (mboc), pp. 1637–1649. ISSN: 1059-1524. DOI: 10.1091/mbc.E19-09-0549. URL: https://www-molbiolcell-org.proxy.uchicago.edu/doi/10.1091/mbc.E19-09-0549 (visited on 03/17/2022).

Cornell-Bell, Ann H. et al. (Jan. 1990). "Glutamate Induces Calcium Waves in Cultured Astrocytes: Long-Range Glial Signaling". In: *Science* 247.4941. Publisher: American Association for the Advancement of Science, pp. 470–473. DOI: 10.1126/science.1967852. URL: https://www.science.org/doi/10.1126/science.1967852 (visited on 02/23/2022).

Cowan, Carrie R. and Anthony A. Hyman (Sept. 2004). "Centrosomes direct cell polarity independently of microtubule assembly in C. elegans embryos". eng. In: *Nature* 431.7004, pp. 92–96. ISSN: 1476-4687. DOI: 10.1038/nature02825.

Curran, Scott et al. (Nov. 2017). "Myosin II Controls Junction Fluctuations to Guide Epithelial Tissue Ordering". en. In: *Developmental Cell* 43.4, 480–492.e6. ISSN: 1534-5807. DOI: 10.1016/j.devcel.2017.09.018. URL: https://www.sciencedirect.com/science/article/pii/S1534580717307712 (visited on 03/06/2022).

Dekoninck, Sophie and Cédric Blanpain (Jan. 2019). "Stem cell dynamics, migration and plasticity during wound healing". en. In: *Nature Cell Biology* 21.1. Number: 1 Publisher: Nature Publishing Group, pp. 18–24. ISSN: 1476-4679. DOI: 10.1038/s41556-018-0237-

6. URL: https://www.nature.com/articles/s41556-018-0237-6 (visited on 03/05/2022).

Dickinson, Daniel J. et al. (2017). "A Single-Cell Biochemistry Approach Reveals PAR Complex Dynamics during Cell Polarization". eng. In: *Developmental Cell* 42.4, 416–434.e11. ISSN: 1878-1551. DOI: 10.1016/j.devcel.2017.07.024.

DiFrancesco, D (1993). "Pacemaker mechanisms in cardiac tissue." In: *Annual Review of Physiology* 55, pp. 455–472. DOI: 10.1146/annurev.ph.55.030193.002323. URL: http://dx.doi.org/10.1146/annurev.ph.55.030193.002323 (visited on 04/11/2020).

Ding, Wei Yung et al. (May 2017). "Plastin increases cortical connectivity to facilitate robust polarization and timely cytokinesis". In: *The Journal of Cell Biology* 216.5, pp. 1371–1386. ISSN: 0021-9525. DOI: 10.1083/jcb.201603070. URL: https://www.ncbi.nlm.nih.gov/pmc/articles/PMC5412556/ (visited on 10/21/2020).

Dockery, J. D. and J. P. Keener (Apr. 1989). "Diffusive Effects on Dispersion in Excitable Media". In: *SIAM Journal on Applied Mathematics* 49.2. Publisher: Society for Industrial and Applied Mathematics, pp. 539–566. ISSN: 0036-1399. DOI: 10.1137/0149031. URL: https://epubs.siam.org/doi/abs/10.1137/0149031 (visited on 10/11/2021).

Doubrovinski, K. and K. Kruse (Dec. 2011). "Cell Motility Resulting from Spontaneous Polymerization Waves". In: *Physical Review Letters* 107.25. Publisher: American Physical Society, p. 258103. DOI: 10.1103/PhysRevLett.107.258103. URL: https://link.aps.org/doi/10.1103/PhysRevLett.107.258103 (visited on 04/01/2022).

Ermentrout, G. B., S. P. Hastings, and W. C. Troy (1984). "Large Amplitude Stationary Waves in an Excitable Lateral-Inhibitory Medium". In: *SIAM Journal on Applied Mathematics* 44.6. Publisher: Society for Industrial and Applied Mathematics, pp. 1133–1149. ISSN: 0036-1399. URL: https://www.jstor.org/stable/2101400 (visited on 10/15/2021).

Ferrell, James E (Dec. 2013). "Feedback loops and reciprocal regulation: recurring motifs in the systems biology of the cell cycle". en. In: *Current Opinion in Cell Biology*. Cell cycle, differentiation and disease 25.6, pp. 676–686. ISSN: 0955-0674. DOI: 10.1016/j.ceb.2013.07.007. URL: https://www.sciencedirect.com/science/article/pii/S095506741300121X (visited on 11/25/2021).

Field, C.M. and B.M. Alberts (1995). "Anillin, a contractile ring protein that cycles from the nucleus to the cell cortex". English. In: *Journal of Cell Biology* 131.1, pp. 165–178. ISSN: 0021-9525. DOI: 10.1083/jcb.131.1.165.

Foe, V.E. and B.M. Alberts (May 1983). "Studies of nuclear and cytoplasmic behaviour during the five mitotic cycles that precede gastrulation in Drosophila embryogenesis". In: *Journal of Cell Science* 61.1, pp. 31–70. ISSN: 0021-9533. DOI: 10.1242/jcs.61.1.31. URL: https://doi.org/10.1242/jcs.61.1.31 (visited on 04/12/2022).

Franke, Josef D., Ruth A. Montague, and Daniel P. Kiehart (Dec. 2005). "Nonmuscle myosin II generates forces that transmit tension and drive contraction in multiple tissues during dorsal closure". eng. In: *Current biology: CB* 15.24, pp. 2208–2221. ISSN: 0960-9822. DOI: 10.1016/j.cub.2005.11.064.

Friedl, Peter and Katarina Wolf (May 2003). "Tumour-cell invasion and migration: diversity and escape mechanisms". en. In: *Nature Reviews Cancer* 3.5. Number: 5 Publisher: Nature Publishing Group, pp. 362–374. ISSN: 1474-1768. DOI: 10.1038/nrc1075. URL: https://www.nature.com/articles/nrc1075 (visited on 03/05/2022).

Gerisch, Günther et al. (Nov. 2004). "Mobile Actin Clusters and Traveling Waves in Cells Recovering from Actin Depolymerization". en. In: *Biophysical Journal* 87.5, pp. 3493–3503. ISSN: 0006-3495. DOI: 10.1529/biophysj.104.047589. URL: https://www.sciencedirect.com/science/article/pii/S000634950473814X (visited on 04/01/2022).

Gierer, A and H Meinhardt (Dec. 1972). "A theory of biological pattern formation." In: *Kybernetik* 12.1, pp. 30–39. DOI: 10.1007/BF00289234. URL: http://dx.doi.org/10.1007/BF00289234 (visited on 09/17/2020).

Glover, James D. et al. (July 2017). "Hierarchical patterning modes orchestrate hair follicle morphogenesis". en. In: *PLOS Biology* 15.7. Publisher: Public Library of Science, e2002117. ISSN: 1545-7885. DOI: 10.1371/journal.pbio.2002117. URL: https://journals.plos.org/plosbiology/article?id=10.1371/journal.pbio.2002117 (visited on 03/09/2022).

Goldman, L. and C. L. Schauf (June 1972). "Inactivation of the sodium current in Myxicola giant axons. Evidence for coupling to the activation process". eng. In: *The Journal of General Physiology* 59.6, pp. 659–675. ISSN: 0022-1295. DOI: 10.1085/jgp.59.6.659.

Gorfinkiel, Nicole et al. (June 2009). "Mechanical control of global cell behaviour during dorsal closure in Drosophila." In: *Development* 136.11, pp. 1889–1898. DOI: 10.1242/dev.030866. URL: http://dx.doi.org/10.1242/dev.030866 (visited on 04/09/2020).

Goryachev, Andrew B and Alexandra V Pokhilko (Apr. 2008). "Dynamics of Cdc42 network embodies a Turing-type mechanism of yeast cell polarity." In: *FEBS Letters* 582.10, pp. 1437–1443. ISSN: 0014-5793. DOI: 10.1016/j.febslet.2008.03.029. URL: http://dx.doi.org/10.1016/j.febslet.2008.03.029 (visited on 04/09/2020).

Gov, Nir S. and Ajay Gopinathan (Jan. 2006). "Dynamics of Membranes Driven by Actin Polymerization". en. In: *Biophysical Journal* 90.2, pp. 454–469. ISSN: 0006-3495. DOI: 10.1529/biophysj.105.062224. URL: https://www.sciencedirect.com/science/article/pii/S0006349506722263 (visited on 04/01/2022).

Graessl, Melanie et al. (Dec. 2017). "An excitable Rho GTPase signaling network generates dynamic subcellular contraction patterns". en. In: *Journal of Cell Biology* 216.12, pp. 4271–4285. ISSN: 0021-9525, 1540-8140. DOI: 10.1083/jcb.201706052. URL: https://rupress.org/jcb/article/216/12/4271/38828/An-excitable-Rho-GTPase-signaling-network (visited on 02/07/2021).

Gu, Zhenyu et al. (Mar. 1998). "The type I activin receptor ActRIB is required for egg cylinder organization and gastrulation in the mouse". en. In: *Genes & Development* 12.6. Company: Cold Spring Harbor Laboratory Press Distributor: Cold Spring Harbor Laboratory Press Institution: Cold Spring Harbor Laboratory Press Label: Cold Spring Harbor Laboratory Press Publisher: Cold Spring Harbor Lab, pp. 844–857. ISSN: 0890-9369, 1549-5477. URL: http://genesdev.cshlp.org/content/12/6/844 (visited on 03/24/2022).

Hamada, Hiroki, Masakatsu Watanabe, et al. (Jan. 2014). "Involvement of Delta/Notch signaling in zebrafish adult pigment stripe patterning". In: *Development* 141.2, pp. 318–324. ISSN: 0950-1991. DOI: 10.1242/dev.099804. URL: https://doi.org/10.1242/dev.099804 (visited on 03/25/2022).

Hamada, Hiroshi, Chikara Meno, et al. (Feb. 2002). "Establishment of vertebrate left–right asymmetry". en. In: *Nature Reviews Genetics* 3.2. Number: 2 Publisher: Nature Publishing Group, pp. 103–113. ISSN: 1471-0064. DOI: 10.1038/nrg732. URL: https://www.nature.com/articles/nrg732 (visited on 03/08/2022).

Hamill, Danielle R. et al. (Nov. 2002). "Centrosome maturation and mitotic spindle assembly in C. elegans require SPD-5, a protein with multiple coiled-coil domains". eng. In: *Developmental Cell* 3.5, pp. 673–684. ISSN: 1534-5807. DOI: 10.1016/s1534-5807(02)00327-1.

Hannezo, Edouard et al. (July 2015). "Cortical instability drives periodic supracellular actin pattern formation in epithelial tubes". In: *Proceedings of the National Academy of Sciences* 112.28. Publisher: Proceedings of the National Academy of Sciences, pp. 8620–8625. DOI: 10.1073/pnas.1504762112. URL: https://www.pnas.org/doi/full/10.1073/pnas.1504762112 (visited on 03/15/2022).

Hansen, Anders S. and Erin K. O'Shea (Nov. 2013). "Promoter decoding of transcription factor dynamics involves a trade-off between noise and control of gene expression". eng. In: *Molecular Systems Biology* 9, p. 704. ISSN: 1744-4292. DOI: 10.1038/msb.2013.56.

Hao, Nan and Erin K. O'Shea (Dec. 2011). "Signal-dependent dynamics of transcription factor translocation controls gene expression". eng. In: *Nature Structural & Molecular Biology* 19.1, pp. 31–39. ISSN: 1545-9985. DOI: 10.1038/nsmb.2192.

Hara, K. (June 1971). "Cinematographic observation of "surface contraction waves" (SCW) during the early cleavage of axolotl eggs". en. In: *Wilhelm Roux' Archiv für Entwicklungsmechanik der Organismen* 167.2, pp. 183–186. ISSN: 1432-041X. DOI: 10.1007/BF00577039. URL: https://doi.org/10.1007/BF00577039 (visited on 02/23/2022).

Hara, K., P. Tydeman, and M. Kirschner (Jan. 1980). "A cytoplasmic clock with the same period as the division cycle in Xenopus eggs". en. In: *Proceedings of the National Academy of Sciences* 77.1. Publisher: National Academy of Sciences Section: Research Article, pp. 462–466. ISSN: 0027-8424, 1091-6490. DOI: 10.1073/pnas.77.1.462. URL: https://www.pnas.org/content/77/1/462 (visited on 02/22/2022).

Hecht, Inbal, David A. Kessler, and Herbert Levine (Apr. 2010). "Transient Localized Patterns in Noise-Driven Reaction-Diffusion Systems". en. In: *Physical Review Letters* 104.15, p. 158301. ISSN: 0031-9007, 1079-7114. DOI: 10.1103/PhysRevLett.104.158301. URL: https://link.aps.org/doi/10.1103/PhysRevLett.104.158301 (visited on 04/30/2021).

Hille, B. (1976). "Gating in sodium channels of nerve". eng. In: *Annual Review of Physiology* 38, pp. 139–152. ISSN: 0066-4278. DOI: 10.1146/annurev.ph.38.030176.001035.

Hodgkin, A. L. and A. F. Huxley (Aug. 1952). "A quantitative description of membrane current and its application to conduction and excitation in nerve". eng. In: *The Journal of Physiology* 117.4, pp. 500–544. ISSN: 0022-3751. DOI: 10.1113/jphysiol.1952.sp004764.

Huang, Chuan-Hsiang et al. (Nov. 2013). "An excitable signal integrator couples to an idling cytoskeletal oscillator to drive cell migration". en. In: *Nature Cell Biology* 15.11. Bandiera_abtest: a Cg_type: Nature Research Journals Number: 11 Primary_atype: Research Publisher: Nature Publishing Group Subject_term: Cell migration;Cell signalling;Cytoskeleton;Dictyostelium discoideum Subject_term_id: cell-migration;cell-signalling;cytoskeleton;dictyostelium-discoideum, pp. 1307–1316. ISSN: 1476-4679. DOI: 10.1038/ncb2859. URL: https://www.nature.com/articles/ncb2859 (visited on 10/10/2021).

Imran Alsous, Jasmin et al. (Mar. 2021). "Dynamics of hydraulic and contractile wave-mediated fluid transport during Drosophila oogenesis". eng. In: *Proceedings of the National Academy of Sciences of the United States of America* 118.10, e2019749118. ISSN: 1091-6490. DOI: 10.1073/pnas.2019749118.

Inaba, Masafumi, Hiroaki Yamanaka, and Shigeru Kondo (Feb. 2012). "Pigment Pattern Formation by Contact-Dependent Depolarization". In: *Science* 335.6069. Publisher: American Association for the Advancement of Science, pp. 677–677. DOI: 10.1126/science.1212821. URL: https://www.science.org/doi/10.1126/science.1212821 (visited on 03/25/2022).

Jacinto, Antonio, Sarah Woolner, and Paul Martin (July 2002). "Dynamic analysis of dorsal closure in Drosophila: from genetics to cell biology". eng. In: *Developmental Cell* 3.1, pp. 9–19. ISSN: 1534-5807. DOI: 10.1016/s1534-5807(02)00208-3.

Jewett, Cayla E. et al. (Sept. 2017). "Planar polarized Rab35 functions as an oscillatory ratchet during cell intercalation in the Drosophila epithelium". en. In: *Nature Communications* 8.1. Number: 1 Publisher: Nature Publishing Group, p. 476. ISSN: 2041-1723. DOI: 10.1038/s41467-017-00553-0. URL: https://www.nature.com/articles/s41467-017-00553-0 (visited on 03/06/2022).

Jung, Han-Sung et al. (Apr. 1998). "Local Inhibitory Action of BMPs and Their Relationships with Activators in Feather Formation: Implications for Periodic Patterning". en. In: *Developmental Biology* 196.1, pp. 11–23. ISSN: 0012-1606. DOI: 10.1006/dbio.

1998.8850. URL: https://www.sciencedirect.com/science/article/pii/S0012160698988509 (visited on 03/14/2022).

Kabaso, Doron et al. (May 2011). "Theoretical Model for Cellular Shapes Driven by Protrusive and Adhesive Forces". en. In: *PLOS Computational Biology* 7.5. Publisher: Public Library of Science, e1001127. ISSN: 1553-7358. DOI: 10.1371/journal.pcbi.1001127. URL: https://journals.plos.org/ploscompbiol/article?id=10.1371/journal.pcbi.1001127 (visited on 04/01/2022).

Kamath, Ravi S. et al. (Jan. 2003). "Systematic functional analysis of the Caenorhabditis elegans genome using RNAi". eng. In: *Nature* 421.6920, pp. 231–237. ISSN: 0028-0836. DOI: 10.1038/nature01278.

Kapoor, Sukriti and Sachin Kotak (Nov. 2019). "Centrosome Aurora A regulates RhoGEF ECT-2 localisation and ensures a single PAR-2 polarity axis in C. elegans embryos". eng. In: *Development (Cambridge, England)* 146.22, dev174565. ISSN: 1477-9129. DOI: 10.1242/dev.174565.

Kinmonth-Schultz, Hannah A., Greg S. Golembeski, and Takato Imaizumi (May 2013). "Circadian clock-regulated physiological outputs: Dynamic responses in nature". en. In: *Seminars in Cell & Developmental Biology*. Plant Circadian Rhythms & Mechanisms of inner ear development 24.5, pp. 407–413. ISSN: 1084-9521. DOI: 10.1016/j.semcdb.2013.02.006. URL: https://www.sciencedirect.com/science/article/pii/S1084952113000244 (visited on 04/08/2022).

Klaasen, Gene A. and William C. Troy (1984). "Stationary Wave Solutions of a System of Reaction-Diffusion Equations Derived from the Fitzhugh-Nagumo Equations". In: *SIAM Journal on Applied Mathematics* 44.1. Publisher: Society for Industrial and Applied Mathematics, pp. 96–110. ISSN: 0036-1399. URL: https://www.jstor.org/stable/2101307 (visited on 10/15/2021).

Klika, Václav et al. (Apr. 2012). "The Influence of Receptor-Mediated Interactions on Reaction-Diffusion Mechanisms of Cellular Self-organisation". en. In: *Bulletin of Mathematical Biology* 74.4, pp. 935–957. ISSN: 1522-9602. DOI: 10.1007/s11538-011-9699-4. URL: https://doi.org/10.1007/s11538-011-9699-4 (visited on 03/09/2022).

Koga, Shinji and Yoshiki Kuramoto (Jan. 1980). "Localized Patterns in Reaction-Diffusion Systems". In: *Progress of Theoretical Physics* 63.1, pp. 106–121. ISSN: 0033-068X. DOI: 10.1143/PTP.63.106. URL: https://doi.org/10.1143/PTP.63.106 (visited on 10/15/2021).

Kondo, Shigeru and Takashi Miura (Sept. 2010). "Reaction-diffusion model as a framework for understanding biological pattern formation." In: *Science* 329.5999, pp. 1616–1620. DOI: 10.1126/science.1179047. URL: http://dx.doi.org/10.1126/science.1179047 (visited on 04/09/2020).

Kress, Geraldine J. et al. (July 2008). "High threshold, proximal initiation, and slow conduction velocity of action potentials in dentate granule neuron mossy fibers". eng. In: *Journal of Neurophysiology* 100.1, pp. 281–291. ISSN: 0022-3077. DOI: 10.1152/jn.90295.2008.

Kumar, K. Vijay et al. (May 2014). "Pulsatory Patterns in Active Fluids". In: *Physical Review Letters* 112.20. Publisher: American Physical Society, p. 208101. DOI: 10.1103/PhysRevLett.112.208101. URL: https://link.aps.org/doi/10.1103/PhysRevLett.112.208101 (visited on 03/16/2022).

Kusano, Kiyoshi (1966). "Electrical activity and structural correlates of giant nerve fibers in Kuruma shrimp (Penaeus japonicus)". en. In: *Journal of Cellular Physiology* 68.3. _eprint: https://onlinelibrary.wiley.com/doi/pdf/10.1002/jcp.1040680315, pp. 361–383. ISSN: 1097-4652. DOI: 10.1002/jcp.1040680315. URL: https://onlinelibrary.wiley.com/doi/abs/10.1002/jcp.1040680315 (visited on 02/23/2022).

Lagage, Valentine and Stephan Uphoff (Sept. 2020). "Pulses and delays, anticipation and memory: seeing bacterial stress responses from a single-cell perspective". In: *FEMS Microbiology Reviews* 44.5, pp. 565–571. ISSN: 0168-6445. DOI: 10.1093/femsre/fuaa022. URL: https://doi.org/10.1093/femsre/fuaa022 (visited on 04/08/2022).

Lam Hui, King, Sae In Kwak, and Arpita Upadhyaya (2014). "Adhesion-dependent modulation of actin dynamics in Jurkat T cells". en. In: *Cytoskeleton* 71.2, pp. 119–135. ISSN: 1949-3592. DOI: 10.1002/cm.21156. URL: https://onlinelibrary.wiley.com/doi/abs/10.1002/cm.21156 (visited on 02/11/2022).

Landino, Jennifer et al. (Dec. 2021). "Rho and F-actin self-organize within an artificial cell cortex". en. In: *Current Biology* 31.24, 5613–5621.e5. ISSN: 0960-9822. DOI: 10.1016/j.

cub.2021.10.021. URL: https://www.sciencedirect.com/science/article/pii/S096098222101410X (visited on 02/24/2022).

Lee, Jen-Yi and Richard M. Harland (Feb. 2010). "Endocytosis Is Required for Efficient Apical Constriction during Xenopus Gastrulation". en. In: *Current Biology* 20.3, pp. 253–258. ISSN: 0960-9822. DOI: 10.1016/j.cub.2009.12.021. URL: https://www.sciencedirect.com/science/article/pii/S0960982209021435 (visited on 03/06/2022).

Levayer, Romain and Thomas Lecuit (July 2013). "Oscillation and polarity of E-cadherin asymmetries control actomyosin flow patterns during morphogenesis." In: *Developmental Cell* 26.2, pp. 162–175. DOI: 10.1016/j.devcel.2013.06.020. URL: http://dx.doi.org/10.1016/j.devcel.2013.06.020 (visited on 04/09/2020).

Levayer, Romain, Anne Pelissier-Monier, and Thomas Lecuit (May 2011). "Spatial regulation of Dia and Myosin-II by RhoGEF2 controls initiation of E-cadherin endocytosis during epithelial morphogenesis." In: *Nature Cell Biology* 13.5, pp. 529–540. ISSN: 1476-4679. DOI: 10.1038/ncb2224. URL: http://dx.doi.org/10.1038/ncb2224 (visited on 04/09/2020).

Levine, Joe H., Michelle E. Fontes, et al. (Jan. 2012). "Pulsed feedback defers cellular differentiation". eng. In: *PLoS biology* 10.1, e1001252. ISSN: 1545-7885. DOI: 10.1371/journal.pbio.1001252.

Levine, Joe H., Yihan Lin, and Michael B. Elowitz (Dec. 2013). "Functional Roles of Pulsing in Genetic Circuits". In: *Science (New York, N.Y.)* 342.6163, pp. 1193–1200. ISSN: 0036-8075. DOI: 10.1126/science.1239999. URL: https://www.ncbi.nlm.nih.gov/pmc/articles/PMC4100686/ (visited on 05/17/2021).

Li, Younan and Edwin Munro (Sept. 2021). "Filament-guided filament assembly provides structural memory of filament alignment during cytokinesis". eng. In: *Developmental Cell* 56.17, 2486–2500.e6. ISSN: 1878-1551. DOI: 10.1016/j.devcel.2021.08.009.

Liu, Ji et al. (Mar. 2010). "NMY-2 maintains cellular asymmetry and cell boundaries, and promotes a SRC-dependent asymmetric cell division". In: *Developmental biology* 339.2, pp. 366–373. ISSN: 0012-1606. DOI: 10.1016/j.ydbio.2009.12.041. URL: https://www.ncbi.nlm.nih.gov/pmc/articles/PMC2903000/ (visited on 01/04/2021).

Locke, James C. W. et al. (Oct. 2011). "Stochastic pulse regulation in bacterial stress response". eng. In: *Science (New York, N.Y.)* 334.6054, pp. 366–369. ISSN: 1095-9203. DOI: 10.1126/science.1208144.

Maddox, Amy Shaub, Bianca Habermann, et al. (June 2005). "Distinct roles for two C. elegans anillins in the gonad and early embryo." In: *Development* 132.12, pp. 2837–2848. DOI: 10.1242/dev.01828. URL: http://dx.doi.org/10.1242/dev.01828 (visited on 04/09/2020).

Maddox, Amy Shaub, Lindsay Lewellyn, et al. (May 2007). "Anillin and the septins promote asymmetric ingression of the cytokinetic furrow." In: *Developmental Cell* 12.5, pp. 827–835. DOI: 10.1016/j.devcel.2007.02.018. URL: http://dx.doi.org/10.1016/j.devcel.2007.02.018 (visited on 04/15/2020).

Maître, Jean-Léon et al. (July 2015). "Pulsatile cell-autonomous contractility drives compaction in the mouse embryo." In: *Nature Cell Biology* 17.7, pp. 849–855. DOI: 10.1038/ncb3185. URL: http://dx.doi.org/10.1038/ncb3185 (visited on 04/09/2020).

Marchesin, Valentina, Guillaume Montagnac, and Philippe Chavrier (Mar. 2015). "ARF6 Promotes the Formation of Rac1 and WAVE-Dependent Ventral F-Actin Rosettes in Breast Cancer Cells in Response to Epidermal Growth Factor". en. In: *PLOS ONE* 10.3. Publisher: Public Library of Science, e0121747. ISSN: 1932-6203. DOI: 10.1371/journal.pone.0121747. URL: https://journals.plos.org/plosone/article?id=10.1371/journal.pone.0121747 (visited on 02/11/2022).

Martin, Adam C, Matthias Kaschube, and Eric F Wieschaus (Jan. 2009). "Pulsed contractions of an actin-myosin network drive apical constriction." In: *Nature* 457.7228, pp. 495–499. ISSN: 1476-4687. DOI: 10.1038/nature07522. URL: http://dx.doi.org/10.1038/nature07522 (visited on 04/09/2020).

Martin, Adam C. and Bob Goldstein (May 2014). "Apical constriction: themes and variations on a cellular mechanism driving morphogenesis". In: *Development* 141.10, pp. 1987–1998. ISSN: 0950-1991. DOI: 10.1242/dev.102228. URL: https://doi.org/10.1242/dev.102228 (visited on 04/08/2022).

Mason, Frank M, Michael Tworoger, and Adam C Martin (Aug. 2013). "Apical domain polarization localizes actin-myosin activity to drive ratchet-like apical constriction." In: *Nature*

Cell Biology 15.8, pp. 926–936. DOI: 10.1038/ncb2796. URL: http://dx.doi.org/10.1038/ncb2796 (visited on 04/09/2020).

Mayer, Mirjam et al. (Sept. 2010). "Anisotropies in cortical tension reveal the physical basis of polarizing cortical flows." In: *Nature* 467.7315, pp. 617–621. DOI: 10.1038/nature09376. URL: http://dx.doi.org/10.1038/nature09376 (visited on 04/09/2020).

Menshykau, Denis, Conradin Kraemer, and Dagmar Iber (Feb. 2012). "Branch Mode Selection during Early Lung Development". en. In: *PLOS Computational Biology* 8.2. Publisher: Public Library of Science, e1002377. ISSN: 1553-7358. DOI: 10.1371/journal.pcbi.1002377. URL: https://journals.plos.org/ploscompbiol/article?id=10.1371/journal.pcbi.1002377 (visited on 03/09/2022).

Meron, Ehud (Sept. 1992). "Pattern formation in excitable media". In: *Physics Reports* 218.1, pp. 1–66. ISSN: 03701573. DOI: 10.1016/0370-1573(92)90098-K. URL: http://linkinghub.elsevier.com/retrieve/pii/037015739290098K (visited on 09/10/2020).

Miao, Hui and J. Todd Blankenship (Sept. 2020). "The pulse of morphogenesis: actomyosin dynamics and regulation in epithelia". In: *Development* 147.17, dev186502. ISSN: 0950-1991. DOI: 10.1242/dev.186502. URL: https://doi.org/10.1242/dev.186502 (visited on 03/06/2022).

Miao, Hui, Timothy E. Vanderleest, et al. (Sept. 2019). "Cell ratcheting through the Sbf RabGEF directs force balancing and stepped apical constriction". In: *Journal of Cell Biology* 218.11, pp. 3845–3860. ISSN: 0021-9525. DOI: 10.1083/jcb.201905082. URL: https://doi.org/10.1083/jcb.201905082 (visited on 03/06/2022).

Michaud, Ani, Zachary T. Swider, et al. (May 2021). "Cortical excitability and cell division". eng. In: *Current biology: CB* 31.10. tex.ids= Michaud2021a publisher: Cell Press, R553–R559. ISSN: 1879-0445. DOI: 10.1016/j.cub.2021.02.053.

Michaux, Jonathan B et al. (Dec. 2018). "Excitable RhoA dynamics drive pulsed contractions in the early C. elegans embryo." In: *The Journal of Cell Biology* 217.12, pp. 4230–4252. DOI: 10.1083/jcb.201806161. URL: http://dx.doi.org/10.1083/jcb.201806161 (visited on 04/10/2020).

Moore, Thomas et al. (Dec. 2014). "Self-Organizing Actomyosin Patterns on the Cell Cortex at Epithelial Cell-Cell Junctions". en. In: *Biophysical Journal* 107.11, pp. 2652–2661. ISSN: 0006-3495. DOI: 10.1016/j.bpj.2014.10.045. URL: https://www.sciencedirect.com/science/article/pii/S000634951401131X (visited on 03/17/2022).

Motegi, Fumio and Asako Sugimoto (Sept. 2006). "Sequential functioning of the ECT-2 RhoGEF, RHO-1 and CDC-42 establishes cell polarity in Caenorhabditis elegans embryos". eng. In: *Nature Cell Biology* 8.9, pp. 978–985. ISSN: 1465-7392. DOI: 10.1038/ncb1459.

Mou, Chunyan et al. (Mar. 2011). "Cryptic Patterning of Avian Skin Confers a Developmental Facility for Loss of Neck Feathering". en. In: *PLOS Biology* 9.3. Publisher: Public Library of Science, e1001028. ISSN: 1545-7885. DOI: 10.1371/journal.pbio.1001028. URL: https://journals.plos.org/plosbiology/article?id=10.1371/journal.pbio.1001028 (visited on 03/09/2022).

Müller, Patrick et al. (May 2012). "Differential Diffusivity of Nodal and Lefty Underlies a Reaction-Diffusion Patterning System". In: *Science* 336.6082. Publisher: American Association for the Advancement of Science, pp. 721–724. DOI: 10.1126/science.1221920. URL: https://www.science.org/doi/10.1126/science.1221920 (visited on 03/08/2022).

Munjal, Akankshi et al. (Aug. 2015). "A self-organized biomechanical network drives shape changes during tissue morphogenesis." In: *Nature* 524.7565, pp. 351–355. DOI: 10.1038/nature14603. URL: http://dx.doi.org/10.1038/nature14603 (visited on 04/09/2020).

Munro, Edwin, Jeremy Nance, and James R Priess (Sept. 2004). "Cortical flows powered by asymmetrical contraction transport PAR proteins to establish and maintain anterior-posterior polarity in the early C. elegans embryo." In: *Developmental Cell* 7.3, pp. 413–424. ISSN: 1534-5807. DOI: 10.1016/j.devcel.2004.08.001. URL: http://dx.doi.org/10.1016/j.devcel.2004.08.001 (visited on 04/09/2020).

Murthy, Kausalya and Patricia Wadsworth (July 2008). "Dual role for microtubules in regulating cortical contractility during cytokinesis". In: *Journal of Cell Science* 121.14, pp. 2350–2359. ISSN: 0021-9533. DOI: 10.1242/jcs.027052. URL: https://doi.org/10.1242/jcs.027052 (visited on 10/15/2021).

Naganathan, Sundar Ram et al. (Dec. 2014). "Active torque generation by the actomyosin cell cortex drives left–right symmetry breaking". In: *eLife* 3. Ed. by James Ferrell. Publisher: eLife Sciences Publications, Ltd, e04165. ISSN: 2050-084X. DOI: 10.7554/eLife.04165. URL: https://doi.org/10.7554/eLife.04165 (visited on 02/25/2022).

Nagumo, J., S. Arimoto, and S. Yoshizawa (Oct. 1962). "An Active Pulse Transmission Line Simulating Nerve Axon". en. In: *Proceedings of the IRE* 50.10, pp. 2061–2070. ISSN: 0096-8390. DOI: 10.1109/JRPROC.1962.288235. URL: http://ieeexplore.ieee.org/document/4066548/ (visited on 10/31/2021).

Nakamura, Tetsuya et al. (Oct. 2006). "Generation of Robust Left-Right Asymmetry in the Mouse Embryo Requires a Self-Enhancement and Lateral-Inhibition System". en. In: *Developmental Cell* 11.4, pp. 495–504. ISSN: 1534-5807. DOI: 10.1016/j.devcel.2006.08.002. URL: https://www.sciencedirect.com/science/article/pii/S1534580706003480 (visited on 03/08/2022).

Neidt, Erin M., Bonnie J. Scott, and David R. Kovar (Jan. 2009). "Formin differentially utilizes profilin isoforms to rapidly assemble actin filaments". eng. In: *The Journal of Biological Chemistry* 284.1, pp. 673–684. ISSN: 0021-9258. DOI: 10.1074/jbc.M804201200.

Neidt, Erin M., Colleen T. Skau, and David R. Kovar (Aug. 2008). "The cytokinesis formins from the nematode worm and fission yeast differentially mediate actin filament assembly". eng. In: *The Journal of Biological Chemistry* 283.35, pp. 23872–23883. ISSN: 0021-9258. DOI: 10.1074/jbc.M803734200.

Nelson, D. E. et al. (Oct. 2004). "Oscillations in NF-kappaB signaling control the dynamics of gene expression". eng. In: *Science (New York, N.Y.)* 306.5696, pp. 704–708. ISSN: 1095-9203. DOI: 10.1126/science.1099962.

Nishikawa, Masatoshi et al. (Jan. 2017). "Controlling contractile instabilities in the actomyosin cortex". In: *eLife* 6. Ed. by Matthieu Piel. Publisher: eLife Sciences Publications, Ltd, e19595. ISSN: 2050-084X. DOI: 10.7554/eLife.19595. URL: https://doi.org/10.7554/eLife.19595 (visited on 02/24/2022).

Nishimura, Tamako, Hisao Honda, and Masatoshi Takeichi (May 2012). "Planar Cell Polarity Links Axes of Spatial Dynamics in Neural-Tube Closure". en. In: *Cell* 149.5, pp. 1084–1097. ISSN: 0092-8674. DOI: 10.1016/j.cell.2012.04.021. URL: https://www.

sciencedirect.com/science/article/pii/S0092867412005259 (visited on 03/25/2022).

Onimaru, Koh et al. (May 2016). "The fin-to-limb transition as the re-organization of a Turing pattern". en. In: *Nature Communications* 7.1. Number: 1 Publisher: Nature Publishing Group, p. 11582. ISSN: 2041-1723. DOI: 10.1038/ncomms11582. URL: https://www.nature.com/articles/ncomms11582 (visited on 03/09/2022).

Ono, Kanako et al. (May 2003). "Specific requirement for two ADF/cofilin isoforms in distinct actin-dependent processes in Caenorhabditis elegans." In: *Journal of Cell Science* 116.Pt 10, pp. 2073–2085. DOI: 10.1242/jcs.00421. URL: http://dx.doi.org/10.1242/jcs.00421 (visited on 04/15/2020).

Pacquelet, Anne et al. (Sept. 2015). "PAR-4 and anillin regulate myosin to coordinate spindle and furrow position during asymmetric division". In: *Journal of Cell Biology* 210.7, pp. 1085–1099. ISSN: 0021-9525. DOI: 10.1083/jcb.201503006. URL: https://doi.org/10.1083/jcb.201503006 (visited on 09/02/2021).

Painter, K. J. et al. (Aug. 2012). "Towards an integrated experimental–theoretical approach for assessing the mechanistic basis of hair and feather morphogenesis". In: *Interface Focus* 2.4. Publisher: Royal Society, pp. 433–450. DOI: 10.1098/rsfs.2011.0122. URL: https://royalsocietypublishing.org/doi/10.1098/rsfs.2011.0122 (visited on 03/09/2022).

Paluch, Ewa et al. (July 2005). "Cortical actomyosin breakage triggers shape oscillations in cells and cell fragments". eng. In: *Biophysical Journal* 89.1, pp. 724–733. ISSN: 0006-3495. DOI: 10.1529/biophysj.105.060590.

Peleg, Barak et al. (Apr. 2011). "Propagating Cell-Membrane Waves Driven by Curved Activators of Actin Polymerization". en. In: *PLOS ONE* 6.4. Publisher: Public Library of Science, e18635. ISSN: 1932-6203. DOI: 10.1371/journal.pone.0018635. URL: https://journals.plos.org/plosone/article?id=10.1371/journal.pone.0018635 (visited on 02/25/2022).

Pérez-Mongiovi, D., P. Chang, and E. Houliston (Feb. 1998). "A propagated wave of MPF activation accompanies surface contraction waves at first mitosis in Xenopus". eng. In: *Journal of Cell Science* 111 (Pt 3), pp. 385–393. ISSN: 0021-9533. DOI: 10.1242/jcs.111.3.385.

Piekny, Alisa J and Michael Glotzer (Jan. 2008). "Anillin is a scaffold protein that links RhoA, actin, and myosin during cytokinesis." In: *Current Biology* 18.1, pp. 30–36. DOI: 10.1016/j.cub.2007.11.068. URL: http://dx.doi.org/10.1016/j.cub.2007.11.068 (visited on 04/15/2020).

Piekny, Alisa J., Jacque-Lynne F. Johnson, et al. (Dec. 2003). "The Caenorhabditis elegans non-muscle myosin genes nmy-1 and nmy-2 function as redundant components of the let-502/Rho-binding kinase and mel-11/myosin phosphatase pathway during embryonic morphogenesis". en. In: *Development* 130.23. Publisher: The Company of Biologists Ltd Section: Research Article, pp. 5695–5704. ISSN: 0950-1991, 1477-9129. DOI: 10.1242/dev.00807. URL: https://dev.biologists.org/content/130/23/5695 (visited on 10/21/2020).

Pikovsky, Arkady S. and Jürgen Kurths (Feb. 1997). "Coherence Resonance in a Noise-Driven Excitable System". In: *Physical Review Letters* 78.5. Publisher: American Physical Society, pp. 775–778. DOI: 10.1103/PhysRevLett.78.775. URL: https://link.aps.org/doi/10.1103/PhysRevLett.78.775 (visited on 03/14/2022).

Pohl, Christian et al. (Nov. 2012). "Actomyosin-based Self-organization of cell internalization during C. elegans gastrulation". In: *BMC Biology* 10.1, p. 94. ISSN: 1741-7007. DOI: 10.1186/1741-7007-10-94. URL: https://doi.org/10.1186/1741-7007-10-94 (visited on 10/09/2021).

Pomerening, Joseph R., Eduardo D. Sontag, and James E. Ferrell (Apr. 2003). "Building a cell cycle oscillator: hysteresis and bistability in the activation of Cdc2". eng. In: *Nature Cell Biology* 5.4, pp. 346–351. ISSN: 1465-7392. DOI: 10.1038/ncb954.

Purvis, Jeremy E. et al. (June 2012). "p53 dynamics control cell fate". eng. In: *Science (New York, N.Y.)* 336.6087, pp. 1440–1444. ISSN: 1095-9203. DOI: 10.1126/science.1218351.

Rankin, Susannah and Marc W. Kirschner (June 1997). "The surface contraction waves of Xenopus eggs reflect the metachronous cell-cycle state of the cytoplasm". en. In: *Current Biology* 7.6, pp. 451–454. ISSN: 0960-9822. DOI: 10.1016/S0960-9822(06)00192-8. URL: https://www.sciencedirect.com/science/article/pii/S0960982206001928 (visited on 02/23/2022).

Raspopovic, J. et al. (Aug. 2014). "Digit patterning is controlled by a Bmp-Sox9-Wnt Turing network modulated by morphogen gradients". In: *Science* 345.6196. Publisher: American As-

sociation for the Advancement of Science, pp. 566–570. DOI: 10.1126/science.1252960. URL: https://www.science.org/doi/10.1126/science.1252960 (visited on 11/22/2021).

Rauzi, Matteo, Pierre-François Lenne, and Thomas Lecuit (Dec. 2010). "Planar polarized actomyosin contractile flows control epithelial junction remodelling." In: *Nature* 468.7327, pp. 1110–1114. ISSN: 1476-4687. DOI: 10.1038/nature09566. URL: http://dx.doi.org/10.1038/nature09566 (visited on 04/09/2020).

Reyes, Ciara C. et al. (June 2014). "Anillin regulates cell-cell junction integrity by organizing junctional accumulation of Rho-GTP and actomyosin". eng. In: *Current biology: CB* 24.11, pp. 1263–1270. ISSN: 1879-0445. DOI: 10.1016/j.cub.2014.04.021.

Ridley, Anne J (Oct. 2015). "Rho GTPase signalling in cell migration". en. In: *Current Opinion in Cell Biology*. Cell adhesion and migration 36, pp. 103–112. ISSN: 0955-0674. DOI: 10.1016/j.ceb.2015.08.005. URL: https://www.sciencedirect.com/science/article/pii/S0955067415001106 (visited on 10/28/2021).

Robin, François B et al. (June 2014). "Single-molecule analysis of cell surface dynamics in Caenorhabditis elegans embryos." In: *Nature Methods* 11.6, pp. 677–682. DOI: 10.1038/nmeth.2928. URL: http://dx.doi.org/10.1038/nmeth.2928 (visited on 04/09/2020).

Rodriguez, Josana et al. (Aug. 2017). "aPKC Cycles between Functionally Distinct PAR Protein Assemblies to Drive Cell Polarity". In: *Developmental Cell* 42.4, 400–415.e9. ISSN: 1534-5807. DOI: 10.1016/j.devcel.2017.07.007. URL: https://www.ncbi.nlm.nih.gov/pmc/articles/PMC5563072/ (visited on 10/28/2021).

Roh-Johnson, Minna et al. (Mar. 2012). "Triggering a cell shape change by exploiting preexisting actomyosin contractions." In: *Science* 335.6073, pp. 1232–1235. ISSN: 1095-9203. DOI: 10.1126/science.1217869. URL: http://dx.doi.org/10.1126/science.1217869 (visited on 04/09/2020).

Ryan, Gillian L. et al. (Apr. 2012). "Excitable Actin Dynamics in Lamellipodial Protrusion and Retraction". en. In: *Biophysical Journal* 102.7, pp. 1493–1502. ISSN: 0006-3495. DOI: 10.1016/j.bpj.2012.03.005. URL: https://www.sciencedirect.com/science/article/pii/S0006349512002858 (visited on 04/01/2022).

Sailer, Anne et al. (Oct. 2015). "Dynamic Opposition of Clustered Proteins Stabilizes Cortical Polarity in the C. elegans Zygote". eng. In: *Developmental Cell* 35.1, pp. 131–142. ISSN: 1878-1551. DOI: 10.1016/j.devcel.2015.09.006.

Segal, Dagan et al. (May 2018). "Feedback inhibition of actin on Rho mediates content release from large secretory vesicles." In: *The Journal of Cell Biology* 217.5, pp. 1815–1826. ISSN: 0021-9525. DOI: 10.1083/jcb.201711006. URL: http://www.jcb.org/lookup/doi/10.1083/jcb.201711006 (visited on 04/12/2020).

Sehring, Ivonne M et al. (Oct. 2015). "Assembly and positioning of actomyosin rings by contractility and planar cell polarity". In: *eLife* 4. Ed. by Mohan Balasubramanian. Publisher: eLife Sciences Publications, Ltd, e09206. ISSN: 2050-084X. DOI: 10.7554/eLife.09206. URL: https://doi.org/10.7554/eLife.09206 (visited on 03/17/2022).

Sha, Wei et al. (Feb. 2003). "Hysteresis drives cell-cycle transitions in Xenopus laevis egg extracts". In: *Proceedings of the National Academy of Sciences of the United States of America* 100.3, pp. 975–980. ISSN: 0027-8424. DOI: 10.1073/pnas.0235349100. URL: https://www.ncbi.nlm.nih.gov/pmc/articles/PMC298711/ (visited on 03/31/2022).

Sheth, Rushikesh et al. (Dec. 2012). "Hox Genes Regulate Digit Patterning by Controlling the Wavelength of a Turing-Type Mechanism". In: *Science* 338.6113. Publisher: American Association for the Advancement of Science, pp. 1476–1480. DOI: 10.1126/science.1226804. URL: https://www.science.org/doi/10.1126/science.1226804 (visited on 11/22/2021).

Shindo, Asako (Jan. 2018). "Models of convergent extension during morphogenesis". eng. In: *Wiley Interdisciplinary Reviews. Developmental Biology* 7.1. ISSN: 1759-7692. DOI: 10.1002/wdev.293.

Shindo, Asako and John B. Wallingford (Feb. 2014). "PCP and septins compartmentalize cortical actomyosin to direct collective cell movement". eng. In: *Science (New York, N.Y.)* 343.6171, pp. 649–652. ISSN: 1095-9203. DOI: 10.1126/science.1243126.

Shlomovitz, R. and N. S. Gov (Apr. 2007). "Membrane Waves Driven by Actin and Myosin". In: *Physical Review Letters* 98.16. Publisher: American Physical Society, p. 168103. DOI: 10.1103/PhysRevLett.98.168103. URL: https://link.aps.org/doi/10.1103/PhysRevLett.98.168103 (visited on 02/24/2022).

Sick, Stefanie et al. (Dec. 2006). "WNT and DKK Determine Hair Follicle Spacing Through a Reaction-Diffusion Mechanism". In: *Science* 314.5804. Publisher: American Association for the Advancement of Science, pp. 1447–1450. DOI: 10.1126/science.1130088. URL: https://www.science.org/doi/10.1126/science.1130088 (visited on 03/09/2022).

Smith, Mark A. et al. (Sept. 2010). "A Zyxin-Mediated Mechanism for Actin Stress Fiber Maintenance and Repair". en. In: *Developmental Cell* 19.3, pp. 365–376. ISSN: 15345807. DOI: 10.1016/j.devcel.2010.08.008. URL: https://linkinghub.elsevier.com/retrieve/pii/S1534580710003837 (visited on 10/31/2021).

Sokolow, Adam et al. (Mar. 2012). "Cell ingression and apical shape oscillations during dorsal closure in Drosophila". eng. In: *Biophysical Journal* 102.5, pp. 969–979. ISSN: 1542-0086. DOI: 10.1016/j.bpj.2012.01.027.

Solon, Jerome et al. (June 2009). "Pulsed forces timed by a ratchet-like mechanism drive directed tissue movement during dorsal closure." In: *Cell* 137.7, pp. 1331–1342. ISSN: 1097-4172. DOI: 10.1016/j.cell.2009.03.050. URL: http://dx.doi.org/10.1016/j.cell.2009.03.050 (visited on 04/09/2020).

Spiliotis, Elias T. and Konstantinos Nakos (May 2021). "Cellular functions of actin- and microtubule-associated septins". en. In: *Current Biology* 31.10, R651–R666. ISSN: 0960-9822. DOI: 10.1016/j.cub.2021.03.064. URL: https://www.sciencedirect.com/science/article/pii/S0960982221004371 (visited on 04/09/2022).

Stephenson, Rachel E. et al. (Feb. 2019). "Rho Flares Repair Local Tight Junction Leaks". en. In: *Developmental Cell* 48.4, 445–459.e5. ISSN: 1534-5807. DOI: 10.1016/j.devcel.2019.01.016. URL: https://www.sciencedirect.com/science/article/pii/S1534580719300449 (visited on 12/07/2021).

Straight, A.F., C.M. Field, and T.J. Mitchison (2005). "Anillin binds nonmuscle myosin II and regulates the contractile ring". English. In: *Molecular Biology of the Cell* 16.1, pp. 193–201. ISSN: 1059-1524. DOI: 10.1091/mbc.E04-08-0758.

Sumi, Angughali et al. (Nov. 2018). "Adherens Junction Length during Tissue Contraction Is Controlled by the Mechanosensitive Activity of Actomyosin and Junctional Recycling". en. In: *Developmental Cell* 47.4, 453–463.e3. ISSN: 1534-5807. DOI: 10.1016/j.devcel.

2018.10.025. URL: https://www.sciencedirect.com/science/article/pii/S1534580718308797 (visited on 03/06/2022).

Sun, Xiaoyu et al. (Nov. 2020). "Mechanosensing through Direct Binding of Tensed F-Actin by LIM Domains". English. In: *Developmental Cell* 55.4. Publisher: Elsevier, 468–482.e7. ISSN: 1534-5807. DOI: 10.1016/j.devcel.2020.09.022. URL: https://www.cell.com/developmental-cell/abstract/S1534-5807(20)30754-1 (visited on 10/31/2021).

Sutherland, Ann and Alyssa Lesko (Feb. 2020). "Pulsed actomyosin contractions in morphogenesis". In: *F1000Research* 9. ISSN: 2046-1402. DOI: 10.12688/f1000research.20874.1. URL: https://www.ncbi.nlm.nih.gov/pmc/articles/PMC7043108/ (visited on 11/02/2020).

Takenawa, Tadaomi and Shiro Suetsugu (Jan. 2007). "The WASP–WAVE protein network: connecting the membrane to the cytoskeleton". en. In: *Nature Reviews Molecular Cell Biology* 8.1. Number: 1 Publisher: Nature Publishing Group, pp. 37–48. ISSN: 1471-0080. DOI: 10.1038/nrm2069. URL: https://www.nature.com/articles/nrm2069 (visited on 04/01/2022).

Tay, Savaş et al. (July 2010). "Single-cell NF-kappaB dynamics reveal digital activation and analogue information processing". eng. In: *Nature* 466.7303, pp. 267–271. ISSN: 1476-4687. DOI: 10.1038/nature09145.

Tian, Dong et al. (May 2015). "Anillin Regulates Neuronal Migration and Neurite Growth by Linking RhoG to the Actin Cytoskeleton". en. In: *Current Biology* 25.9, pp. 1135–1145. ISSN: 0960-9822. DOI: 10.1016/j.cub.2015.02.072. URL: https://www.sciencedirect.com/science/article/pii/S0960982215002742 (visited on 03/02/2021).

Timmons, L., D. L. Court, and A. Fire (Jan. 2001). "Ingestion of bacterially expressed dsRNAs can produce specific and potent genetic interference in Caenorhabditis elegans". eng. In: *Gene* 263.1-2, pp. 103–112. ISSN: 0378-1119. DOI: 10.1016/s0378-1119(00)00579-5.

Tse, Yu Chung, Alisa Piekny, and Michael Glotzer (Sept. 2011). "Anillin promotes astral microtubule-directed cortical myosin polarization". eng. In: *Molecular Biology of the Cell* 22.17, pp. 3165–3175. ISSN: 1939-4586. DOI: 10.1091/mbc.E11-05-0399.

Turing, A. M. (Aug. 1952). "The chemical basis of morphogenesis". In: *Philosophical Transactions of the Royal Society B: Biological Sciences* 237.641, pp. 37–72. ISSN: 0962-8436. DOI: 10.1098/rstb.1952.0012. URL: http://rstb.royalsocietypublishing.org/cgi/doi/10.1098/rstb.1952.0012 (visited on 09/17/2020).

Vanderleest, Timothy E et al. (July 2018). "Vertex sliding drives intercalation by radial coupling of adhesion and actomyosin networks during Drosophila germband extension". In: *eLife* 7. Ed. by Sally Horne-Badovinac and Didier YR Stainier. Publisher: eLife Sciences Publications, Ltd, e34586. ISSN: 2050-084X. DOI: 10.7554/eLife.34586. URL: https://doi.org/10.7554/eLife.34586 (visited on 03/06/2022).

Vicker, Michael G (2002). "F-actin assembly in Dictyostelium cell locomotion and shape oscillations propagates as a self-organized reaction–diffusion wave". en. In: *FEBS Letters* 510.1-2. _eprint: https://onlinelibrary.wiley.com/doi/pdf/10.1016/S0014-5793%2801%2903207-0, pp. 5–9. ISSN: 1873-3468. DOI: 10.1016/S0014-5793(01)03207-0. URL: https://onlinelibrary.wiley.com/doi/abs/10.1016/S0014-5793%2801%2903207-0 (visited on 02/11/2022).

Vishnoi, Monika et al. (2013). "Triggering sporulation in Bacillus subtilis with artificial two-component systems reveals the importance of proper Spo0A activation dynamics". en. In: *Molecular Microbiology* 90.1. _eprint: https://onlinelibrary.wiley.com/doi/pdf/10.1111/mmi.12357, pp. 181–194. ISSN: 1365-2958. DOI: 10.1111/mmi.12357. URL: https://onlinelibrary.wiley.com/doi/abs/10.1111/mmi.12357 (visited on 02/17/2022).

Watanabe, Sadanori et al. (Sept. 2010). "Rho and anillin-dependent control of mDia2 localization and function in cytokinesis". eng. In: *Molecular Biology of the Cell* 21.18, pp. 3193–3204. ISSN: 1939-4586. DOI: 10.1091/mbc.E10-04-0324.

Weiner, Orion D et al. (Sept. 2007). "An actin-based wave generator organizes cell motility." In: *PLoS Biology* 5.9, e221. ISSN: 1545-7885. DOI: 10.1371/journal.pbio.0050221. URL: http://dx.doi.org/10.1371/journal.pbio.0050221 (visited on 04/09/2020).

Winkelman, Jonathan D. et al. (Oct. 2020). "Evolutionarily diverse LIM domain-containing proteins bind stressed actin filaments through a conserved mechanism". en. In: *Proceedings of the National Academy of Sciences* 117.41. Publisher: National Academy of Sciences Section: Biological Sciences, pp. 25532–25542. ISSN: 0027-8424, 1091-6490. DOI: 10.1073/pnas.

2004656117. URL: https://www.pnas.org/content/117/41/25532 (visited on 02/24/2022).

Wu, Min, Xudong Wu, and Pietro De Camilli (Jan. 2013). "Calcium oscillations-coupled conversion of actin travelling waves to standing oscillations." In: *Proceedings of the National Academy of Sciences of the United States of America* 110.4, pp. 1339–1344. DOI: 10.1073/pnas.1221538110. URL: http://dx.doi.org/10.1073/pnas.1221538110 (visited on 04/09/2020).

Wu, Zhanghan, Maohan Su, et al. (Jan. 2018). "Membrane shape-mediated wave propagation of cortical protein dynamics". en. In: *Nature Communications* 9.1. Number: 1 Publisher: Nature Publishing Group, p. 136. ISSN: 2041-1723. DOI: 10.1038/s41467-017-02469-1. URL: https://www.nature.com/articles/s41467-017-02469-1 (visited on 02/11/2022).

Xiong, Ding et al. (Mar. 2016). "Frequency and amplitude control of cortical oscillations by phosphoinositide waves." In: *Nature Chemical Biology* 12.3, pp. 159–166. DOI: 10.1038/nchembio.2000. URL: http://dx.doi.org/10.1038/nchembio.2000 (visited on 07/21/2020).

Yamaguchi, Motoomi, Eiichi Yoshimoto, and Shigeru Kondo (Mar. 2007). "Pattern regulation in the stripe of zebrafish suggests an underlying dynamic and autonomous mechanism". In: *Proceedings of the National Academy of Sciences* 104.12. Publisher: Proceedings of the National Academy of Sciences, pp. 4790–4793. DOI: 10.1073/pnas.0607790104. URL: https://www.pnas.org/doi/full/10.1073/pnas.0607790104 (visited on 03/07/2022).

Yamanaka, Hiroaki and Shigeru Kondo (Feb. 2014). "In vitro analysis suggests that difference in cell movement during direct interaction can generate various pigment patterns in vivo". In: *Proceedings of the National Academy of Sciences* 111.5. Publisher: Proceedings of the National Academy of Sciences, pp. 1867–1872. DOI: 10.1073/pnas.1315416111. URL: https://www.pnas.org/doi/full/10.1073/pnas.1315416111 (visited on 03/25/2022).

Yang, Hee Won, Sean R. Collins, and Tobias Meyer (Feb. 2016). "Locally excitable Cdc42 signals steer cells during chemotaxis". en. In: *Nature Cell Biology* 18.2. Number: 2 Publisher:

Nature Publishing Group, pp. 191–201. ISSN: 1476-4679. DOI: 10.1038/ncb3292. URL: https://www.nature.com/articles/ncb3292 (visited on 02/11/2022).

Yang, Qiong and James E. Ferrell (May 2013). "The Cdk1-APC/C cell cycle oscillator circuit functions as a time-delayed, ultrasensitive switch". In: *Nature cell biology* 15.5, pp. 519–525. ISSN: 1465-7392. DOI: 10.1038/ncb2737. URL: https://www.ncbi.nlm.nih.gov/pmc/articles/PMC3728279/ (visited on 03/31/2022).

Young, Jonathan W., James C. W. Locke, and Michael B. Elowitz (Mar. 2013). "Rate of environmental change determines stress response specificity". eng. In: *Proceedings of the National Academy of Sciences of the United States of America* 110.10, pp. 4140–4145. ISSN: 1091-6490. DOI: 10.1073/pnas.1213060110.

Zaidel-Bar, Ronen, Guo Zhenhuan, and Chen Luxenburg (June 2015). "The contractome – a systems view of actomyosin contractility in non-muscle cells". In: *Journal of Cell Science* 128.12, pp. 2209–2217. ISSN: 0021-9533. DOI: 10.1242/jcs.170068. URL: https://doi.org/10.1242/jcs.170068 (visited on 03/05/2022).

Zhang, Donglei and Michael Glotzer (Aug. 2015). "The RhoGAP activity of CYK-4/MgcRacGAP functions non-canonically by promoting RhoA activation during cytokinesis". In: *eLife* 4. Ed. by Mohan Balasubramanian. Publisher: eLife Sciences Publications, Ltd, e08898. ISSN: 2050-084X. DOI: 10.7554/eLife.08898. URL: https://doi.org/10.7554/eLife.08898 (visited on 04/01/2022).

Zhao, Peng et al. (Mar. 2019). "Aurora-A Breaks Symmetry in Contractile Actomyosin Networks Independently of Its Role in Centrosome Maturation". eng. In: *Developmental Cell* 48.5, 631–645.e6. ISSN: 1878-1551. DOI: 10.1016/j.devcel.2019.02.012.

Zhu, Jianjian et al. (Apr. 2008). "Uncoupling Sonic Hedgehog Control of Pattern and Expansion of the Developing Limb Bud". In: *Developmental cell* 14.4, pp. 624–632. ISSN: 1534-5807. DOI: 10.1016/j.devcel.2008.01.008. URL: https://www.ncbi.nlm.nih.gov/pmc/articles/PMC8284562/ (visited on 03/24/2022).